Materials Science and Engineering, 29 (2000) 49–113

R Reports: *A Review Journal*

www.elsevier.com/locate/mser

Microstructural and mechanical characteristics of in situ metal matrix composites

S.C. Tjong*, Z.Y. Ma[1]

Department of Physics and Materials Science, City University of Hong Kong, 83 Tat Chee Avenue, Kowloon, Hong Kong

Accepted 10 July 2000

Abstract

During the past decade, considerable research effort has been directed towards the development of in situ metal matrix composites (MMCs), in which the reinforcements are formed in situ by exothermal reactions between elements or between elements and compounds. Using this approach, MMCs with a wide range of matrix materials (including aluminum, titanium, copper, nickel and iron), and second-phase particles (including borides, carbides, nitrides, oxides and their mixtures) have been produced. Because of the formation of ultrafine and stable ceramic reinforcements, the in situ MMCs are found to exhibit excellent mechanical properties. In this review article, current development on the fabrication, microstructure and mechanical properties of the composites reinforced with in situ ceramic phases will be addressed. Particular attention is paid to the mechanisms responsible for the formation of in situ reinforcements, and for creep failure of the aluminum-based matrix composites.

Keywords: Metal matrix composites; In situ formed particles; Fabrication; Microstructure; Creep; Wear

1. Introduction

Metal matrix composites (MMCs) refer to a kind of material in which rigid ceramic reinforcements are embedded in a ductile metal or alloy matrix. MMCs combine metallic properties (ductility and toughness) with ceramic characteristics (high strength and modulus), leading to greater strength in shear and compression and to higher service temperature capabilities. The attractive physical and mechanical properties that can be obtained with MMCs, such as high specific modulus, strength, and thermal stability, have been documented extensively [1–7]. Interest in MMCs for use in the aerospace and automotive industries, and other structural applications, has increased over the past 20 years as a result of the availability of relatively inexpensive reinforcements and the development of various processing routes which result in reproducible microstructure and properties [8].

The family of discontinuously reinforced MMCs includes both particulates and whiskers or short fibers. More recently, this class of MMCs has attracted considerable attention as a result of (a) availability of various types of reinforcement at competitive costs, (b) the successful development of manufacturing processes to produce MMCs with reproducible structure and properties, and (c) the availability of standard or near-standard metal working methods which can be utilized to fabricate

* Corresponding author. Tel.: +852-2788-7702; fax: +852-2788-7830.
E-mail address: aptjong@cityu.edu.hk (S.C. Tjong).
[1] On leave from: Institute of Metal Research, Chinese Academy of Sciences, Shenyang 110015, PR China.

0927-796X/00/$ – see front matter
PII: S0927-796X(00)00024-3

these MMCs [9]. The particulate-reinforced MMCs are of particular interest due to their ease of fabrication, lower costs, and isotropic properties.

Traditionally, discontinuously reinforced MMCs have been produced by several processing routes such as powder metallurgy, spray deposition, mechanical alloying (MA) and various casting techniques, i.e. squeeze casting, rheocasting and compocasting [1–18]. All these techniques are based on the addition of ceramic reinforcements to the matrix materials which may be in molten or powder form. For the conventional MMCs, the reinforcing phases are prepared separately prior to the composite fabrication. Thus, conventional MMCs can be viewed as ex situ MMCs. In this case, the scale of the reinforcing phase is limited by the starting powder size, which is typically of the order of microns to tens of microns and rarely below 1 μm. Other main drawbacks that have to be overcome are the interfacial reactions between the reinforcements and the matrix, and poor wettability between the reinforcements and the matrix due to surface contamination of the reinforcements.

It is widely recognized that the properties of MMCs are controlled by the size and volume fraction of the reinforcements as well as the nature of the matrix–reinforcement interfaces. An optimum set of mechanical properties can be achieved when fine and thermally stable ceramic particulates are dispersed uniformly in the metal matrix. Efforts have been made to meet such requirements. The work has led to the development of novel composites — in situ MMCs in which the reinforcements are synthesized in a metallic matrix by chemical reactions between elements or between element and compound during the composite fabrication. Compared to the conventional MMCs produced by ex situ methods, the in situ MMCs exhibit the following advantages: (a) the in situ formed reinforcements are thermodynamically stable at the matrix, leading to less degradation in elevated-temperature services; (b) the reinforcement–matrix interfaces are clean, resulting in a strong interfacial bonding; (c) the in situ formed reinforcing particles are finer in size and their distribution in the matrix is more uniform, yielding better mechanical properties.

Because of the great potential that in situ MMCs offer for widespread applications, a variety of processing techniques have been developed for production during the past decade. Using these routes, in situ MMCs with a wide range of matrix materials (including aluminum, titanium, copper, nickel and iron) and second-phase particles (including borides, carbides, nitrides, oxides and their mixtures) have been produced [19–24]. Commercial application of these in situ processing technologies requires an understanding of several key processing steps. However, common processing features of in situ MMCs, including fabricating routes themselves, are not well established. Moreover, the mechanisms responsible for in situ formation of ceramic reinforcements in the metallic matrix are not well understood.

In this review article, current developments in fabrication, microstructure and mechanical properties of the composites reinforced with in situ ceramic phases will be addressed. Particular attention is paid to the mechanisms responsible for the formation of in situ reinforcements, and for creep failure of the aluminum-based matrix composites.

2. Main fabrication methods

A variety of processing techniques have evolved over the last decade in an effort to optimize the structure and properties of in situ ceramic phase reinforced MMCs. However, the terminology in the literature for the processing routes is inconsistent and confused. Koczak and Premkumar [25] have suggested that the in situ reactions can be categorized in terms of the starting phases, such as gas–liquid, liquid–solid, liquid–liquid etc., but an effective categorization and naming of the processing routes have not so far been established. Here, we categorize the processing methods utilized to

manufacture the in situ MMCs according to the temperature of the metallic matrix and reactants during processing. Accordingly, the processing routes can be classified into four categories: (a) solid–liquid reaction process; (b) vapor–liquid–solid reaction process; (c) solid–solid reaction process, and (d) liquid–liquid reaction process.

2.1. Solid–liquid reaction process

In this process, reactants (elements or compounds) react in situ to form reinforcing phases in the presence of a third liquid metallic phase, or reactants react with some component in the melt to form in situ ceramic reinforcements. In essence, this process is a solvent-assisted reaction wherein the reinforcing particles are generated in the solvent medium (the matrix) via diffusion of the components. This process has been widely adopted to fabricate in situ MMCs. According to the processing features, this process can be further grouped into the following processing routes.

2.1.1. Self-propagating high-temperature synthesis (SHS)

Self-propagating high-temperature synthesis (SHS), developed by Merzhanov and coworkers [26–29] in the late 1960s, refers to a process in which materials with a sufficiently high heat of formation are synthesized in a combustion wave, which after ignition, spontaneously propagates throughout the reactants and converts them into the products. An important feature of SHS reactions is the self-sustaining reaction front. Three basic requirements must be met in order for a reaction to be self-sustaining [30]. The first is that the reaction must be highly exothermic. The heat given off during the reaction helps to maintain the propagation front by heating the unreacted portion of the sample to its ignition temperature. A heat of reaction of the order of -167 kJ/g mol is sufficient to maintain a propagating front [30]. The second requirement is that one of the reactants should form a liquid or vapor phase in order to facilitate the diffusion of the fluid phase reactant to the reaction front. The third requirement is that the rate of heat dissipation (via conduction or radiation) must be less than the rate of heat generation. This ensures that the reaction will not be extinguished due to extreme heat losses to the surroundings. SHS is extremely attractive, its main advantages being the self-generation of energy required for the process, the high-purity products due to volatilization of low boiling point impurity at elevated temperature, and high productivity due to very high reaction rates.

The SHS process has been extensively employed for the production of ceramic [31–35], intermetallic [36,37], and intermetallic matrix composites (IMCs) [38–42]. However, reports on in situ SHS processing of MMCs are very limited [43,44]. In principle, SHS processing appears to be much more problematic for MMCs than it is for IMCs. For IMCs, both the reactions for the reinforcement formation and matrix formation are exothermic, whereas for MMCs, the ‘inert’ matrix acts as a diluent which may cause damping of the combustion wave. Therefore, only ceramic reinforcements with a high heat of formation are suitable for SHS processing of MMCs. Another basic requirement is that the high fraction of ceramic reinforcement (i.e. low fraction of metal matrix) should be maintained. This ensures that the reaction does not cease owing to an excessive dilution of the matrix material. For Al-based MMCs, TiC and TiB_2 seem to be feasible reinforcements, both from the point of view of the exothermicity of the reactions of their formation and their stability in the Al matrix.

Choi et al. [43] were the first to report the fabrication of Al-based MMCs reinforced with fibrous TiC formed by SHS reaction. In the process, a blend of Al and Ti powders and carbon fibers was pressed at 17–28 kPa by a hydrostatic press. The resulting compact was preheated in an electrical furnace before ignition. The ignition was carried out in an inert argon atmosphere

Table 1
Composition of reactant powder mixture, measured maximum temperatures, and average propagation rates[a]

Sample	Mole ratio			T_{max} (K)	Velocity (10^{-3} m/s)
	Ti	C	Al		
1[b]	1	1	–	2911	9.8
2[c]	1	1	–	2361	4.8
3[c]	1	1	0.1	2337	0.8
4[d]	1	1	0.5	–	–

[a] Reprinted from Y. Choi et al., Fabrication of metal matrix composites of TiC–Al through self-propagating synthesis reaction, Metallurgical Transaction A 23A (1992) 2389, with permission from TMS and ASM [43].
[b] Graphite.
[c] PAN-type carbon fibers.
[d] No reaction with preheating up to the melting point of Al.

(<0.2 ppm O_2) using a low arc source or a high-power argon plasma torch. The combustion parameters used in their experiment are summarized in Table 1. Choi et al. [43] indicated that the self-propagating reaction front cannot be sustained when more than 0.1 mole ratio of Al is added to the Ti–C mixture at room temperature. However, the combustion reaction of the above concentration propagates well by preheating the compact to a temperature of at least 523 K. They suggested that the increase in the enthalpy of the compact due to preheating compensates for a decrease in heat generation per unit mass caused by the aluminum diluent. When the green compact is preheated above the melting point of aluminum, where titanium aluminide is formed, they also observed that the combustion reaction between Ti and carbon does not take place for a compact containing 0.5 mole ratio of Al. Furthermore, it is noted from Table 1 that the combustion velocity for the compact containing Al is about one order of magnitude lower than for pure Ti–C. The density of a composite with a fairly low-volume content of metal matrix produced by the SHS process is relative low, i.e. 78% of the theoretical density. Even after hot isostatic pressing (HIP) treatment at 773 K, the actual density of the product is only 92% of its theoretical density. This is mainly attributed to the formation of a high volume fraction of ceramic phase in the products.

Gotman et al. [44] have prepared an Al matrix composite reinforced with 30 vol.% TiC, TiB_2 and $TiC + TiB_2$ ceramic reinforcements via SHS, followed by high-pressure consolidation to full density. In their study, powder blends of Al–Ti–C, Al–Ti–B, Al–Ti–B_4C, and Al–Ti–C–B were prepared by ball milling. Very small amounts (less than 1%) of halogenide-based gas transport agents were added to the starting powder mixture to activate the combustion process. Cylindrical compacts (32 mm diameter × 100 mm height) with about 36–38% theoretical density were placed in a reactor with thermally insulated walls. On top of each compact, 15 g of an igniting Ti–C mixture (1:1 mole ratio) was placed. The mixture was ignited by passing electric current through a tungsten wire. All SHS experiments were performed in argon at atmospheric pressure. After the combustion process, cylindrical samples with porosity were obtained.

Table 2 summarizes the measured, calculated and estimated combustion parameters for four different powder mixtures (starting composition, final composition based on thermodynamic equilibrium, adiabatic temperature T_{ad}, combustion temperature T_{exp}, combustion wave velocity u and cooling time from T_{exp} to the freezing (melting) temperature of Al, t_{cool}). Gotman et al. [44] reported that, for all four compositions investigated, very low combustion velocities (at least one order of magnitude lower than those of pure Ti–C and Ti–B) are observed, which is in good agreement with the result reported by Choi et al. [43]. The propagation of the combustion wave is unstable, indicating that the rate of heat dissipation into the 'inert' Al matrix approaches the rate of

Table 2
Combustion parameters of the powder mixtures used[a]

Starting powder mixture (wt.%)	Equilibrium combustion products (wt.%)	Volume fraction of ceramic particles	Adiabatic temperature T_{ad} (K)	Combustion temperature T_{exp} (K)	Combustion velocity u (10^{-3} m/s)	t_{cool} (min)
Al 57.5 Ti 34.0 C 8.5	Al 57.4 TiC 42.45 Al_4C_3 0.15	0.29	1401	1373	0.9	45
Al 58.6 Ti 28.5 B 12.9	Al 58.6 TiB_2 41.4	0.30	1600	1533	1.9	54
Al 57.6 Ti 30.6 B_4C 11.8	Al 57.6 TiB_2 29.6 TiC 12.8	TiB_2 0.22 TiC 0.09	1449	1428	0.8	42
Al 57.6 Ti 30.6 B 9.2 C 2.6	Al 57.6 TiB_2 29.6 TiC 12.8	TiB_2 0.22 TiC 0.09	1570	1513	1.4	48

[a] Reprinted from Gotman et al., Fabrication of Al matrix in situ composites via self-propagating synthesis, Materials Science and Engineering A A187 (1994) 192, with permission from Elsevier [44].

heat generation. The non-steady-state oscillatory motion of the wave during combustion results in a typical layered structure of the reaction products. Gotman et al. [44] pointed out that the heat required to maintain the propagation front of these reactions for the formation of 30 vol.% TiC and/or TiB_2 appears to be close to the lower limit required for the self-sustained synthesis process.

X-ray diffraction (XRD) analyses indicate that the phase compositions of the synthesized MMCs closely fit the predictions based on thermodynamic equilibrium, i.e. the materials contain high fractions of TiC, TiB_2, and TiC + TiB_2, respectively. Microstructural examination reveals that very fine ceramic particles ranging from tens of nanometers up to 1–2 μm are formed in situ in the Al matrix. XRD and microstructural analyses of the reaction products also confirm TiB_2/Al and (TiB_2 + TiC)/Al composites containing the Al_3Ti phase. This implies that full conversion of Ti to TiC or TiC + TiB_2 is not achieved.

In subsequent consolidation processing, two procedures were adopted by Gotman et al. [44]. In the first procedure, SHS-processed porous materials were directly consolidated inside a high-pressure cell. In the second procedure, SHS-processed porous materials were milled into powders of ~100 μm size which were compacted into approximately 70% dense green compacts. Both types of specimens were treated in a vacuum of 10^{-5} Torr at 573 K for 1 h in order to remove the hydrate layer from the Al surface. They were consolidated at high pressure (3 GPa) at room or slight elevated (~573 K) temperature. After consolidation, practically 100% density was achieved.

2.1.2. Exothermic dispersion (XD)

In the 1980s, an exothermic dispersion (XD) process, termed XD™ technology, was developed by Martin Marietta Laboratories, Baltimore, MD, USA [20,45–47]. In this technology (Fig. 1), powders of the elemental components of a high-temperature (ceramic) phase (X, Y) are heated in the presence of a third metallic phase (A), with A constituting all or part of the matrix of the eventual product. At some temperature, usually above the melting point of phase A but well below that normally required to produce the ceramic phase XY, the component elements X and Y interact exothermally, forming submicroscopic hardening particles in the solvent phase. After the initial

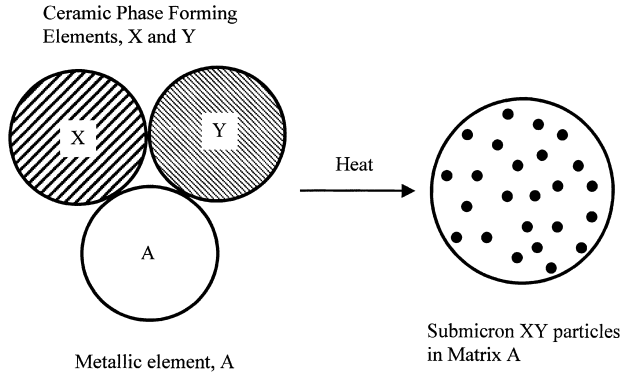

Fig. 1. Schematic of process for making XD dispersion-hardened composites.

exothermic production step, a master alloy with as high as 20–75 vol.% reinforcement is obtained. This master alloy can be added to any compatible matrix material to achieve required levels of reinforcement. The conventional metallurgical processing can be used to produce final shapes such as castings, forgings, and extrusions. Research that is now in progress is focused on the 'design' of microstructures containing hard phases for strength, resilient phases for toughness, and whiskers for creep resistance.

Kuruvilla et al. [48] have fabricated the in situ TiB_2 reinforced Al composite using XD process. Powder blends of Ti, Al and B are first cold-isostatically pressed at a pressure of 200 MPa and subsequently degassed in vacuum at 723 K for 1 h. The Al–Ti–B compact is heated to 1073 K in an argon atmosphere and held at that temperature for 15 min. The resulting porous composite is canned and section-rolled into rods of 6 mm in diameter. TiB_2 particles with a size of ~1 μm are formed in situ. In addition, some coarse Al_xTi particles are formed in the composite. Similarly, in situ TiB_2/2024Al composite reinforced with TiB_2 particulates of 1.3 μm average size, TiC/Al composite reinforced with TiC particulates of 0.7 μm average size, and TiC/2219Al alloy composites reinforced with TiC particulates of 3.3 μm average size have been fabricated successfully [49–55].

2.1.3. Reactive hot pressing (RHP)

The reactive hot pressing (RHP) process has been developed by Ma et al. [56,57] for fabricating the aluminum matrix composites reinforced with TiB_2 particulates on the basis of the XD technique [48]. It encompasses both the exothermic conversion of reactants to in situ reinforcements and the subsequent hot compaction of the porous composite product. Thus, dense Al-based composites can be produced in one processing step. In this process, stoichiometric Ti and B powders, and an appropriate amount of Al powders, are blended thoroughly and cold-compacted to a theoretical density of ~65%. The as-compacted green billet is heated to above 1073 K in vacuum and maintained for 10 min, then cooled down to 873 K and hot-pressed. This process results in an in situ Al-based composite product of 60 mm diameter × 100 mm height with a theoretical density of nearly 100%. The dense as-pressed composites can be subsequently subjected to extrusion or rolling. TiB_2 particulates with a size of 0.1–5 μm are formed in situ. Furthermore, Ma et al. [56,57] reported that a certain amount of irregular Al_3Ti blocks was detected in the composite. The existence of Al_3Ti was also reported in in situ composites fabricated by other processes [53,54].

In order to reduce the size of in situ reinforcements further and eliminate Al_3Ti in the in situ composites, a novel reactive system TiO_2–Al–B is adopted by Ma et al. to fabricate in situ Al_2O_3 and TiB_2 particulate, mixture-reinforced, Al-based composites [20,58–60]. In their studies, mixture

Table 3
Molecular ratio of in starting TiO_2–Al–B materials and nominal content of generated phases (vol.%) in composite products [58]

B/TiO_2	Al_2O_3	TiB_2	Al_3Ti
0	10.5	–	23.7
4/3	10.5	6.3	7.9
5/3	10.5	7.9	4.0
2/1	10.5	9.5	–

powders of B and TiO_2 with various B/TiO_2 molecular ratios are used (Table 3). For the TiO_2–Al system without B, XRD patterns show the presence of Al, Al_2O_3 and Al_3Ti diffraction peaks (Fig. 2a), indicating that a reaction between TiO_2 and Al, i.e. a thermite reaction [61], has taken place forming Al_2O_3 and Al_3Ti. When B is incorporated into the TiO_2–Al system, TiB_2 diffraction peaks appear and the intensity of the Al_3Ti peaks is significantly weakened (Fig. 2b). This indicates that the Ti displaced from the thermite reaction reacts preferentially with B to form TiB_2 in the presence of B. The intensity of the Al_3Ti peaks is further reduced with increasing B content in the TiO_2–Al–B system (Fig. 2c). As the molecular ratio of B/TiO_2 reaches 2/1, the Al_3Ti diffraction lines disappear (Fig. 2d). Ma et al. [58] suggested that the reaction between TiO_2, Al and B takes place as follows:

$$3TiO_2 + 4Al + 6B \rightarrow 2Al_2O_3 + 3TiB_2 \quad (R1)$$

Accordingly, Al_2O_3 and TiB_2 are in situ generated and the Al_3Ti phase is eliminated. Thus, in situ Al-based composites reinforced with fine Al_2O_3 and TiB_2 particulates (average size of 0.31 μm) can be produced by means of the RHP route using the novel TiO_2–Al–B system [20,58,59]. Furthermore, Ma and Tjong [59] have investigated the possibility of fabricating $(Al_2O_3 + TiB_2)$/Al composite from a TiO_2–Al–B_2O_3 system. They reported that Al_2O_3 and TiB_2 particulates are in situ formed through the reactions between TiO_2, Al, and B_2O_3. However, a certain amount of plate-like Al_3Ti blocks with a size of several tens of micrometers are generated in this composite. Finally Ma et al. [59,60] have fabricated Al_2O_3 and TiB_2 particulate reinforced Al–Cu alloy matrix composites by incorporating CuO into the TiO_2–Al–B system.

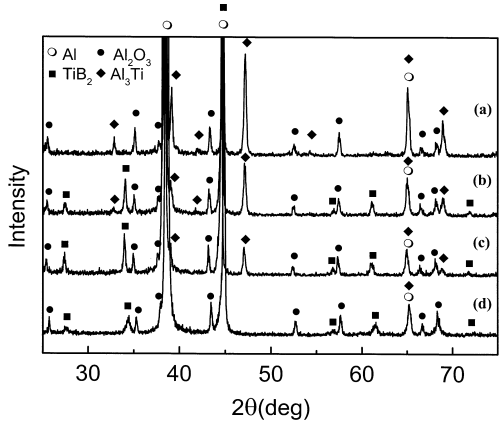

Fig. 2. X-ray diffraction pattern of composites for B/TiO_2 molecular ratio of (a) 0; (b) 4/3; (c) 5/3 and (d) 2/1 [58].

2.1.4. Combustion assisted cast (CAC)

Combustion assisted cast (CAC), also known as combustion assisted synthesis (CAS), refers to a process in which the combustion synthesis and traditional ingot metallurgy (IM) are combined to produce in situ MMCs. Generally, a stoichiometric amount of reactant powders is first blended thoroughly and then compacted into pellets. The compacted pellet and the required amount of matrix are melted and then cast into a graphite mold. The ceramic reinforcements are formed in situ during melting via exothermic reactions between the reactants.

Lin et al. [62] performed a preliminary study on the fabrication of in situ TiC particulate reinforced Ti matrix composites by means of the CAC. In the process, Ti, C, and Al powders are placed in a graphite crucible and then heated in an oven with an argon atmosphere at 473 K for 12 h, to remove water vapor in the graphite crucible and charge materials. Melting of Ti, C, Al powders is conducted in an induction furnace. An ultrasonic vibrator is used to enhance stirring and reduce entrained gas in the melt. An in situ Ti matrix composite reinforced with 45 vol.% of three-dimensional TiC is successfully produced.

Ranganath et al. [21] have carried out the CAS of (TiB + TiC)/Ti composites via the casting route. In their study, compacted pellets of Ti and B_4C and a required amount of titanium sponge are melted in a water-cooled copper crucible using non-consumable vacuum arc melting. Ranganath et al. [21] suggested that the chemical reaction between B_4C and Ti takes place as follows:

$$5Ti + B_4C \rightarrow 4TiB + TiC \quad \text{(R2)}$$

Subsequently, in situ ceramic reinforcements are yielded by the exothermic reaction between Ti and B_4C in the melt, resulting in the formation of TiB and TiC reinforcing particles in the Ti matrix. From the literature, several workers also fabricated in situ TiC/Ti, TiB/Ti and (TiB + TiC)/Ti composites from Ti–C, Ti–B and Ti–B_4C systems, respectively, by means of the CAC technique [63–66].

2.1.5. Direct reaction synthesis (DRS)

Direct reaction synthesis (DRS) refers to a process in which reactant powders, or compacts of reactant powders, are directly added into molten metal and the ceramic reinforcing particles are formed in situ through the exothermic reaction between reactants or between reactant and some component of the melt.

Maity et al. [67] have investigated the possibility of fabricating in situ Al_2O_3 reinforced Al composite by means of the DRS process. A required amount of TiO_2 particles is slowly added into the vortex developed in molten Al at 973 K by stirring with a graphite impeller. After reaction, the composite melt is subsequently solidified in a crucible in air. Al_2O_3 particles with a size of $\sim$3 μm are formed in situ in the composite.

Nakata et al. [68] have prepared in situ formed carbide particulate reinforced Al-based composites based on the reaction between liquid aluminum alloys, containing a thermodynamically stable carbide formation element and a relative unstable carbide such as SiC and Al_4C_3 as a solid carbon source. Two fabrication procedures were adopted by Nakata et al. [68]. In the first method, aluminum containing a carbide-forming element (Ti, Zr, and Ta) was melted in an MgO crucible of an induction furnace under an argon atmosphere. Then, SiC or Al_4C_3 particles were incorporated into the melt by the melt-stirring method. During stirring, TiC, ZrC and TaC particles are formed in situ in the liquid aluminum and the melt is then cast in a permanent mold. Nakata et al. [68] reported that the size of the SiC particles added has an effect, not only on the rate of the in situ reaction, but also on the dispersion behavior of in situ-formed TiC particles. When adding small SiC particles (0.6

and 3 μm) into the melt, fine TiC particles with a size of less than 1 μm are formed in situ, dispersed uniformly in the Al matrix. In the case of large SiC particles of 14 μm size, a circular TiC phase appears to aggregate near the remaining raw SiC particles due to a decrease in the in situ reaction rate and to the presence of large Al_3Ti intermetallic compounds, formed from the remaining titanium. In the second method, a powder mixture of Al_4C_3 (3 μm) and Ti (~350 mesh) is added to the Al melt at 1473 K. After the in situ reaction ceases, magnesium or copper is alloyed at a lowered temperature. Thus, in situ TiCp/Al–5 wt.% Mg and TiCp/Al–4.5 wt.% Cu composites are produced.

For Cu-based composites, Chrysanthou and Erbaccio [69] have used the DRS process to form TiC or TiB_2 reinforcing particles. In their study, C powders or powder mixtures of B_2O_3 and C, respectively, are added to the Cu–Ti alloy melt at a temperature of 1673–1873 K. They suggested that the following two reactions take place in the melt:

$$[Ti]_{cu} + C \rightarrow TiC \quad (R3)$$

$$[Ti]_{cu} + B_2O_3 + 3C \rightarrow TiB_2 + 3CO \quad (R4)$$

They indicate that in situ TiC particles with a size of 1–10 μm and a content of as high as 55 wt.% are achieved in the TiC/Cu composite, whereas TiB_2 particles up to 18 wt.% with a size of 3–5 μm are formed in situ in the TiB_2/Cu composite.

Recently, the DRS technique has been further developed as a novel in situ process to prepare Al-based MMCs at the Harbin Institute of Technology (HIT), Harbin, PR China [70–75]. First stoichiometric reactant powders (Ti and C or Ti and B) and an appropriate amount of matrix (Al) powder are mixed thoroughly and uniaxially pressed into green compacts with a theoretical density of 50–60%. The powder compacts are placed in an aluminum melt. The reaction is carried out at a constant temperature for an appropriate length of time to ensure complete conversion to ceramic reinforcement of the reactants in the powder compact. The processing time and temperature depend on the molar ratio of the mixed powders, the matrix chemistry, and the melt quantity and desired reinforcement content. Processing time can range from 2 to 20 min and the processing temperature varies between 1073 and 1273 K. After completion of the in situ reaction, the melt is agitated and then cast. Using this process, Al-based composites reinforced with submicron-sized in situ TiC or TiB_2 particulates have been successfully fabricated [70–75].

2.1.6. Flux-assisted synthesis (FAS)

A patented process termed flux-assisted synthesis (FAS) (also known as mixed-salt reaction or reaction cast) was developed by the London Scandinavian Metallurgical Company (LSM) to produce in situ aluminum matrix composites (Fig. 3). Such a technique, based on their existing technology, has produced fine-grained aluminum alloys [76]. During the synthesis, mixed salts of potassium hexafluorotitanate (K_2TiF_6) and potassium tetrafluororate (KBF_4) are introduced into a stirred aluminum melt with an atomic ratio in accordance with Ti/2B. Exothermal reactions between the salts and the molten aluminum take place according the following sequences [77]:

$$3K_2TiF_6 + 13Al \rightarrow 3TiAl_3 + 3KAlF_4 + K_3AlF_6 \quad (R5)$$

$$2KBF_4 + 3Al \rightarrow AlB_2 + 2KAlF_4 \quad (R6)$$

$$AlB_2 + TiAl_3 \rightarrow TiB_2 + 4Al \quad (R7)$$

After the reaction stirring is stopped in order to remove the slug containing $KAlF_4$ and K_3AlF_6, the molten composite is cast into a mold. The maximum amount of in situ formed TiB_2 is determined by

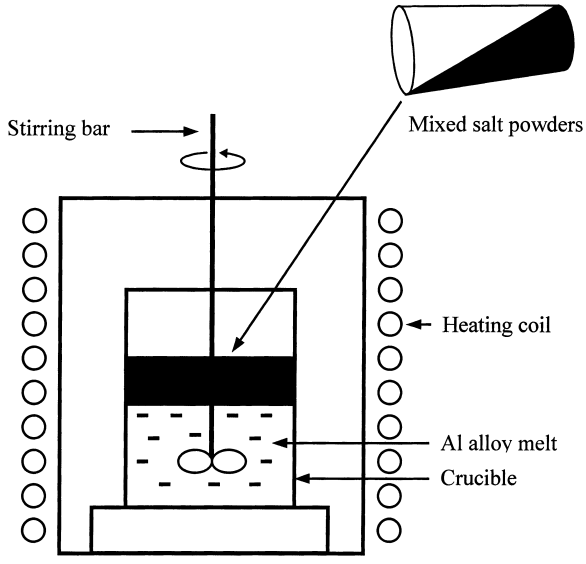

Fig. 3. Schematic diagram of an apparatus for fabricating in situ MMCs by means of FAS.

the viscosity of the subsequent melt. Values of up to 12% have been reported by Kellie and Wood [77]. Pure Al, Al–4 wt.% Cu and A356 composites reinforced with in situ TiB_2 particles were successfully fabricated [77–80].

Using a similar approach, Chen and Chung [81] have fabricated 10 vol.% in situ TiB particle reinforced 2024Al composite by adding mixed powders of TiO_2, Na_3AlF_6 and KBF_4 into an Al alloy melt. Furthermore, they also fabricated a strong, ductile, $TiAl_3$ particle reinforced Al matrix composite by using a new reaction scheme [82]. In this scheme, mixed powders of TiO_2 and Na_3AlF_6 were added to an Al melt and the following reactions were assumed to occur:

$$2TiO_2 + 2Na_3AlF_6 \rightarrow 2Na_2TiF_6 + Na_2O + Al_2O_3 \quad \text{(R8)}$$

$$2Na_2TiF_6 + 6Al \rightarrow 4NaF + 4F_2 + 2TiAl_3 \quad \text{(R9)}$$

$$Al_2O_3 + 2Na_3AlF_6 \rightarrow 3Na_2O + 4Al + 6F_2 \quad \text{(R10)}$$

Owing to the ability of Na_3AlF_6 to reduce TiO_2 as well as Al_2O_3, TiO_2 was consumed fully in the reaction and no Al_2O_3 retained in the resulting composite. In this way, an aluminum matrix composite containing $TiAl_3$ particles with a size of 1–2 μm was produced [82].

Since the FAS process is based on a well-established technology, it could be readily amenable for scaling up for the commercial production of composites. However, Koczak and Premkumar [25] and Davies et al. [78] indicate that the nature of the particle–matrix interface in the composites prepared by FAS process is unclear. They suggest that the TiB_2 particles formed are coated with some undesirable reaction products due to the presence of salts in the reaction process. In this case, the effectiveness of borides on the composite strengthening would be diminished. This issue was further investigated by Chen et al. very recently [83]. They fabricated in situ TiB_2/Al–4 wt.% Cu composites by using both mixed salt K_2TiF_6–KBF_4–Na_3AlF_6, and mixed oxide TiO_2–H_3BO_3–Na_3AlF_6 systems, respectively. They reported that the mechanical properties of the TiB_2/Al–4 wt.% Cu composite fabricated from the mixed salt system is lower than that from the mixed oxide system, which is attributed to the presence of molten salts around the TiB_2 particles as reported by Davies

et al. [78]. Chen et al. [83] further indicated that the reaction rate in the mixed salt system is markedly lower than that in the mixed oxide system. Also, it is rather difficult to produce composites reinforced with a higher loading of TiB_2 particles (>8 vol.%) using the mixed salt system. They suggest that the TiO_2–H_3BO_3–Na_3AlF_6 mixed oxide system is more suitable for fabricating in situ TiB_2/Al composites than the K_2TiF_6–KBF_4–Na_3AlF_6 mixed salt system.

2.1.7. Reactive spontaneous infiltration (RSI)

This process involves simultaneous infiltration and reaction of a porous solid preform with the melt to form a very fine, and thermodynamically stable, reinforcing ceramic phase [84]. In the process, a powder mixture of the reactants is poured into an alumina crucible of 12 mm inner diameter and 100 mm height, and then an Al or Al alloy ingot is placed above the loose bed of the powder mixture. The crucible containing ingot–powder pairs are then placed in a nitrogen or argon atmosphere controlled, induction furnace. The specimens are then heated to desired temperature for a specified time. This process can be used to fabricate the in situ boride (TiB_2, NbB_2, TaB_2, HfB_2) reinforced Al matrix composites by using powder mixtures of $TiN(TC_xN_{1-x})$–B, Ti(Nb,Ta,Hf)–B_4C [85,86]. It offers the advantage of producing composites with a high ceramic content and near-net-shape fabrication [87].

Recently, Nanabe and Aswath [88,89] have synthesized Al matrix composites reinforced with micro Al_2O_3/Al particles via reactive infiltration of molten Al into preforms of SiO_2 or $Mg + SiO_2$ mixtures at 1348 K. In this RSI reaction, SiO_2 particulate preform placed inside a quartz tube of 9 mm diameter and 15 mm length is immersed in the Al melt. The melt infiltrates the preform and the following reaction is expected to occur:

$$3SiO_2 + 4Al \rightarrow 2Al_2O_3 + 3Si \quad \text{(R11)}$$

Si released from the reaction diffuses out of the preform and dissolves into the bulk melt. Thus, Al matrix composite reinforced with in situ formed microcomposite Al_2O_3/Al particle is produced.

2.1.8. Directed melt/metal oxidation (DIMOX)

The directed melt oxidation (DIMOX) process was developed by Lanxide Corporation, USA, as a novel synthesis route to obtain flexible metal–ceramic composites. Its primary advantages include the ability to form relatively complex, fully dense composites with tailor-made properties to meet the needs of a wide range of applications. This technique is widely used to produce reinforced ceramics and metals [90–93].

In the DIMOX process, the liquid metal melt, such as Mg-containing Al alloys, is oxidized at elevated temperatures (usually from 1273 to 1673 K for Al alloy) and the reaction product grows outwards from the original metal poll surface, either into free space or into a filler material. The growth continues by transportation of the liquid through tortuous microscopic channels of the reaction product to reach the oxide–gas interface. Growth proceeds until the metal supply is exhausted or until the reaction front is stopped by an inhibitor barrier coating. The final reaction product is an interconnected oxide network with metal-filled interstices. Further, the growth kinetics are accelerated by placing filler materials (e.g. particles, whiskers, or fibers) in the path of the reaction front. In this case, a ceramic preform is continuously infiltrated by a molten alloy that undergoes an oxidation reaction. The high-temperature reaction of the molten alloy in the interstices of the ceramic preform produces a matrix material consisting of a mixture of ceramic oxides and unreacted metal alloy. The growth of the oxide occurs continuously away from the initial

molten-alloy–ceramic-preform interface, while fresh alloy is supplied to the gas–metal reaction interface by fine microscopic channels through the oxide product. The final composite consists of the ceramic preform in an interconnected matrix (ceramic reaction product and residual metal alloy).

2.1.9. Rapid solidification processing (RSP)

This processing route combines traditional IM and a rapid solidification technique to produce in situ MMCs. For example, rapid solidification processing (RSP) of Ti–B or Ti–Si alloys accompanied by large undercoolings and high cooling rates has been shown to be very effective in producing in situ Ti-based composites containing large volume fractions of reinforcing particles [94]. These particles are formed in situ in Ti–B or Ti–Si alloys either upon solidification, or subsequently by the controlled decomposition of the resulting supersaturated solid solutions. In the preparation of in situ Ti-based composites via the RSP route, rapidly solidified powders of Ti alloys containing B or Si are initially produced by the plasma arc melting/centrifugal atomization (PAMCA) technique [95]. Powders of 1 kg are packed inside the extrusion cans, vacuum-outgassed and sealed. The cans are then subjected to hot extrusion at 1338 K. Needle-like TiB whiskers with a length of $\sim$4 μm and aspect ratios between 5 and 10, and $TiSi_2$ particles with a size of $\sim$1 μm, are generated in situ [96–98].

More recently, the RSP route has been used by Tong and coworkers [99–102] to fabricate in situ TiC particulate reinforced Al-based composites. In their work, master material ingots were prepared by melting a mixture of Al, Ti and graphite powder in a graphite-lined induction furnace under an argon atmosphere, followed by direct chill cast. Rapidly solidified samples were prepared in a ribbon form by chill block melt spinning. These resultant ribbons were further milled into powders (100–250 μm), subsequently canned and degassed and then extruded into rods of 12 mm diameter. In situ formed TiC particles of 40–80 nm were reported to be distributed uniformly in the aluminum matrix with a grain size of 0.3–0.85 μm [102]. One main advantage of RSP is its ability to produce alloy compositions not obtainable by conventional processing methods. Furthermore, RSP materials have excellent compositional homogeneity, small grain sizes, and homogeneously distributed fine precipitates or dispersoids.

2.1.10. Reactive squeeze casting (RSC)

Reactive squeeze casting (RSC) was first adopted by Fukunaga et al. to fabricate in situ Al_2O_3 particles reinforced intermetallic compound matrix composites [103]. In their study, anatase TiO_2 whiskers or powders were first shaped to a preform and placed inside a preheated metal die. Molten aluminum was then poured into the die and squeezed into the preform at a relatively low speed. In this case, α-Al_2O_3, Al_3Ti and TiAl were generated in situ through the reaction between TiO_2 and liquid Al. However, they reported that it is rather difficult to make intermetallic composites of uniform and fine structure through a simple combination of TiO_2 and Al by means of RSC.

Recently, Pan [104] and Pan et al. [105] reported the fabrication of Al-based composites reinforced with hard phase α-Al_2O_3 and Al_3Ti by means of the RSC route. They showed that the reaction is too drastic to control. Furthermore, the metallographical structure of the composites so prepared is heterogeneous owing to the volume shrinkage during the reaction. Alternatively, macroscopically non-reacted TiO_2/Al composites can be prepared by squeeze casting at a relatively lower temperature. The in situ formation of Al_2O_3 and Al_3Ti can be achieved by heat-treating the TiO_2–Al bulk materials at 1073 K [105–107]. In this way, dense (Al_2O_3 + Al_3Ti)/Al composite with an uniform microstructure can be produced.

2.2. Vapor–liquid–solid (VLS) reaction process

Koczak and Kumar [108] have developed a patented vapor–liquid–solid (VSL) reaction processing technique. In the process, Al–Ti alloy is melted under vacuum, and subsequently, the chamber is back-filled with purified argon gas, which is also the carrier gas. Upon reaching the appropriate processing temperature, clean carbon-bearing gas, typically, a mixture of argon and CH_4 gas, is bubbled through the Al–Ti melt via a gas diffusion system. It is suggested that the carbon released from the injected gas reacts with Ti in the melt to form TiC [109,110]. The reaction is carried out at a constant temperature for an appropriate length of time to ensure complete conversion of the titanium in the melt to TiC. After completion of the reaction, the melt is allowed to solidify. The processing time and temperature depend on the gas partial pressure and the alloy chemistry. The processing time can range from 20 min to 2 h and the processing temperature varies between 1473 and 1573 K. Using this processing technique, Al–4.5 wt.% Cu and 2519Al alloy composites, reinforced with TiC particulates of size 0.1–3 μm were successfully fabricated [109–112].

Although the TiC/Al system has been the most extensively studied one, AlN/Al, TiN/Al, SiC/Al–Si, TiC/Cu, TiC/Ni, as well as HfC/Al, TaC/Al, and NbC/Al composites have also been processed successfully [113]. Recently, Chu et al. [114] fabricated Al–Mg alloy composite reinforced with in situ AlN particulates and TiN whiskers by using the gas–liquid reaction method under an intensive electromagnetic mixing. This method is similar to the VLS reaction processing technique. First of all, Al–4.5Mg–6.2Ti (in wt.%) parent alloy was melted in an induction furnace, and subsequently, the chamber was back-filled with purified argon. Upon reaching an appropriate processing temperature, clean N_2 gas was introduced into the Al alloy melt. Chu et al. [114] suggested that Ti atoms in the Al liquid react with the N atoms to form TiN crystal nuclei, i.e.

$$2Ti + N_2 \rightarrow 2TiN \quad \text{(R12)}$$

This reaction is an intensive exothermic reaction [115] and the reaction heat results in an increase in the temperature of the melt. In order to hold at a constant melt temperature, the power of the furnace should be reduced, leading to a weakening of electromagnetic mixing. Thus, TiN crystal nuclei can easily grow into a whisker with typically a mean diameter of 0.5 μm and a mean aspect ratio of 5.8–7.5 [114]. During TiN formation, the reaction between N_2 and Al also proceeds as follows:

$$2Al + N_2 \rightarrow 2AlN \quad \text{(R13)}$$

The in situ formed AlN particulates usually have a size of about 2–5 μm.

2.3. Solid–solid reaction process

2.3.1. Mechanical alloying (MA)

Mechanical alloying (MA) is a solid state powder processing method which involves repeated cold drawing and fracture of particles as a result of the high energy ball–sample collisions. This method can be used to produce fine-grained alloyed powder particles in metal–metal and metal–ceramic systems [116–120]. In situ formation of Al_4C_3 was first introduced by Jangg [121,122] as result of the development of alloy glass by Koch et al. [123]. The Al_4C_3 particles are formed via MA of Al with C and subsequent annealing of as-milled mixture powders. After annealing of as-milled powder mixtures at 873 K, Al_4C_3 particles with a length of 0.1–0.3 μm and a diameter of 0.02–0.03 μm were formed in situ [124].

In recent years, the MA technique has been extensively used to fabricate in situ ceramic particle reinforced MMCs. Ma et al. [125] have fabricated in situ Al_4C_3 dispersoid and SiC particulate mixture-reinforced Al composites via the MA process. In this process C, Al, and SiC powder mixture is subjected to ball milling. The as-milled powder mixture is then annealed at 873 K. Finally, the as-annealed powder compact is extruded into rods at 673 K.

Biselli et al. [22] have fabricated the in situ TiB_2 particle reinforced copper composites by means of mechanical milling techniques, followed by suitable heat treatments. They reported that the reaction between Ti and B does not occur during milling, but instead takes place during annealing for short time periods at temperatures of 873–1073 K.

Recently, Lu et al. [126] investigated the possibility of forming in situ TiB_2 particulate via the MA of elemental Ti and B powders in a system diluted with Al. They reported that a low volume concentration of TiB_2 phase is formed in situ after an extensive period of milling (>40 h). However, there is no evidence for the formation of the Al_3Ti phase. This is due to the fact that the enthalpy for the formation of TiB_2 (−323.6 kJ/mol) at room temperature is significantly lower than that of Al_3Ti (−75.3 kJ/mol). Annealing treatment of as-milled powder at 723 K can, however, lead to the formation of the Al_3Ti phase. At a higher annealing temperature of 873 K, the content of reinforcing TiB_2 phase tends to increase, while that of the Al_3Ti phase is reduced significantly. Lu et al. [126] suggested that three stages of solid reaction are responsible for the formation of in situ TiB_2 particles. In the first stage, Ti and B are homogeneously distributed in the Al matrix as a solid solution and only a very small amount of TiB_2 is formed. At the second stage, Al_3Ti precipitates from the Al matrix during the annealing process at about 723 K. At the third stage, Al_3Ti decomposes at 873 K and Ti decomposed from Al_3Ti reacts with fine B to form the TiB_2 phase.

2.3.2. Reactive hot pressing (RHP)

Reactive hot pressing (RHP) refers to a process in which ceramic reinforcement is in situ formed through chemical reaction between elements or between element and compound during hot pressing of mixture powders. Lu et al. [127] have prepared in situ TiB whisker reinforced Ti–6Al–4V composites by means of RHP. The powder mixtures of Ti, Al–V master alloy, and TiB_2 are initially hot pressed at 1473 K in a vacuum. The as-pressed billets are then subjected to hot extrusion at 1323 K. They reported that TiB whiskers with a diameter of 0.1–3.5 μm and an aspect ratio of 10–20 are in situ generated through the reaction between Ti and TiB_2. Thus, TiB whisker reinforced Ti matrix composite with a good TiB/Ti interfacial bonding can be produced by the RHP route [127,128].

Similarly, Wang et al. have fabricated Ti–6Al–2Sn–4Zr–2Mo alloy matrix composites, reinforced with various volume fractions of TiB particles, by means of the RHP route [129]. Recently, Sahay et al. have also prepared TiB/Ti composites containing high volume contents of TiB whiskers (30–92%) [130]. They reported that TiB is the predominant phase for the composites containing less than 86% volume content of reinforcing particles. In the case of TiB/Ti composites with TiB above 86%, a significant amount of TiB_2 phase remains.

More recently, Ma et al. [131] have examined the possibility of producing in situ TiB particle reinforced Ti composites by means of the RHP route from four different systems, i.e. Ti–B, Ti–TiB_2, Ti–B_4C, and Ti–BN. The compositions of the composites are listed in Table 4. The powders from these systems are first blended thoroughly and then cold compacted. The compacted green billets are degassed in a vacuum and hot pressed at 1523 K for 1 h. The as-pressed billets of 75 mm diameter and 80 mm height are extruded into rods at 1373 K at an extrusion ratio of 20:1. XRD analyses indicate that the TiB phase is generated in the systems investigated (Fig. 4). Furthermore, the TiC phase is also detected in the Ti–B_4C system. It is noted that a certain amount of TiB_2 remains in the

Table 4
Nominal content of generated phases (vol.%) in in situ Ti-based composites by assuming in situ reactions take place completely in all systems [131]

System	TiB	TiC
Ti–B	15	–
Ti–TiB_2	15	–
Ti–B_4C	12.1	2.9
Ti–BN	11.8	–

Ti–TiB_2 system, indicating an incomplete conversion of TiB_2 to TiB. Finally, no titanium nitrides are detected in the Ti–BN system.

2.3.3. Isothermal heat treatment (IHT)

Satyaprasad et al. [132] have studied the reaction strengthening of the PM TiCp/Al composites by isothermal heat treatment. They indicated that isothermal heat treatment at 873 K results in the reaction between TiC and the aluminum matrix:

$$13Al + 3TiC \rightarrow 3Al_3Ti + Al_4C_3 \quad \text{(R14)}$$

thereby yielding Al_3Ti and Al_4C_3 particles. The in situ formation of Al_3Ti and Al_4C_3 leads to obvious increases in strength and modulus of the composites. Further, Mitra et al. [133] investigated the effect of isothermal heat treatment on the XD-processed TiCp/Al composites. The heat treatment at 913 K results in the emergence of large particles with high aspect ratios and an increase in the volume fraction of the dispersed phases. This implies that stable reaction products Al_3Ti and Al_4C_3 are generated, due to the reaction between TiC and Al during heat treatment.

2.4. Liquid–liquid reaction process

This technique was developed by Sutek Corporation and termed the Mixalloy Process [134]. The process involves the reaction between two metal streams to form refractory particles. Two or more high-speed, turbulent, molten-metal streams containing components of a high- temperature (ceramic) phase, for example Cu–Ti and Cu–B, are made to impinge upon one another in a mixing

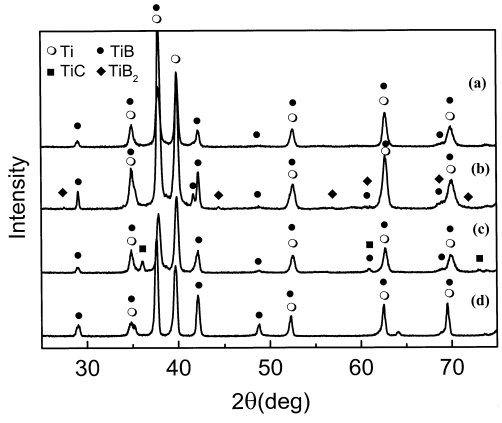

Fig. 4. X-ray diffraction patterns of in situ Ti-based composites fabricated from (a) Ti–B system; (b) Ti–TiB_2 system; (c) Ti–B_4C system and (d) Ti–BN system [131].

chamber, resulting in intimate mixing and reaction to produce the second phase. The resulting mixture can then be cast in a mold or rapidly solidified via melt spinning or atomization. This technology is effective in producing copper matrix composites reinforced with nanoscale TiB_2 particulates (50 nm) for the electrical applications [135].

3. Thermodynamics of in situ reaction

During the past decade, a great variety of processing techniques have been developed to fabricate in situ MMCs. A number of reactive systems have been adopted by various researchers. Furthermore, the thermodynamical feasibility of the in situ reactions involved in fabricating in situ composites has been considered by a number of researchers [65,66,109,136–138]. In the following text, the thermodynamics of in situ reactions for some typical and important reactive systems, i.e. Al–Ti–C, Al–Ti–B, Ti–C, Ti–B_4C, and Ti–TiB_2, is reviewed.

3.1. Al–Ti–C system

Al–Ti–C is one of the reactive systems widely used for fabricating in situ MMCs. In situ TiC/Al composites have been fabricated using this system by means of various processing routes [43,44,51–55,70–75,99–102,108–113]. In a multicomponent system such as Al–Ti–C, it is possible that a variety of compounds can be formed, depending on the prevailing conditions. TiC, Al_4C_3, and Al_3Ti can all be generated during the in situ reaction. In fabricating in situ TiC/Al composites through the VLS route, Sahoo and Koczak [109] have calculated the free-energy change, ΔG, for TiC and Al_4C_3 formation. They reported that the changes in free energy for TiC and Al_4C_3 formation are negative, indicating that the reactions can proceed spontaneously. In general, the more negative the standard free energy change of formation, the more stable the carbide is. They show that titanium is a very strong carbide former relative to Al_4C_3.

In a liquid aluminum solution containing Ti and C as dilute solutes, Rapp and Zheng [136] suggested the following possible reactions and their accompanying free-energy changes:

$$\underline{\mathrm{Ti}} + \mathrm{C(s)} \rightarrow \mathrm{TiC(s)} \tag{R15}$$

$$\Delta G_1\ (\mathrm{J\,mol^{-1}}) = -91951 + 34.377T + 0.460 \times 10^{-3}T^2 + \frac{3.096 \times 10^5}{T} - 0.962T \ln T \tag{E1}$$

$$\underline{\mathrm{Ti}} + \underline{\mathrm{C}} \rightarrow \mathrm{TiC(s)} \tag{R16}$$

$$\Delta G_2\ (\mathrm{J\,mol^{-1}}) = -163382 + 80.347T + 0.460 \times 10^{-3}T^2 + \frac{3.096 \times 10^5}{T} - 0.962T \ln T \tag{E2}$$

$$\tfrac{4}{3}\mathrm{Al(l)} + \mathrm{C(s)} \rightarrow \tfrac{1}{3}\mathrm{Al_4C_3(s)} \tag{R17}$$

$$\Delta G_3\ (\mathrm{J\,mol^{-1}}) = -89.611 + 32.841T \tag{E3}$$

$$\tfrac{4}{3}\mathrm{Al(l)} + \underline{\mathrm{C}} \rightarrow \tfrac{1}{3}\mathrm{Al_4C_3(s)} \tag{R18}$$

$$\Delta G_4\ (\mathrm{J\,mol^{-1}}) = -161042 + 78.811T \tag{E4}$$

where $\underline{\mathrm{Ti}}$ and $\underline{\mathrm{C}}$ are dilute solutes in the liquid aluminum solution. The change of free-energy against temperature for Reactions (R15) and (R17) is shown in Fig. 5. This figure reveals that the formation

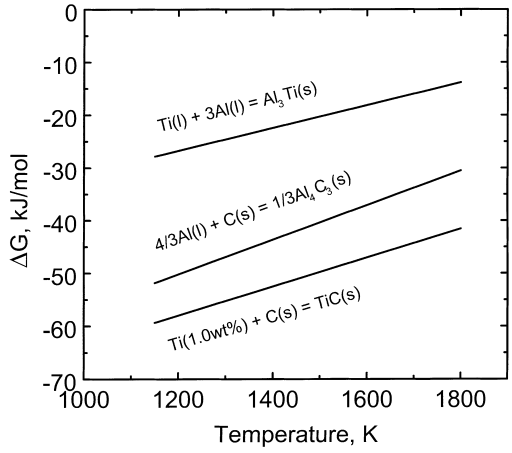

Fig. 5. Change of Gibbs free energy ΔG as a temperature for TiC, Al_4C_3 and Al_3Ti formation (reprinted from R.A. Rapp, X. Zheng, Thermodynamic consideration of grain refinement of aluminum alloys by titanium and carbon, Metallurgical Transaction A 22A (1991) 3074, with permission from TMS and ASM [136]).

of TiC is more favorable than that of Al_4C_3. Furthermore, Rapp and Zheng [136] reported that the standard Gibbs energy of formation of Al_3Ti in liquid aluminum can be considered as

$$\mathrm{Ti(l)} + 3\mathrm{Al(l)} \rightarrow \mathrm{Al_3Ti(s)} \tag{R19}$$

$$\Delta G_5\,(\mathrm{J\,mol^{-1}}) = -52503 + 21.483T \tag{E5}$$

The change in free energy for the formation of Al_3Ti with temperature is also plotted in Fig. 5. Although the free-energy change of Reaction (R19) is negative in the temperature range investigated, TiC is more stable than Al_3Ti in the Al–Ti–C system.

Nukami and Flemings [137] have investigated the in situ reactions for synthesizing TiC particulates reinforced Al composite by heating the infiltrated Ti–Al–C preform with liquid aluminum. On the basis of the differential thermal analysis (DTA) and XRD analyses, they suggested that the following reactions can take place during heating:

$$\mathrm{Ti(s)} + 3\mathrm{Al(s)} \rightarrow \mathrm{Al_3Ti(s)} \tag{R20}$$

$$\mathrm{Al(s)} \rightarrow \mathrm{Al(l)} \tag{R21}$$

$$\mathrm{Ti(s)} + 3\mathrm{Al(l)} \rightarrow \mathrm{Al_3Ti(s)} \tag{R22}$$

$$3\mathrm{Al_3Ti(s)} + \mathrm{Al_4C_3(s)} \rightarrow 3\mathrm{TiC(s)} + 13\mathrm{Al(l)} \tag{R23}$$

$$\mathrm{Al_3Ti(s)} + \mathrm{C(s)} \rightarrow \mathrm{TiC(s)} + 3\mathrm{Al(l)} \tag{R24}$$

Nukami and Flemings [137] calculated both ΔH and ΔG for Reactions (R23) and (R24) using data from [139]. These are plotted in Figs. 6 and 7 as a function of temperature. From Fig. 6, both ΔH and ΔG for Reaction (R23) are positive up to about 1050 K; above this temperature, ΔG becomes negative, which permits the reaction to proceed endothermically at higher temperatures. By contrast, Fig. 7 reveals that both ΔH and ΔG for Reaction (R24) are negative at all temperatures. Hence, this reaction can occur with heat evolution at any temperature.

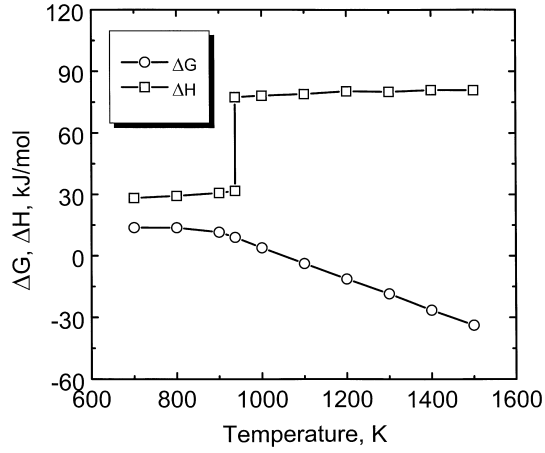

Fig. 6. Thermodynamic data as a function of temperature for the reaction $3Al_3Ti(s) + Al_4C_3(s) \rightarrow 3TiC(s) + 13Al(l)$ (reprinted from T. Nukami, M.C. Flemings, In situ synthesis of TiC particle-reinforced aluminum matrix composites, Metallurgical and Materials Transaction A 26A (1995) 1881, with permission from TMS and ASM [137]).

3.2. Al–Ti–B system

In situ TiB_2/Al composites have been fabricated by several researchers using an Al–Ti–B system by means of various processing routes [44,48,56,57]. In an investigation of TiB_2/Al composite fabrication by means of the DRS process, Yang et al. [138] suggested that the following chemical reactions may take place:

$$Al + 2B \rightarrow AlB_2 \quad \text{(R25)}$$

$$3Al + Ti \rightarrow Al_3Ti \quad \text{(R26)}$$

$$Al_3Ti + 2B \rightarrow TiB_2 + 3Al \quad \text{(R27)}$$

$$Ti + 2B \rightarrow TiB_2 \quad \text{(R28)}$$

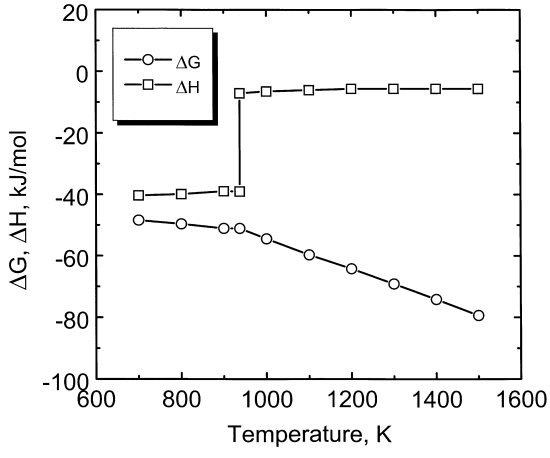

Fig. 7. Thermodynamic data as a function of temperature for the reaction $3Al_3Ti(s) + C(s) \rightarrow TiC(s) + 3Al(l)$ (reprinted from T. Nukami, M.C. Flemings, In situ synthesis of TiC particle-reinforced aluminum matrix composites, Metallurgical and Materials Transaction A 26A (1995) 1882, with permission from TMS and ASM [137]).

Yang et al. [138] calculated the Gibbs free energy, ΔG, for Reactions (R25)–(R28) according to [139]. They reported that the ΔG for Reaction (R28) is much less than that for Reaction (R25), indicating that TiB_2 forms preferentially to AlB_2 throughout the temperature range. Furthermore, the Al_3Ti phase is unstable in the system and will react further with B to form TiB_2, according to Reaction (R27).

3.3. Ti–C system

In situ TiC reinforced Ti matrix composites have been fabricated from Ti and C by means of the CAC route [62,63,65]. Lu et al. [65] calculated the reaction formation enthalpy, ΔH, and Gibbs free energy, ΔG, for the reaction between Ti and C according to [140]. They show that, when the temperature is lower than 1939 K,

$$\Delta H_1 = -184571.8 + 5.042T - 2.425 \times 10^{-3}T^2 - \frac{1.958 \times 10^6}{T} \quad \text{(E6)}$$

$$\Delta G_6\,(\mathrm{J\,mol^{-1}}) = -184571.8 + 41.382T + 2.425 \times 10^{-3}T^2 - \frac{9.79 \times 10^5}{T} - 5.042T \ln T \quad \text{(E7)}$$

and when the temperature is higher than 1939 K,

$$\Delta H_2 = -160311.5 - 24.79T + 2.732 \times 10^{-3}T^2 - \frac{1.862 \times 10^6}{T} \quad \text{(E8)}$$

$$\Delta G_7\,(\mathrm{J\,mol^{-1}}) = -160311.5 - 186.97T - 2.732 \times 10^{-3}T^2 - \frac{9.31 \times 10^5}{T} + 24.79T \ln T \quad \text{(E9)}$$

The variations of ΔH and ΔG with temperature are plotted in this study. ΔG is negative for the temperature ranges investigated, indicating that the reaction for the formation of TiC is feasible thermodynamically. Moreover, the ΔH values are very large, indicating that a high quantity of heat will be released during the reaction.

3.4. Ti–B_4C system

TiB and TiC mixture-reinforced Ti matrix composites were fabricated by Ranganath et al. [21] and Zhang et al. [66] by means of the CAC route, and recently by Ma et al. [131] by means of the RHP route. For the B_4C–Ti system, a chemical reaction between B_4C and Ti may take place as follows:

$$5\mathrm{Ti} + \mathrm{B_4C} \rightarrow 4\mathrm{TiB} + \mathrm{TiC} \quad \text{(R2)}$$

$$3\mathrm{Ti} + \mathrm{B_4C} \rightarrow 2\mathrm{TiB_2} + \mathrm{TiC} \quad \text{(R29)}$$

The reaction formation enthalpy, ΔH, and Gibbs free energy, ΔG, for Reactions (R2) and (R29) have been calculated by Zhang et al. [66] using thermodynamic data from [140]. These results are shown in Figs. 8 and 9, respectively. From Fig. 8, the ΔG of Reaction (R2) is less than that of Reaction (R29). This indicates that Reaction (R2) is more likely to take place viz. TiB forms in preference to TiB_2 throughout the temperature range of 1200–2200 K. Moreover, the reaction formation enthalpy, ΔH, of the two reactions are all very large, indicating that considerable amounts of heat will be released during reactions.

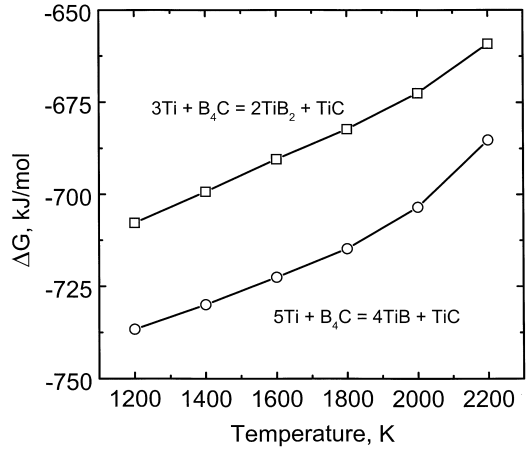

Fig. 8. Change of Gibbs free energy ΔG as a temperature for the reactions $5Ti + B_4C \rightarrow 4TiB + TiC$ and $3Ti + B_4C \rightarrow 2TiB_2 + TiC$, respectively (reprinted from X. Zhang et al., In situ technique for synthesizing (TiB + TiC)/Ti composites, Scripta Materialia 41 (1999) 40, with permission from Elsevier [66]).

3.5. *Ti–TiB_2 system*

The Ti–TiB_2 system was first adopted by Lu et al. [127], and more recently by Wang et al. [129], Sahay et al. [130] and Ma et al. [131], to fabricate in situ TiB whisker reinforced titanium matrix composites. According to thermodynamic calculation [66], TiB_2 is not stable when an excess of titanium exists in the Ti–TiB_2 system and can be converted to TiB, according to following reaction:

$$TiB_2 + Ti \rightarrow 2TiB \quad \text{(R30)}$$

The reaction formation enthalpy, ΔH, and Gibbs free energy, ΔG, for Reaction (R30) versus temperature is shown in Fig. 10. Apparently, Reaction (R30) can occur due to a negative free-energy change. Moreover, ΔH is also negative, indicating that the reaction is exothermic, making it favored to occur.

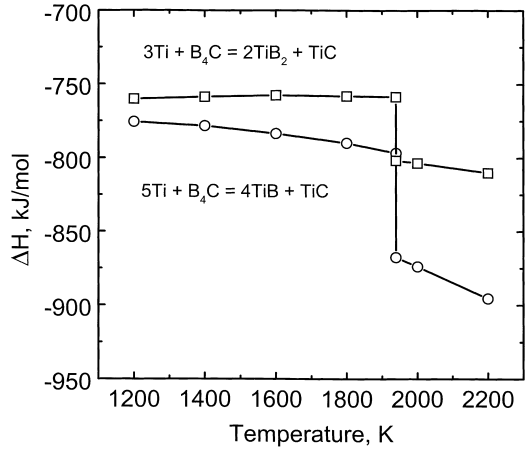

Fig. 9. Change of formation enthalpy ΔH as a temperature for the reactions $5Ti + B_4C \rightarrow 4TiB + TiC$ and $3Ti + B_4C \rightarrow 2TiB_2 + TiC$, respectively (reprinted from X. Zhang et al., In situ technique for synthesizing (TiB + TiC)/Ti composites, Scripta Materialia 41 (1999) 40, with permission from Elsevier [66]).

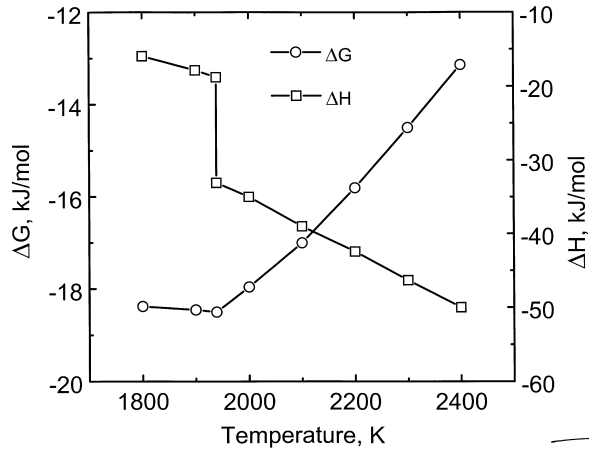

Fig. 10. Change of Gibbs free energy ΔG and formation enthalpy ΔH as a temperature for the reaction $TiB_2 + Ti \rightarrow 2TiB$ (reprinted from X. Zhang et al., In situ technique for synthesizing (TiB + TiC)/Ti composites, Scripta Materialia 41 (1999) 43, with permission from Elsevier [66]).

4. Formation mechanism of in situ ceramic phases

4.1. Solution–precipitation

4.1.1. Al–Ti–C system

In a saturated metal solution such as carbon (or boron)- and titanium-saturated aluminum melt, it is very likely that the formation of TiC or TiB_2 is achieved via a mechanism of multiple nucleation and growth in situ of TiC or TiB_2 phase from the aluminum melt.

Chu and Premkumar [141] analyzed a mixture of Al–6 wt.% Ti alloy powders and high-purity graphite powders with an arbitrary weight ratio of 1:1 using DTA. They reported that an exothermal reaction associated with the formation of TiC appears at 1533 K. The microstructure of the DTA sample reveals several important aspects. Firstly, all the TiC particles within the matrix are significantly finer than the original graphite particles used in the mixture. Secondly, neither unreacted cores nor surface reaction zones are observed in the carbon in contact with the metal droplets. Thirdly, the fine TiC particles are not only round in shape but also relatively uniform in size. On the basis of these observations, Chu and Premkumar [141] suggested that the formation of TiC is achieved via a mechanism of multiple nucleation and growth in situ of TiC from the carbon-saturated Al–Ti melt during isothermal holding [141], i.e. a solution–precipitation mechanism. The fine submicron-size carbides, with a narrow size distribution, indicate that nucleation is easier than growth. Nucleation would require the dissolution and rapid diffusion of carbon from the large graphite flakes into the melt. Diffusion of C in molten aluminum is sufficiently fast for nucleation of TiC, even though the solubility of C in Al at the processing temperature (1533 K) is of the order of 0.35 wt.% [142]. On the other hand, diffusivity of Ti at the processing temperature is lower than that of carbon, and thus, the growth of TiC would be determined by the diffusion of Ti.

Zhang et al. [72] have carried out DSC analyses for Al–Ti and Al–Ti–C compacts at a rate of 20 K/min under an argon atmosphere. For the Al–Ti system, exothermic peaks near 973 and 1023 K are detected, indicating that exothermic reactions between Al and Ti take place. For the Al–Ti–C system, another exothermic reaction peak is detected at 1144 K. This reaction corresponds to the synthesis reaction of TiC. Furthermore, Zhang et al. [72] conducted a series of quenching

experiments, in which Al–Ti–C compacts with a 50–60% of theoretical density are heated to the preset temperatures at a fast rate and then water quenched immediately. XRD analyses on the quenched specimens indicate that, at 943 K, in addition to Al, Ti and C diffraction peaks, Al_3Ti peaks are detected, indicating the occurrence of the reaction between Ti and Al at this temperature. When the temperature of the compact is increased up to 1043 K, TiC diffraction peaks appear and no evidence of residual Ti is found, indicating that, at this temperature, both the reaction between Al and Ti and the synthesis reaction of TiC take place. With further increase in temperature, the diffraction intensity of the TiC peak increases rapidly, whereas the intensity of Al_3Ti decreases markedly. At 1773 K, only TiC and Al phases are observed.

More recently, the kinetic process of the reaction synthesis of TiC has been further investigated by Zhang et al. [74]. In their study, Al–Ti–C compact with a 50–60% theoretical density is put on a platen and ignited at the top by an ignition heater (electric resistant). When the reaction propagates to the middle of the compact, the compact is quenched immediately. The quenched sample consists of three parts with quite separate microstructural characteristics, i.e. an unreacted region, a reaction region, and a product region. XRD analyses reveal that, in the unreacted region, only diffraction peaks of Al, Ti and C occur; no new phase is found. In the reaction region, Al_3Ti and TiC phases are detected, indicating that some reactions have taken place. In the product region, the diffraction peaks of Ti, C and Al_3Ti disappear. TiC is the only phase in situ formed.

Zhang et al. [74] divided the unreacted region into three subregions — original subregion, preheating subregion, and melting subregion. SEM examinations reveal that, in the original subregion and the preheating subregion, there is no change in the microstructure and morphology of the powders. In the melting subregion, the Al powder begins to partly melt. As a result, the graphite and titanium powders are surrounded by the aluminum melt. However, the morphology of the graphite and the titanium powders does not change. In the reaction region, near the melting subregion, a spherical Al_3Ti phase is found around or near the titanium powders. In the center of the reaction region, the graphite powders are surrounded by a Ti-rich layer. In the microstructure of the reaction region near the product region, there exist many fine spherical-shaped TiC particles around the graphite powders. Finally, the product region is characterized by TiC particles with a small size and smooth surface.

Based on the above experimental results [72,74], Zhang et al. [74] suggested that the micromechanism of reaction synthesis of TiC is a solution–precipitation mechanism. Accordingly, they divided the whole process of synthesizing TiC into four stages — a heating and melting stage, an initial reaction stage, a complete reaction stage, and a cooling stage [74]. Further, they established a mathematical kinetic model to express the reaction rate of in situ synthesizing TiC [75]. The model reveals that an increase in temperature and decreases in the aluminum content of the compact and the thickness of the Ti-rich layer, as well as the size of carbon particle, can accelerate the reaction rate, thereby resulting in a reduction of reaction time. They reported that the experimental results are in good agreement with the numerical calculated ones.

4.1.2. Al–Ti–B system

Compared to the Al–Ti–C system, investigations on the Al–Ti–B system are limited. Although the Al–Ti–B system has been adopted to fabricate in situ TiB_2 particle reinforced Al-based composites by several researchers [44,48,56,57], existing studies [143–147] agree that there is a lack of understanding of the reaction mechanisms, which hinders the optimization of the process and the TiB_2/Al product.

In an investigation of in situ TiB_2/Al composite fabrication, Kuruvilla et al. [48] suggested a possible mechanism for the TiB_2 formation which involves the solution of Ti and B in liquid

aluminum, and a solvent-assisted reaction, leading to the in situ formation of micron-size TiB_2 particles. On the basis of microstructural characterization showing that the whole population of considerably fine-scale (~0.1 μm) in situ particles are homogeneously distributed in the Al matrix of the SHS-processed TiB_2/Al composite, Gotman et al. [44] suggested that these fine in situ particles are not formed by an interfacial reaction between boron and titanium, but rather than by precipitation from the solution.

Recently, the reaction mechanisms and phase formation sequence of the reactive sintering of elemental powder Al, Ti and B were investigated by Brinkman et al. [148]. On the basis of DSC and XRD studies on the reactive sintering of the Al–40 vol.% (Ti + 2B) and Al–2B systems, they identified AlB_2 and Al_3Ti as transient phases during the reactive sintering of the Al–Ti–B system. Further, it is shown that the AlB_2 phase is formed prior to the Al_3Ti phase. Moreover, if there is no unreacted Al left after the formation of two intermediate phases AlB_2 and Al_3Ti, the formation reaction of TiB_2 does not proceed until the decomposition of the AlB_2 phase into a thermodynamically more stable AlB_{12} phase with an Al liquid phase containing a small amount of B in solution. This newly formed liquid phase enables the reaction between Ti and B in solution to form TiB_2. These results definitely indicate that the formation of TiB_2 is assisted by the aluminum solvent via a solution–precipitation mechanism [148].

Brinkman et al. [149] further investigated the effect of matrix alloying elements on the reactive synthesis of in situ TiB_2/Al composites. They reported that the alloying elements do not exert a significant effect on the reaction mechanism and phase formation sequence in the Al–Ti–B system. However, the presence of Cu leads to an increase in the reaction rate during the formation of intermediate reaction products leading to a more complete conversion of the intermediate Al_3Ti in the final composite products.

However, it should be pointed out that Brinkman et al. [148] do not show how the intermediate Al_3Ti phase transforms during the reactive process, nor how the AlB_{12} phase disappears in the final composite product. Further study is needed to elucidate the exact reaction mechanism of the Al–Ti–B system.

4.1.3. Ti–C (Ti–B_4C) system

During the processing of the titanium matrix composite by means of the CAC route, the temperature of the melt is so high that the TiC and TiB reinforcements synthesized by SHS undergo disintegration and dissolution. When the melt is solidified, the TiC or TiB tends to precipitate from the Ti melt by means of nucleation and growth. Thus, the size and morphology of the in situ reinforcements are controlled by the solidification paths. Lin et al. [62] have investigated the effect of cooling rate and aluminum addition on the morphology and size of in situ formed TiC reinforcements in a Ti matrix. They show that both aluminum addition and an increase in the cooling rate of the melt can result in refinement of the reinforcements.

4.2. Solid–liquid interface reaction

The solid–liquid interface reaction is considered to be another possible formation mechanism for in situ reinforcements [150]. In a multicomponent system such as Al–Ti–C, molten titanium surrounds the carbon powder precursor and reacts at its outer surface. The molten titanium then diffuses through the product TiC layer, and reacts with the unreacted portion of the carbon powder particles. As the reaction progresses, the diameter of the carbon powder decreases with time. In the outlying melt, the Ti concentration decreases and the product concentration increases with time.

Sahoo and Koczak [109] analyzed the in situ formation of TiC in aluminum alloys during the VLS reaction process. They suggest that nucleation of the TiC occurs via titanium diffusing into the carbon and precipitating out as a carbide via a solid–liquid chemical reaction. In the initial stage of the process, the rate-limiting feature is the supply of carbon in the carrier gas. Towards the latter part of the process, with titanium depletion, diffusion of titanium across the boundary layer is the rate-limiting step.

The in situ formation of TiC in aluminum alloys during the VLS reaction process has been further analyzed by Khatri and Koczak [151]. Based on their experimental observations, it is suggested that TiC formation occurs in several stages. Following CH_4 decomposition, solid amorphous carbon particles with a size of 40–50 nm are distributed and trapped in the alloy. The reaction to form TiC is limited at first by diffusion of titanium to carbon and thereafter by the carbide. During the in situ reaction, the first phase to form is aluminum carbide or aluminum–titanium carbide. Given sufficient time for completion, the reaction proceeds to form the most stable carbide, TiC.

Taheri-Nassaj et al. [85,86] fabricated in situ, boride reinforced, Al matrix composites by the RSI process. For a powder mixture of TiN and B, they suggest that the reaction can take place as follows [85]:

$$\mathrm{TiN} + 2\mathrm{B} + \mathrm{Al} \rightarrow \mathrm{TiB_2} + \mathrm{AlN} \tag{R31}$$

This reaction has a ΔH of -325 kJ at 1500 K, which makes it favorable. For the powder mixture of Ti and B_4C, Al_3Ti is formed first, followed by a reaction between Al_3Ti and B_4C [86]:

$$3\mathrm{Al_3Ti} + \mathrm{B_4C} \rightarrow 2\mathrm{TiB_2} + \mathrm{TiC} + 9\mathrm{Al} \tag{R32}$$

This reaction has a ΔH of -217.4 kJ/mol at 1300 K, making it favorable. Taheri-Nassaj et al. [85,86] suggest that infiltration in the system is driven by exothermic reactions between the starting powders and the melt. These reactions result in an increase in temperature in the infiltration fronts and a decrease in the interfacial tension of the Al melt in contact with solid particles. This will in turn enhance a reaction between the moving infiltration front and fresh reactants.

4.3. Combination mechanism of solid–liquid reaction and solution–precipitation

Tong and Fang [101] reported that the formation of TiC particles in liquid aluminum may be considered to occur according to both Reactions (R15) and (R16). According to [136], the solubility of Ti and C, in equilibrium with TiC in the liquid aluminum for Eqs. (E15) and (E16), are given, respectively, by

$$C_{\underline{\mathrm{Ti}}}\,(\mathrm{wt.\%}) = \exp\left(4.135 + 5.533 \times 10^{-5}T - \frac{1.106 \times 10^4}{T} + \frac{3.724 \times 10^4}{T^2} - 0.116 \ln T\right) \tag{E10}$$

$$C_{\underline{\mathrm{Ti}}}C_{\underline{\mathrm{C}}}\,(\mathrm{wt.\%}) = \exp\left(9.664 + 5.533 \times 10^{-5}T - \frac{1.965 \times 10^4}{T} + \frac{3.724 \times 10^4}{T^2} - 0.116 \ln T\right) \tag{E11}$$

Diagrammatic expressions of Reactions (R15) and (R16), Eqs. (E10) and (E11), are shown in Figs. 11 and 12. For temperatures up to 2100 K, the values of free-energy change, ΔG, for Reactions (R15) and (R16) are negative, indicating that TiC formation is thermodynamically viable. Tong and Fang

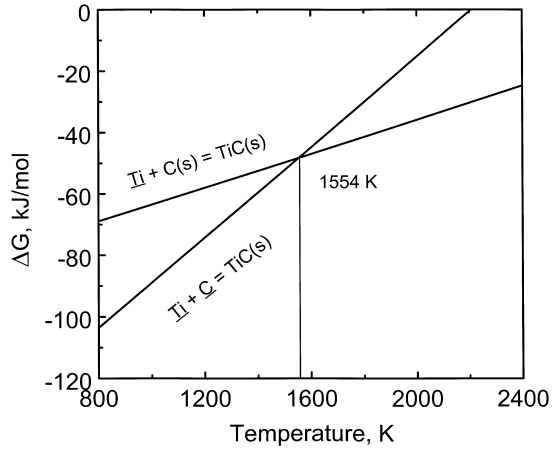

Fig. 11. Variation of standard free energy changes with temperature for $\underline{\mathrm{Ti}} + \mathrm{C(s)} \rightarrow \mathrm{TiC(s)}$ and $\underline{\mathrm{Ti}} + \underline{\mathrm{C}} \rightarrow \mathrm{TiC(s)}$ (reprinted from X.C. Tong, H.S. Fang, Al–TiC composites in situ-processed by ingot metallurgy and rapid solidification technology. Part I. Microstructural evolution, Metallurgical and Materials Transaction A 29A (1998) 884, with permission from TMS and ASM [101]).

[101] reported that there is an intersection at a temperature of 1554 K between the ΔG_1 and ΔG_2 plots and between the $C_{\underline{\mathrm{Ti}}}$ and the $C_{\underline{\mathrm{Ti}}}C_{\underline{\mathrm{C}}}$ curves. When the temperature is greater than 1554 K, $\Delta G_1 < \Delta G_2$ and $C_{\underline{\mathrm{Ti}}} < C_{\underline{\mathrm{Ti}}}C_{\underline{\mathrm{C}}}$, so that TiC formation via Reaction (R15) is more favorable. Otherwise, TiC formation via Reaction (R16) is favored. Tong and Fang [101] proposed that TiC formation may proceed via both Reactions (R15) and (R16) at the same time, provided the temperature is abound 1554 K and the following conditions are met:

$$C_{\mathrm{Ti}} > C_{\underline{\mathrm{Ti}}} \quad \text{for Reaction (R15)}$$

$$C_{\mathrm{Ti}}C_{\mathrm{C}} > C_{\underline{\mathrm{Ti}}}C_{\underline{\mathrm{C}}} \quad \text{for Reaction (R16)}$$

where C_{Ti} and C_{C} are solutes of Ti and C in the liquid aluminum.

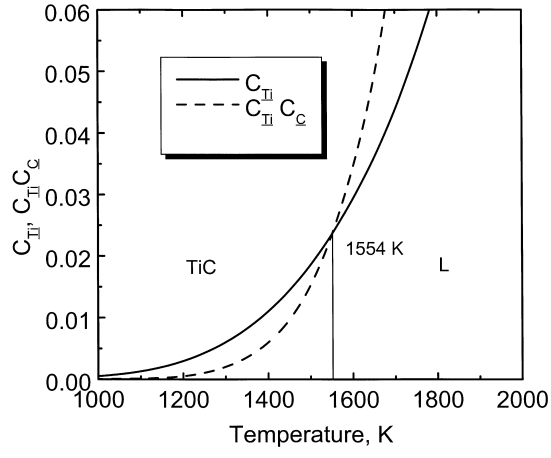

Fig. 12. Variation of Ti, C equilibrium solubility with TiC, $C_{\underline{\mathrm{Ti}}}(\underline{\mathrm{Ti}} + \mathrm{C(s)} \rightarrow \mathrm{TiC(s)})$, and $C_{\underline{\mathrm{Ti}}}C_{\underline{\mathrm{C}}}(\underline{\mathrm{Ti}} + \underline{\mathrm{C}} \rightarrow \mathrm{TiC(s)})$ with temperature (reprinted from X.C. Tong, H.S. Fang, Al–TiC composites in situ-processed by ingot metallurgy and rapid solidification technology. Part I. Microstructural evolution, Metallurgical and Materials Transaction A 29A (1998) 884, with permission from TMS and ASM [101]).

Tong and Fang [101] suggest that the synthesis of TiC in liquid aluminum at temperatures from 1373 to 1673 K is a complex process, which includes both solid–liquid reaction and solution–precipitation.

4.4. Solid–solid interfacial reaction in metal melt

In SHS processing of TiC/Al and TiB_2/Al composites from Ti–Al–C and Ti–Al–B systems, Gotman et al. [44] suggested that the solid–solid interfacial reactions are important mechanisms for ceramic reinforcement formation. These reactions should yield relatively coarse TiC and TiB_2 particles, comparable in size with the starting powder particles. They proposed that reinforcing TiC and TiB_2 particles of 1–2 μm size for SHS-processed TiC/Al and TiB_2/Al composites were formed via the solid–solid (or solid–liquid) interfacial reaction [44]. Further Gotman et al. [44] suggested that the combustion reactions are preceded by the melting of Al, followed by the capillary spreading of the molten Al along the solid Ti and carbon, boron or B_4C powder particles. This ensures intimate contact between Al and Ti, while there are only occasional points of contact between Ti and carbon, boron or B_4C. Upon heating, Al_3Ti is the first phase to be formed due to a direct reaction between Ti particles and molten Al. The Al_3Ti formed is solid and remains solid throughout the combustion process due to the fact that the T_m of Al_3Ti (1613 K) is higher than T_{exp} (Table 2). According to thermodynamic equilibrium, Al_3Ti should further react with carbon or boron to form a more thermodynamically stable TiC or TiB_2. Appreciable amounts of the Al_3Ti phase in the final products (for Al–Ti–B, Al–Ti–B_4C, and Al–Ti–C–B starting mixtures) show that, under the conditions of a propagating combustion wave, the dwell time of the material in the combustion zone is not long enough to achieve the equilibrium compositions.

Nukami and Flemings [137] investigated the reaction process of in situ synthesized, TiC particulate reinforced, Al composite. In their study, a powder mixture of titanium, carbon and aluminum was compacted into preform and infiltrated with molten aluminum. The infiltrated preform was subsequently heated in a differential thermal analyzer (DTA) to about 1573 K in an argon atmosphere. DTA scans revealed that three exothermic reactions occur, starting at about 890, 940, and 1155 K, respectively, and two endothermic reactions, which start at about 930 and 1150 K, respectively. Elements and compounds were determined at various temperatures by XRD and optical microscopic examination. Furthermore, Nukami and Flemings [137] examined the microstructures of the infiltrated preforms, heated to 891, 943, 1109, and 1306 K, using SEM. Based on these results, it is suggested that the first and second exothermic reactions are associated with the synthesis of Al_3Ti. The former is a reaction between solid titanium and solid aluminum, while the latter is a reaction between solid titanium and liquid aluminum. As the Al_3Ti coarsens with increasing synthesis temperature, TiC particles begin to form during the second endothermic reaction at about 1150 K. Al_4C_3 is first detected prior to the occurrence of the second endothermic reaction. Thus, the synthesis of TiC is related to the formation of Al_4C_3. The synthesis of TiC occurs at temperatures ranging from 1155 to 1260 K and is complete at about 1260 K.

From these results and analyses, Nukami and Flemings [137] propose that TiC is formed according to Reactions (R23) and (R24). As discussed in Section 3.1, both ΔH and ΔG values of Reaction (R24) are negative at all temperatures. Hence, this reaction can occur with heat evolution at any temperature. For Reaction (R23), both ΔH and ΔG are positive up to about 1050 K. Above this temperature, ΔG becomes negative, which permits the reaction to proceed endothermically at higher temperatures. In order to further confirm the validity of Reaction (R23), Nukami and Flemings [137] analyzed a preform made by mixing mechanically alloyed Al_3Ti and Al_4C_3 powders, using a DTA

apparatus. The DTA scan reveals an endothermic reaction that starts at 1150 K, which is very close to the temperature of Reaction (R23).

Recently, Feng and Froyen [152] investigated the reaction mechanism and phase formation sequence of reactive sintering of a Al–TiO_2–B system by heating the starting materials up to 1373 K at 10 K/min. They reported that Ti_2O_3, γ-Al_2O_3, and AlB_2 are the transitional phases during the reactive sintering process on the basis of XRD and DSC/DTA analyses. They suggest that TiB_2 is formed according to following two reactions:

$$Ti_2O_3(s) + 2AlB_2(s) \rightarrow 2TiB_2(s) + \alpha\text{-}Al_2O_3(s) \quad \text{(R33)}$$

$$3TiO_2(s) + 3AlB_2(s) + Al(l) \rightarrow 3TiB_2(s) + 2\alpha\text{-}Al_2O_3(s) \quad \text{(R34)}$$

This means that TiB_2 is formed via a solid–solid interfacial reaction mechanism. It is important to point out that the formation mechanism of in situ reinforcing phases, fabricated from powder mixtures, is dependent on the method used for preparing the green powder mixtures and on the type, size and morphology of the starting reactants. Feng and Froyen [152,153] have noticed the distinct difference between DSC scans of green compacts of Al, TiO_2 and B, which are mixed by different methods.

4.5. Solid diffusion reaction

In the MA process, powder particles are subjected to high-energy collisions in a ball mill that cause them to be cold-welded together and fractured apart [117–120]. Cold-welding and fracturing enable the powder particles to be always in contact with each other, with atomically clean surfaces and with minimized diffusion distance. Up to now, two kinds of reaction mechanism are widely accepted for MA: (a) the colliding balls cause severe plastic deformation in the powder particles, leading to flattened powder particles contact with clean surface, so that alloyed particles form through gradual diffusion of thin layers [118,154,155], and (b) alloys form through an SHS or self-sustained reaction within a short period of time after certain milling time, and with the liberation of large amounts of heat [156–160].

It was reported that, during the MA of an elemental powder mixture of titanium and graphite in a high-energy SPEX mill, the formation of TiC undergoes an abrupt, exothermic reaction, i.e. an SHS reaction [161]. However, Ye et al. [162] reported that different reaction mechanisms are responsible for the MA of $Ti_{50}C_{50}$ and $Ti_{33}B_{67}$ in a planetary ball mill. They showed that a gradual reaction occurs during the milling of $Ti_{50}C_{50}$, while a sustained reaction is obtained during the milling of $Ti_{33}B_{67}$ under the same conditions. The different formation mechanisms have been attributed to the different formation heat releases of TiC ($\Delta H_{TiC} = 184$ kl/mol) and TiB_2 ($\Delta H_{TiB_2} = 324$ kl/mol) [162]. Ye et al. [162] suggested that the impact energy generated in the planetary ball mill is not enough to self-sustain the reaction of $Ti_{50}C_{50}$. Thus, the formation of TiC is obtained by a gradual reaction. By contrast, the larger formation heat of TiB_2 (about 1.8 times as that of TiC) compensates for the insufficiency of impact energy, leading to the formation of TiB_2 via SHS for $Ti_{33}B_{67}$.

However, the SHS reaction cannot occur in a multicomponent system diluted by metal, such as in an Al–Ti–B system during the fabrication of MMCs via the MA route. This is due to a very low formation heat release in the process. Thus, the in situ reinforcement is formed via a gradual reaction during milling, or during the subsequent annealing at elevated temperature through interfacial diffusion. Lu et al. [126] reported that only a low volume concentration of the TiB_2 phase is generated, even after long durations of milling (>40 h). The complete conversion of TiB_2 is achieved

during elevated-temperature annealing because the diffusion rate of Ti and B atoms is significantly increased at elevated temperatures.

For fabricating in situ MMCs via RHP or isothermal treatment, the formation of in situ reinforcement is achieved via solid diffusion in a gradual way. Thus, higher synthesis temperatures and shorter diffusion distances contribute to speed up the in situ reaction [133].

5. Microstructural characteristics of in situ MMCs

5.1. Morphology, size and distribution of in situ reinforcements

5.1.1. Al-based composites

Compared to conventional ex situ composites, one of the advantages of the in situ MMCs is that finer reinforcing particles are distributed more uniformly in the metal matrix. Typically, fine in situ reinforcing particles with a size ranging from 0.1 to 3.0 μm are generated in an aluminum matrix by means of XD, SHS, RHP, FAS, DRS, and VLS processes [20,44,48,58–60,71–74,80,83,109–112]. Recently, Tong and coworkers [99–102] have shown that fine-scale dispersion of TiC particles with a size of 40–80 nm are formed in situ in RSP-processed TiC/Al composites. Furthermore, it is reported that the in situ particles are not preferentially segregated to the grain boundaries, and their distribution in the aluminum matrix is uniform [20,51–54,58–60,68,73,111,112].

A typical microstructure of in situ Al_2O_3 and TiB_2 particulates mixture-reinforced aluminum matrix composite, fabricated by means of the RHP process from the Al–TiO_2–B system, is shown in Fig. 13. Fine and equiaxed in situ Al_2O_3 and TiB_2 particulates are uniformly distributed in the aluminum matrix. Image analyzer examinations of particulates taken from the composite demonstrate that the in situ particulates have an average size of 0.31 ± 0.04 μm, the largest size of the particulates being 1.88 μm and the smallest size 0.096 μm [58]. Some smaller particulates could not be resolved by the image analyzer. However, the transmission electron microscopic (TEM) observations reveal that a large number of the in situ particulates have a size of less than 50 nm (Fig. 14). TEM examinations also verified that the in situ Al_2O_3 and TiB_2 particulates have an

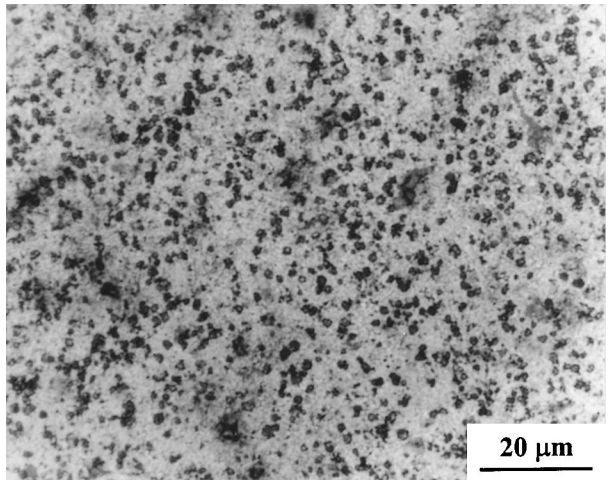

Fig. 13. Optical micrograph showing uniform distribution of fine Al_2O_3 and TiB_2 particulates in aluminum matrix. The composite was fabricated by the RHP route from TiO_2–Al–B system [58].

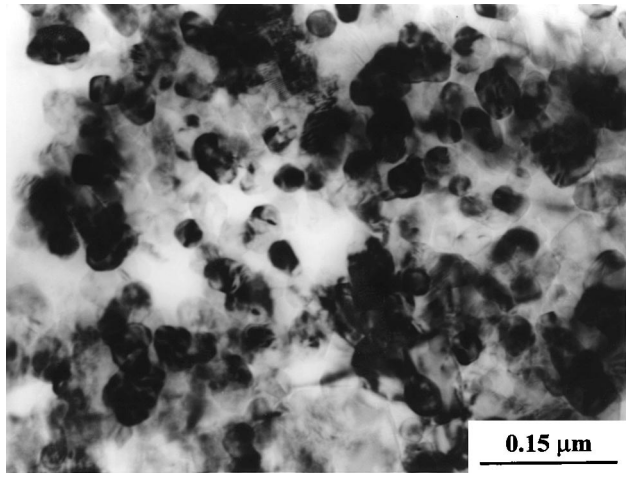

Fig. 14. TEM micrograph showing fine Al_2O_3 and TiB_2 particulates and clean interfaces in 20 vol.% (Al_2O_3 + TiB_2)/Al composite.

equiaxed shape. Equiaxed morphology of in situ particulate TiB_2 and TiC has also been reported by other researchers [48–55,71–73,109–112]. Valencia et al. [163] suggest that growth normal to planes containing both titanium and boron atoms, in the same stoichiometry as the crystal, would be faster than growth along directions involving alternating planes of Ti and B atoms. Since the slowest growing planes in TiB_2 are of the basal $\{0\,0\,0\,1\}$ and prism $\{1\,0\,\bar{1}\,0\}$ families, TiB_2 should exhibit a fairly equiaxed morphology [164].

5.1.2. Ti-based composites

The in situ TiC reinforced titanium composites prepared by means of CAC have been studied extensively by several workers [21,62,63,65,66]. Generally, three-dimensional (3-D) TiC dendrites are generated in the composites. Lu et al. [65] and Zhang et al. [66] suggest that the formation of the dendritic TiC reinforcements in the cast structure of CAC-processed titanium matrix composites is mainly attributed to over-cooling of the composition during solidification. It should be pointed out that TiC exhibits an NaCl-type structure [165]; the position of Ti and C atoms in the lattice is center-symmetric. Thus, when TiC nucleates, the growth rate in symmetric crystal planes is similar, leading to the formation of equiaxed spherical particles. The in situ formation of equiaxed spherical TiC particles in the aluminum matrix composites have been extensively reported [51–55,71–74].

On the other hand, Li et al. [128] reported that TiB whiskers developed in the RHP-processed TiB/Ti composite were in the form of elongated needles with a roughly hexagonal cross-section. The cross-sectional size of TiB whiskers is 1–2 μm and their aspect ratio is ~20. They suggested that the growth direction of the TiB whisker is parallel to $[0\,1\,0]_{TiB}$. Ranganath et al. [166] also reported the formation of rod-like TiB with a cross-sectional size of 2–6 μm, and an aspect ratio of 10–15 in the CAC-processed (TiB + Ti_2C)/Ti composites. They suggest that TiB should exhibit a much faster growth along the [0 1 0] direction than normal to the (1 0 1) and (1 0 0) planes, thus leading to a rod-like morphology. Similarly, the formation of rod-like TiB reinforcements is also reported in RSP-processed titanium matrix composites [94–97].

Recently, Ma et al. [131] have fabricated in situ titanium composites by means of the RHP route from Ti–B, Ti–TiB_2, Ti–B_4C and Ti–BN systems. They report that rod-like TiB reinforce-

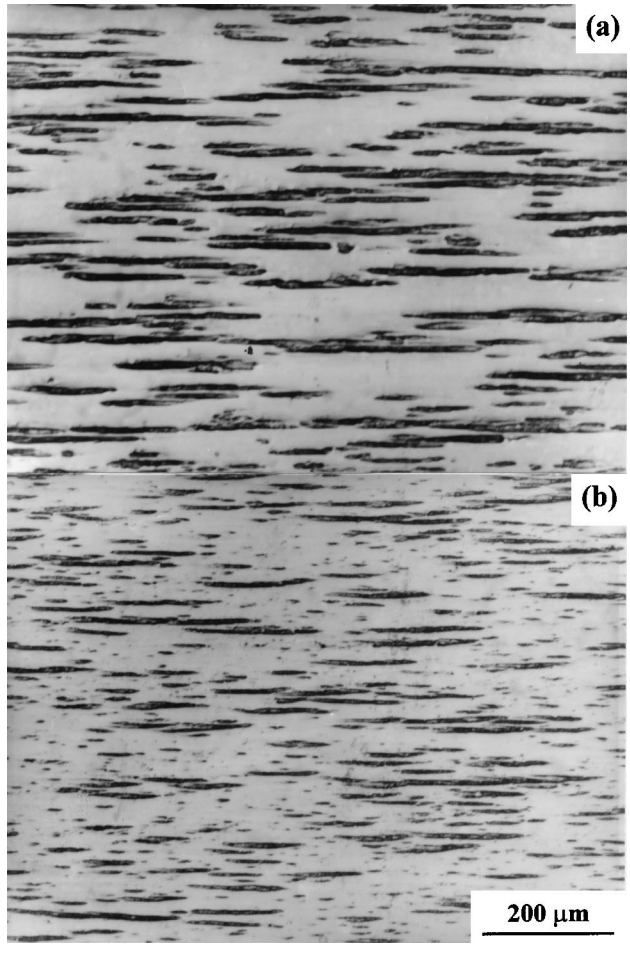

Fig. 15. Optical micrograph showing typical microstructure of (a) 15 vol.% TiB/Ti composite and (b) 15 vol.% (TiB + TiC)/Ti composite. The composites were fabricated by the RHP route from Ti–TiB_2 and Ti–B_4C systems, respectively [131].

ments are formed in situ in all the composites. Fig. 15 shows the typical microstructure of the TiB/Ti and (TiB + TiC)/Ti composites made from the Ti–TiB_2 and Ti–B_4C systems, respectively. The microstructure of both composites is characterized by numerous rod-like reinforcements, i.e. TiB whiskers along the extrusion direction. Furthermore, some fine TiC particles are dispersed in the titanium matrix, in addition to TiB whiskers in the (TiB + TiC)/Ti composite. It is evident that the size of reinforcements in the (TiB + TiC)/Ti composite is much smaller than that in the TiB/Ti composites. TiB whiskers in the TiB/Ti composite have a diameter of ~10 μm and a length of 40–400 μm, while those in the (TiB + TiC)/Ti composite have a diameter of ~6 μm and a length of 25–250 μm. TEM examination provides more evidence for the formation of TiB whiskers and TiC particulates in the (TiB + TiC)/Ti composite (Fig. 16). Apparently, the TiB exhibits a rod shape, while the TiC has a spherical shape. TEM examination also reveals that a clean interface exists between the in situ reinforcements and the titanium matrix. It should be pointed out that the spherical TiC particulates in RHP-processed titanium matrix composites are quite different from dendritic TiC reinforcements formed in CAC-processed composites [21,62,63, 65,66].

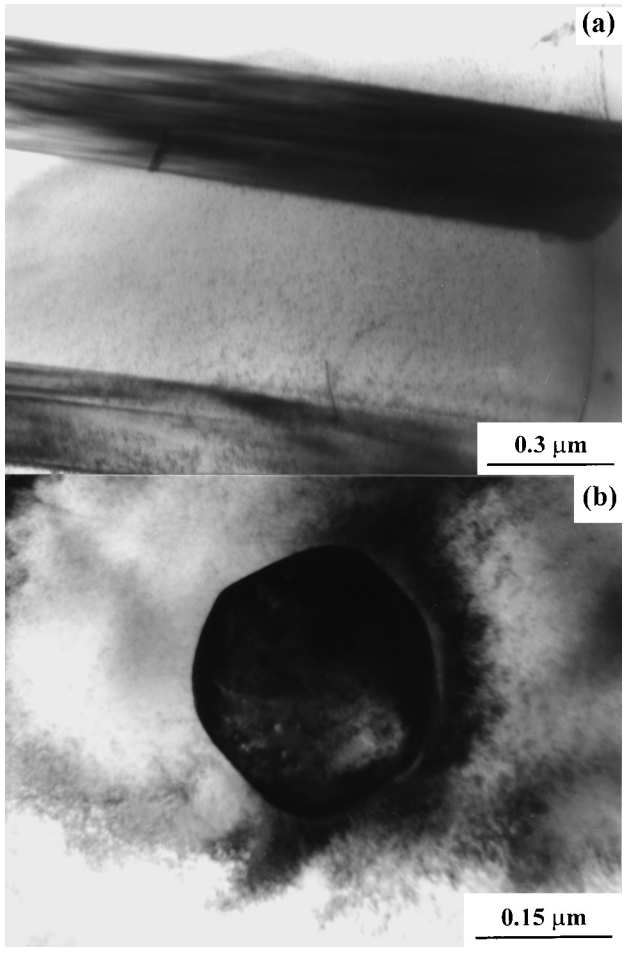

Fig. 16. TEM micrograph showing (a) rod-like TiB whisker and (b) equiaxed TiC particulate in 15 vol.% (TiB + TiC)/Ti composite fabricated by RHP route [131].

5.2. Factor influencing particle size and morphology

5.2.1. Cooling rate of the melt

For fabricating in situ titanium matrix composites by means of CAC, the cooling rate of the melt exerts a significant effect on the microstructures of the generated composites. In general, faster cooling yields smaller dendrites of TiC, encourages the formation of TiC dendrite arrays, and decreases the stoichiometry of the TiC materials [62].

Tong and coworkers [99–102] fabricated in situ TiC particulate reinforced Al-based composites by means of the RSP route. They reported that RSP can significantly refine the microstructure of the composites. For IM-prepared TiC/Al composites, the microstructure is characterized by the presence of agglomerated TiC particles. These particles, with a size of 0.2–1.0 μm, accumulated at the α-Al subgrain or at the grain boundaries. The larger particles have a polyhedral morphology, while the smaller ones are round or globular. In comparison, the typical, rapidly solidified, microstructures consist of a uniform, fine-scale dispersion of TiC particles with a size of 40–80 nm in an α-Al supersaturated matrix of 0.30–0.85 μm grain size.

5.2.2. Synthesis temperature and holding time

Chu and Premkumar [141] report that there is a drastic difference in the size of the TiC particles between samples reacted with carbon-bearing gas for 5 min and samples reacted with carbon-bearing gas for 30 min at 1533 K. The TiC particles in the former sample are as small as 2 μm, while the TiC particle in the latter sample are as large as 10 μm. Coarsening of the in situ particles with increasing holding time is also reported by other researchers [137]. Recently, Nukami [167] conducted a detailed study on the growth of TiC in the aluminum matrix by heating the aluminum-infiltrated Al–Ti–C preform. The average radius of the TiC particles at each synthesis temperature, for different holding times, was measured by means of image analysis. The relationship between holding time and TiC particle radius at various temperatures was determined. He reported that the size of the TiC particles tends to increase with increasing synthesis temperature and holding time. Further, Nukami [167] estimated the activation energy for TiC coarsening. This is determined to be 1.2×10^5 J/mol. The value is very close to that for Ti diffusion in the aluminum melt (1.16×10^5 J/mol). Therefore, Nukami [167] suggests that coarsening of TiC particles is controlled by diffusion of Ti in the aluminum melt.

5.2.3. Chemistry of matrix and reactants

Lin et al. [62] have shown that the addition of aluminum can suppress the formation of large globular-shaped particles during slow cooling of the Ti melt. The TiC tends to grow into large randomly orientated dendrites rather than globular particles. Similarly, in fabricating the (TiB + TiC)/Ti composites by the CAC route, Zhang et al. [66] showed that the addition of aluminum exerts a significant effect on primary TiC structure. However, they reported that there is a trend for primary TiC to grow into an equiaxed-shaped and fine structure after the addition of aluminum. A similar trend is also reported by Lu et al. [65] in fabricated TiC/Ti composites using the same processing technique.

Ma et al. [131] fabricated TiB/Ti and (TiB + TiC)/Ti composites from Ti–TiB_2 and Ti–B_4C systems, respectively, under identical processing conditions. Although the reactants, i.e. TiB_2 and B_4C, have the same 3 μm size, the in situ formed TiB whiskers in the Ti–B_4C system are much smaller than those in the Ti–TiB_2 system (Fig. 15).

5.3. Interfaces between in situ reinforcement and metal matrix

5.3.1. Al-based composites

Ma et al. [58] have investigated the particulate–matrix interface of ($Al_2O_3 + TiB_2$)/Al composites fabricated by means of RHP. They show that the interfaces between in situ Al_2O_3 and TiB_2 particulates and the aluminum matrix are clean and free from any interfacial phase (Fig. 17). Further, no specific orientation relationship (OR) is observed between in situ particulates and aluminum matrix.

Mitra and coworkers [50,168] have carried out a detailed study on the microstructure and particulate–matrix interfaces of the TiC/Al and TiB_2/Al composites prepared by the XD process. They reported that the TiC surfaces are parallel to low index {1 1 1} and {1 0 0} planes. These were considered to form strong bonds with Al of a highly metallic character [50,168]. The interfaces between TiC and the Al matrix are atomically abrupt, and no impurities were detected (Fig. 18). Direct contact on an atomic scale is established between in situ particulates and Al matrix, thereby allowing chemical bonds to form. Both incoherent and semicoherent interfaces are observed. They suggested that the interfacial characteristics depend on the size of the particles and on their orientation with respect to neighboring Al grains [50,168]. Similarly, Tong et al. [100] reported that

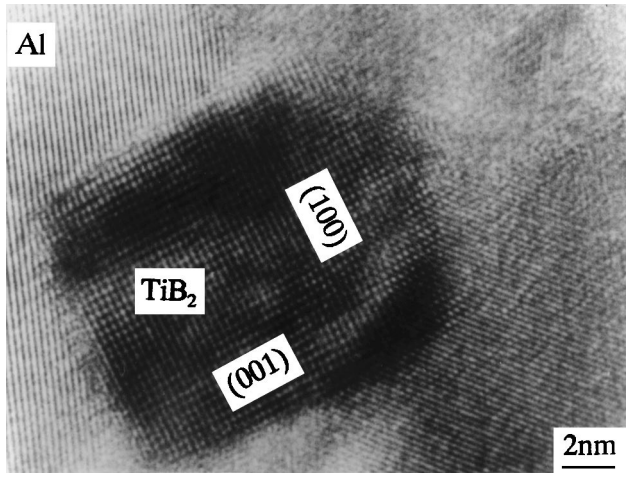

Fig. 17. HREM micrograph showing clean interface between TiB_2 and aluminum in 20 vol.% $(Al_2O_3 + TiB_2)$/Al composite [58].

TiC-dispersed particles in RSP-processed TiC/Al composites generally have a semicoherent relationship with the α-Al matrix.

5.3.2. Ti-based composites

Li et al. [128] studied the ultrafine structure of RHP-processed TiBw/Ti–6Al–4V composite by means of high-resolution electron microscopy. They reported that an orientation relationship exists

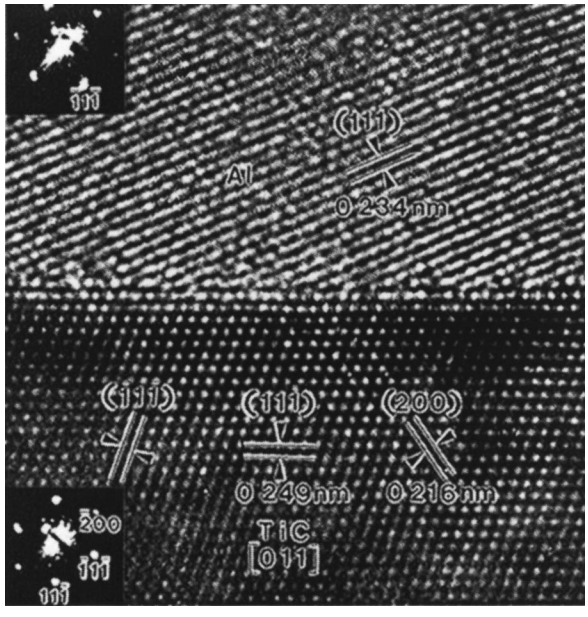

Fig. 18. HREM micrograph showing a TiC/Al interface. The lattices of Al and TiC are undistorted up to the boundary. The optical diffraction pattern (0 1 1) from inside the lattices of Al and TiC are shown. (Reprinted from R. Mitra et al., Interface in As-extruded XD Al/TiC and Al/TiB_2 metal matrix composites, Journal of Materials Research 8 (1993) 2388, with permission from Materials Research Society [168]).

between α-Ti or β-Ti and TiB. There are three types of specific orientation relationships (ORs) between β-Ti and TiB, namely,

OR I:

$$(1\,0\,0)_{TiB}||(1\,0\,0)_{\beta\text{-}Ti}, \qquad [0\,1\,0]_{TiB}||[0\,1\,0]_{\beta\text{-}Ti}$$

OR II:

$$(1\,0\,0)_{TiB}||(1\,1\,0)_{\beta\text{-}Ti}, \qquad [0\,1\,0]_{TiB}||[0\,0\,1]_{\beta\text{-}Ti}$$

OR III:

$$(1\,0\,0)_{TiB}||(1\,1\,\bar{2})_{\beta\text{-}Ti}, \qquad [0\,1\,0]_{TiB}||[1\,1\,1]_{\beta\text{-}Ti}$$

Also, there is a unique orientation relationship between α-Ti and TiB:

$$(0\,0\,1)_{TiB}||(0\,0\,0\,1)_{\alpha\text{-}Ti}, \qquad [0\,1\,0]_{TiB}||[1\,1\,\bar{2}\,0]_{\alpha\text{-}Ti}$$

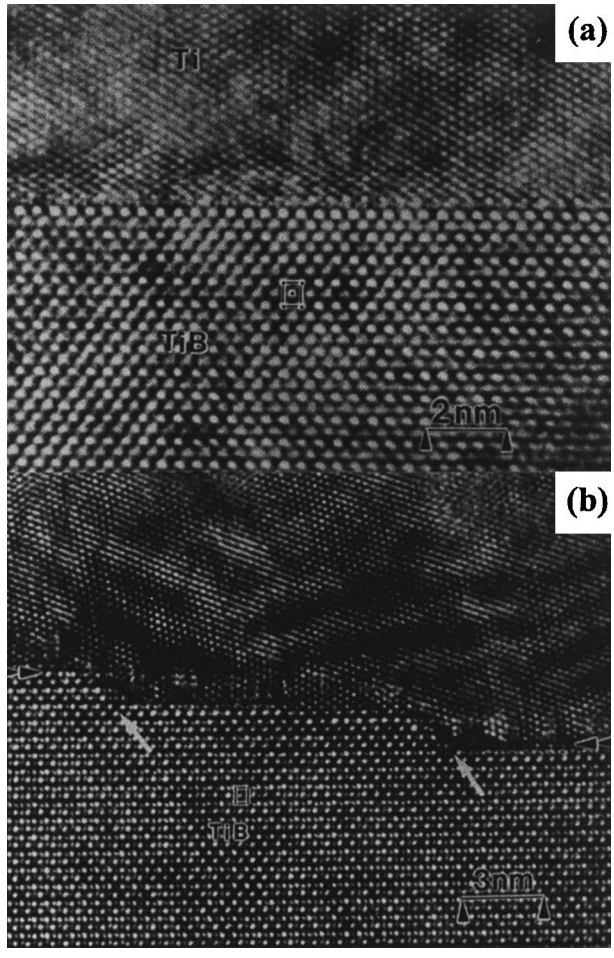

Fig. 19. HREM micrograph of TiB/β-Ti interface observed along $[0\,1\,0]_{TiB}||[1\,1\,1]_{\beta\text{-}Ti}$ in TiBw/Ti-6Al-4V composite fabricated by RHP route (reprinted from D.X. Li et al., Characterization of the microstructure in TiB-whisker reinforced Ti alloy matrix composite, Materials Letters 16 (1993) 326, with permission from Elsevier Science [128]).

Fig. 19a shows a high-resolution TEM image of the TiB/β-Ti interface observed along $[0\,1\,0]_{TiB}||[1\,1\,1]_{\beta\text{-}Ti}$. The interface plane is parallel to $(1\,0\,0)_{TiB}||(1\,1\,\overline{2})_{\beta\text{-}Ti}$. Apparently, the interface between TiB and β-Ti is quite smooth, sharp and free from any interfacial phase. The lattice mismatch ($f = 2.9\%$) between $(0\,0\,2)_{TiB}$ and $(1\,1\,0)_{\beta\text{-}Ti}$ is completely accommodated by the elastic strain of the lattice. The HREM image of the TiB/β-Ti interface observed along $[0\,1\,0]_{TiB}||[1\,1\,1]_{\beta\text{-}Ti}$ is shown in Fig. 19b. Li et al. [128] reported that the $(1\,1\,\overline{2})_{\beta\text{-}Ti}$ plane is tilted by 9° with respect to $(1\,0\,0)_{TiB}$. However, the $(1\,1\,\overline{2})_{\beta\text{-}Ti}$ plane remains parallel to $(1\,0\,0)_{TiB}$ in the vicinity of the interface and the orientation relationship, as shown in Fig. 19a. Some steps with a height of two to three times the *a* axis are frequently observed, and the inclined interface at the step region is parallel to the $\{1\,0\,1\}_{TiB}$ plane. The $(1\,0\,0)_{TiB}||(1\,0\,0)_{\beta\text{-}Ti}$ interface is also atomically flat and free from any interfacial phase. However, Li et al. [128] report that some misfit dislocations are observed due to a large lattice mismatch (8.15%) between TiB and β-Ti at the $(1\,0\,0)_{TiB}||(1\,0\,0)_{\beta\text{-}Ti}$ interface. Further, the features of the TiB/α-Ti interface are quite similar to those of the TiB/β-Ti interface.

6. Mechanical properties of in situ MMCs

The homogeneity of composite materials is of crucial importance for high-performance engineering applications such as those in the automotive and aircraft industries. A uniform reinforcement distribution in MMCs is essential to achieve effective load-bearing capacity of the reinforcement. Non-uniform distribution of reinforcement could lead to lower ductility, strength and toughness of the composites. Conventional fabrication of ex situ MMCs involves the introduction of ceramic particles into the matrices via casting and PM route. The homogeneity of ex situ MMCs is relatively poor. This is because the ceramic reinforcements are not distributed uniformly in the metallic matrices. Agglomeration of ceramic particles is known to occur frequently during casting due to the density difference between the reinforcement and molten metal, and the surface tension of the melt. Similarly, ex situ MMCs produced by the PM process also exhibit such a drawback. This is because fine ceramic particles have a higher tendency to segregate into clusters during blending of the matrix and reinforcing powders with different sizes [11,18]. On the other hand, fine ceramic particles synthesized in situ are dispersed more uniformly in the matrices of MMCs, leading to significant improvements in the yield strength, stiffness, creep and wear resistance of the materials.

6.1. Tensile properties

6.1.1. Al-based composites

The excellent properties of the in situ MMCs were first reported by Westwood and Winzer [169]. They showed that XD TiB_2/Al composites exhibit moduli up to 40% higher than that of pure aluminum, and improved strength retention at elevated temperatures, and a useful increase in wear and fatigue resistance [19,169]. Kuruvilla et al. [48] compare the tensile properties of the in situ XD TiB_2/Al composite with those of the ex situ one. Their results are summarized in Table 5. Apparently, the strength, modulus and hardness of the in situ TiB_2/Al composite are much higher than in the ex situ composite, although the ex situ composite exhibits considerably improved properties compared to unreinforced pure aluminum. The tensile and yield strengths of the in situ TiB_2/Al composite are twice as large as that of the ex situ composite. Furthermore, the modulus of the in situ TiB_2/Al composite is almost double that of unreinforced aluminum. Kuruvilla et al. [48] suggest that strengthening in the in situ composite is mainly attributed to fine dispersion of the high-modulus TiB_2 particles which are well bonded to the matrix.

Table 5
Tensile properties of in situ and ex situ 20 vol.% TiB_2/Al composites[a]

Materials	*E* (GPa)	UTS (MPa)	YS (MPa)	Elongation (%)	Hardness (VHN)
Pure Al	70	90	64	21	37
Ex situ TiB_2/Al	96	166	121	16	85
In situ TiB_2/Al	131	334	235	7	110

[a] Reprinted from A.K. Kuruvilla et al., Microstructure–property correlation in Al/TiB_2 (XD*) composites, Scripta Metallurgica et Materialia 24 (1990) 876, with permission from Elsevier [48].

Table 6
Tensile properties of in situ ($Al_2O_3 + TiB_2$)/Al and ex situ SiC(w,p)/Al composites

Materials (volume content)	UTS (MPa)	YS (MPa)	Elongation (%)	Reference
10.5% Al_2O_3 + 23.7% Al_3Ti/Al	145	110	5	[59]
10.5% Al_2O_3 + 6.3% TiB_2 + 7.9% Al_3Ti/Al	311	271	5	[59]
10.5% Al_2O_3 + 7.9% TiB_2 + 4.0% Al_3Ti/Al	328	301	5	[59]
10.5% Al_2O_3 + 9.5% TiB_2/Al	353	320	6	[59]
11.0% Al_2O_3 + 9.0% TiB_2/Al–3.2 wt.% Cu	478	427	2	[59]
11.4% Al_2O_3 + 8.6% TiB_2/Al–6.0 wt.% Cu	618	588	2	[59]
20% SiCp (1.5 μm)/Al	200	117	10	[170]
20% SiCw/Al	278	176	11	[15]

Ma et al. [20,58,59] have examined the tensile properties of ($Al_2O_3 + TiB_2$)/Al composites prepared by means of the RHP process (Table 6). As discussed in Section 2.1.3, with increasing boron content in the Al–TiO_2–B system, the amount and size of the detrimental Al_3Ti phase are apparently reduced and more TiB_2 particulates are formed in situ. This leads to a significant increase in the strength of the composites. Fig. 20 clearly shows the dependence of the strength of the composites on TiB_2 contents. Further, Ma et al. [20] compared the tensile properties of in situ ($Al_2O_3 + TiB_2$)/Al composite with those of ex situ SiC whisker or particulate reinforced aluminum composites. They showed that in situ ($Al_2O_3 + TiB_2$)/Al sample exhibits superior properties compared to SiC reinforced composites, although SiC is generally considered to be one of the best reinforcements for the aluminum matrix. In addition, Ma et al. [59,60] studied the effect of the

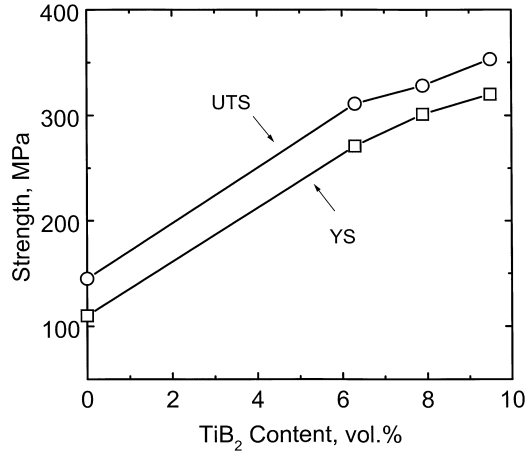

Fig. 20. Variation of strength of ($Al_2O_3 + TiB_2$)/Al composite with TiB_2 content [58].

Table 7
Tensile properties of in situ titanium matrix composites fabricated by the CAC route

Materials	UTS (MPa)	YS (MPa)	Elongation (%)	E (GPa)	Reference
Pure Ti	467	393	20.7	109	63
10 vol.% TiC/Ti	697	651	3.7	–	63
5 vol.% TiB/Ti	787	639	12.5	121	64
10 vol.% TiB/Ti	902	706	5.6	131	64
15 vol.% TiB/Ti	903	842	0.4	139	64
15 vol.% (TiB + Ti_2C)/Ti	757	690	2	–	166
25 vol.% (TiB + Ti_2C)/Ti	680	635	<0.2	–	166
22.5 vol.% (TiB + TiC)/Ti	635	471	1.2	–	21

addition of CuO on the tensile properties of (Al_2O_3 + TiB_2)/Al composites. They indicated that the Al_2Cu precipitates generated from the reduced Cu provide an additional strengthening to the composite, and the strength of the composites increases with increase in the Cu or Al_2Cu content (Table 6).

Tong et al. [102] have fabricated in situ TiC reinforced Al, Al–Si, and Al–Fe–V–Si matrix composites by means of the RSP route. They report that, compared to the IM process, the RSP technique is more effective in improving the tensile properties of the in situ composites due to the formation of a refined microstructure. The in situ composites exhibit excellent room- and elevated-temperature strengths.

6.1.2. Ti-based composites

The tensile properties of typical in situ TiC particle and/or TiB whisker reinforced titanium composites are tabulated in Table 7 [21,63,64,166]. Apparently, both strength and modulus of the composites are significantly higher than those of unreinforced titanium, and further increase with increasing particle content. However, it is noted that increasing particle content to a high level of 25 vol.% decreases the strength of the composites accordingly. Moreover, the ductility of the composites is significantly reduced with increasing particle content. Table 7 also reveals that the TiB whisker exhibits a much larger reinforcing effect on the titanium matrix than the TiC particle.

Lin et al. [62] have investigated the effect of melt cooling rate on the tensile properties of the in situ TiC/Ti composites. In their study, an increase by a factor of 2 or more is found in the ultimate tensile strength (UTS) and elongation-to-failure by increasing the cooling rate from 5 to 900 K/s. They attribute this to a decrease in the secondary dendrite arm spacing (SDAS) of in situ formed TiC. The UTS of the composites exhibits a linear dependence on SDAS. Furthermore, Lin et al. [62] report that aluminum addition could increase the room- and elevated-temperature strengths of the composites without decreasing the ductility of the composites.

6.1.3. Cu-based composites

High-strength Cu alloys can be achieved by reinforcing or dispersing ceramic phase particles, e.g. oxides, borides, carbides, in the copper matrix. These alloys are also known as dispersion strengthened (DS) copper alloys. Compared to Al- and Ti-based composites, less information is available on the tensile properties of Cu-based composites. In general, the tensile strength of Cu-based composites prepared by MA or spray forming process appears to increase with increasing particle content (Fig. 21). By contrast, the ductility of Cu-based composites decreases with increasing reinforcing particle content (Fig. 21, Table 8). These are typical tensile characteristics of MMCs. It is worth noting that TiB_2 reinforcing particle is more effective than Al_2O_3 in improving

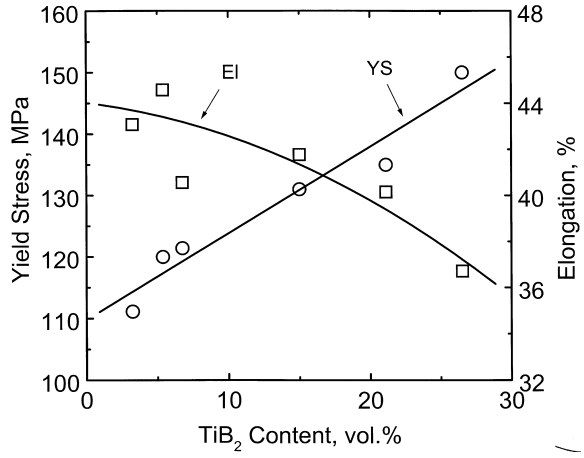

Fig. 21. Variation of yield stress and elongation-to-failure with TiB_2 volume fraction for TiB_2/Cu composite (reprinted from J. Lee et al., The Influence of reinforced particle fracture on strengthening of spray formed Cu–TiB_2 composite, Scripta Materialia 39 (1998) 1065, with permission from Elsevier Science [171]).

Table 8
Tensile properties of in situ 15 vol.% TiB_2/Cu composite and unreinforced Cu fabricated by MA and subsequent RHP [172]

Materials	UTS (MPa)	YS (MPa)	Elongation (%)
Cu	191.5	82.6	45.5
TiB_2/Cu	317.2	266.3	10.4

the mechanical strength of copper at elevated temperatures. Fig. 22 shows the variation of the strength with annealing temperature for the MA-prepared 5 vol.% TiB_2/Cu and 5 vol.% Al_2O_3/Cu composites. Apparently, the TiB_2/Cu composite exhibits a higher strength and better stability at elevated temperature compared to the Al_2O_3/Cu composite.

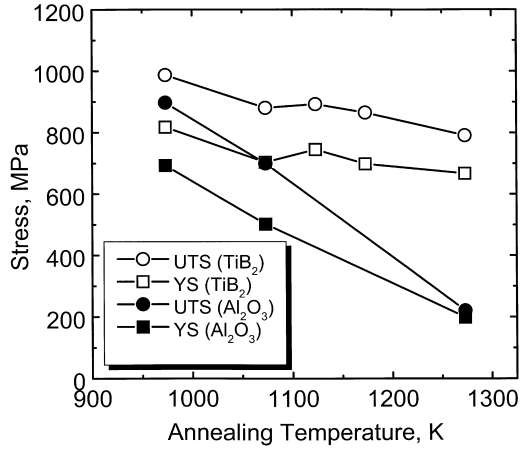

Fig. 22. Variation of strength of 5 vol.% TiB_2/Cu and 5 vol.% Al_2O_3/Cu composites with temperature. The composites are prepared by milling powders for 20 h and extruding at 973 K (reprinted from C. Biselli et al., Mechanical alloying of high-strength copper alloys containing TiB_2 and Al_2O_3 dispersoid particles, Scripta Metallurgica 30 (1994) 1330, with permission from Elsevier Science [22]).

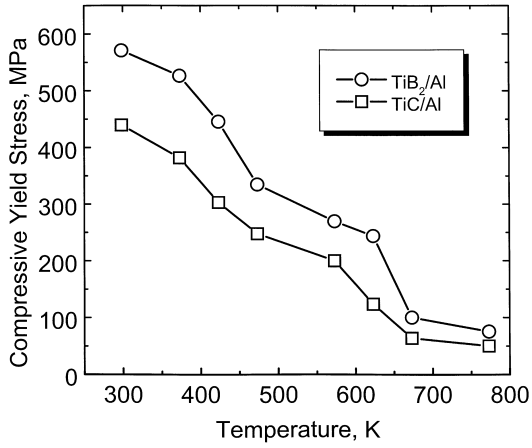

Fig. 23. Compressive yield stress of consolidated ($P = 3$ GPa, $T = 573$ K) SHS-processed 29 vol.% TiC/Al and 30 vol.% TiB_2/Al in situ composites as a function of temperature (reprinted from Gotman et al., Fabrication of Al matrix in situ composites via self-propagating synthesis, Materials Science and Engineering A A187 (1994) 197, with permission from Elsevier Science [44]).

6.2. Compressive properties

Gotman et al. [44] have investigated the compressive properties of consolidated, SHS-processed 29 vol.% TiC/Al and 30 vol.% TiB_2/Al in situ composites. Yield stress values of 430 and 560 MPa have been obtained at room temperature for the TiC/Al and TiB_2/Al composites, respectively. Moreover, the yield stress of the TiB_2/Al composite is much higher than that of the TiC/Al composite from room temperature to 773 K (Fig. 23).

For Ti-based composites, reinforced with in situ TiB and Ti_2C, the compressive yield strength values of the composites determined from the stress–strain curves at different strain rates and temperatures [166] are summarized in Table 9. Typical true stress–true strain plots for 15 vol.% (TiB + Ti_2C)/Ti composites for various strain rates at 873 K are shown in Fig. 24. This shows that, for a constant strain rate of 2×10^{-5} s^{-1} at 873 K, no further work hardening of the composite can take place after initial straining up to 1% deformation. This is because the dislocation generation process for strengthening is balanced by recovery under such a low strain rate. However, work hardening up to 12% deformation is observed at higher strain rates of 2×10^{-3} and 2×10^{-2} s^{-1}.

Recently, Ma et al. [131] have investigated the compressive properties of in situ titanium composites prepared by means of the RHP route. The variation of compressive yield strength with temperature of the composites and unreinforced titanium at strain rates of 7×10^{-4} s^{-1} is shown in Fig. 25. Clearly, the strength of the composites is significantly higher than that of the unreinforced titanium at temperatures ranging from 623 to 923 K. It is noted from Fig. 25 that the strength of (TiB + TiC)/Ti composite fabricated from the Ti–B_4C system is obviously higher than that of TiB/Ti composite from a Ti–TiB_2 system. Ma et al. [131] suggest that the high strength of the (TiB + TiC)/Ti composite is derived from the presence of smaller reinforcements (see Section 5.1.2), as the strength of the composites generally increases with decreasing size of the reinforcements.

6.3. Dynamic mechanical response

During the past two decades the static or quasistatic mechanical properties of discontinuously reinforced MMCs have been extensively investigated [1–18]. However, one important aspect of the

Table 9
Yield strength of ($TiB + Ti_2C$)/Ti composites at different strain rates and temperatures[a]

$TiB + Ti_2C$ (vol.%)	T (K)	Strain rates (s^{-1})			
		2×10^{-5}	2×10^{-4}	2×10^{-3}	2×10^{-2}
0	298	311.5	–	347.1	–
	573	100.4	–	120	–
	723	98.9	100	101.8	–
	873	74.3	74.5	76.2	77.4
10	298	610.7	–	739.3	–
	573	289.8	–	378	–
	723	285.2	332	351.6	–
	873	145	246.7	248.2	259.6
15	298	639.3	–	807	–
	573	401.6	–	418	–
	723	337.5	361.5	372.5	–
	873	154	253.9	272.5	289.8
20	298	922.1	–	1091	–
	573	708.6	–	783.8	–
	723	485.6	494.8	504	–
	873	282.2	370.7	385.5	424.2

[a] Reprinted from S. Ranganath et al., Microstructure and deformation of $TiB + Ti_2C$ reinforced titanium matrix composites, Materials Science and Technology 12 (1996) 223, with permission from IM Communications Ltd. [166].

mechanical behavior which has received less attention is the effect of strain rate on the mechanical response of MMCs. As MMCs are inevitably subjected to impact loading when used in structural applications, it is necessary to understand their behavior under high strain rate loading. Recent studies have indicated that the strength of Al-based MMCs, such as SiCw/2124Al and Al_2O_3/6061Al composites, increases with increasing strain rate [173–177].

Up till recently, information on dynamic response of in situ MMCs has been sparse in the literature. Recently, Tjong et al. [178] have examined the dynamic mechanical response of in situ ($Al_2O_3 + TiB_2$)/Al composites under compression at strain rates ranging from 1.7×10^{-3} to

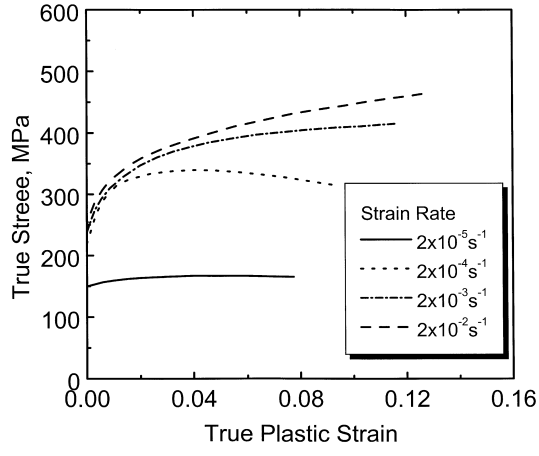

Fig. 24. True stress–true strain plots of 15 vol.% ($TiB + Ti_2C$)/Ti composite at 873 K. The composite was fabricated by CAC route (reprinted from S. Ranganath et al., Microstructure and deformation of $TiB + Ti_2C$ reinforced titanium matrix composites, Materials Science and Technology 12 (1996) 225, with permission from IM Communications Ltd. [166]).

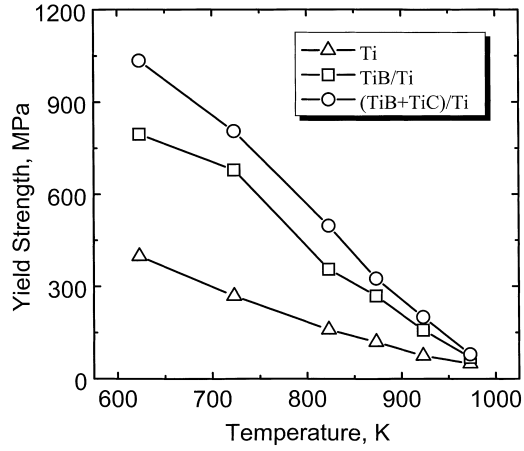

Fig. 25. Variation of compressive yield strength with temperature for 15 vol.% TiB/Ti and 15 vol.% (TiB + TiC)/Ti composites and unreinforced Ti. Materials were fabricated by RHP route [131].

$1.5 \times 10^3\ s^{-1}$. The composites were fabricated by means of RHP from a TiO_2–Al–B system [20,58–60]. They indicate that the strain rate has significant effects on the overall strength and strain hardening properties of in situ MMCs. For $(Al_2O_3 + TiB_2)$/Al composites reinforced with 10 and 20 vol.% in situ particles, the strength and the initial hardening rate increase considerably with increasing strain rate. In order to illustrate the effect, the strain hardening rate versus strain for 20 vol.% $(Al_2O_3 + TiB_2)$/Al composite is plotted in Fig. 26. For an applied strain less than 3%, strain hardening rates of the composite at high strain rates (5.5×10^2 and $1.1 \times 10^3\ s^{-1}$) are considerably larger than those at a lower rate ($1.7 \times 10^{-3}\ s^{-1}$). As the strain is increased above 3%, the strain hardening rates at various strain rates are nearly identical. Fig. 27 shows the variation of the flow stress at 6% strain with the strain rate for these in situ composites. It can be seen that the flow stress increases substantially with increasing stain rate, particularly for the sample containing 20 vol.% of reinforcing particles. It is also noted that this increasing tendency lessens when the strain rate exceeds $5.5 \times 10^2\ s^{-1}$.

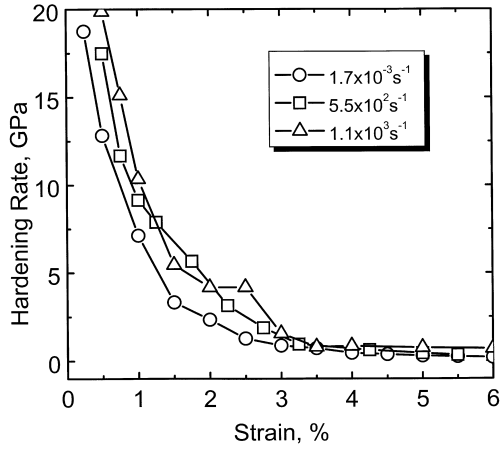

Fig. 26. Plot of strain hardening rate vs. strain at various rates for 20 vol.% $(Al_2O_3 + TiB_2)$/Al composite fabricated by RHP route [178].

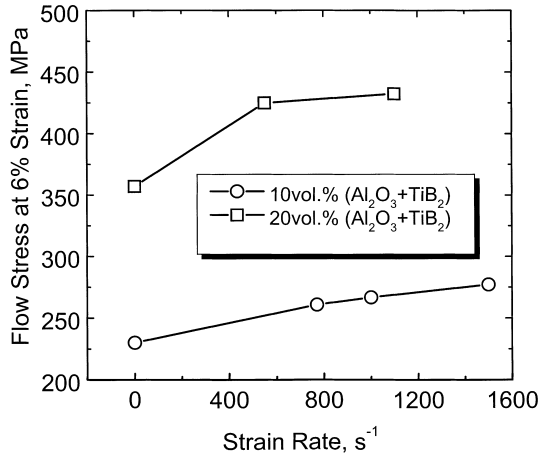

Fig. 27. Variation of flow stress at 6% strain with strain rate for $(Al_2O_3 + TiB_2)$/Al composites [178].

Tjong et al. [178] estimate the strain-rate sensitivity R_s from the following two relations, proposed by Guden and Hall [179] and Hong et al. [180], respectively:

$$R_s = \frac{\sigma_d - \sigma_q}{\sigma_q} \tag{E12}$$

$$R_s = \frac{d\ln\sigma}{d\ln\dot{\varepsilon}} \tag{E13}$$

where σ and $\dot{\varepsilon}$ are flow stress and strain rate, and σ_d, and σ_q are the dynamic and quasistatic flow stresses, respectively, at constant strain. Taking flow stresses at 6% strain, calculated values of the strain-rate sensitivity R_s are listed in Table 10. This table shows that the increasing volume fraction of the in situ Al_2O_3 and TiB_2 particulate leads to an increase in the strain-rate sensitivity of the composites. The increase in strength and initial strain hardening rate at high strain rate, for these in situ composites, can be attributed to an increase in the dislocation density in the matrix of the composites on the basis of TEM examination [178].

6.4. Wear properties

6.4.1. Lubricated sliding wear

It is well known that the aluminum alloys exhibit poor seizure and wear resistance during sliding owing to their softness. Such drawbacks can restrict their uses in tribological environments. Generally, ceramic reinforcing phases, in the form of fibers, whiskers and particles, confer a beneficial effect in improving the wear resistance of aluminum alloys. In the case of particulate reinforcement, most investigations of the wear properties of aluminum MMCs have been carried out

Table 10
Strain-rate sensitivity R_s of $(Al_2O_3 + TiB_2)$/Al composites calculated using Eqs. (E12) and (E13) [178]

Particle content (vol.%)	Using Eq. (E12)	Using Eq. (E13)
10	0.13 (1.7×10^{-3}–7.7×10^{2} s^{-1})	0.012
20	0.19 (1.7×10^{-3}–5.5×10^{2} s^{-1})	0.014

on aluminum alloy systems reinforced with SiC and Al_2O_3 particles. It appears that less information is available on the wear behavior of Al-based alloys reinforced with TiB_2 particles, particularly for composites containing in situ TiB_2 particles. TiB_2 particles are attractive for use in wear applications because their hardness is higher than that of SiC particles [181]. Moreover, TiB_2 particles can be formed in situ in metal matrices, thereby promoting a strong particle–matrix bonding. This can reduce the pull-out of particles from MMCs during sliding. Accordingly, Al-based MMCs reinforced with TiB_2 are expected to exhibit better wear performance than those reinforced with SiC or Al_2O_3 particles.

Caracostas et al. [182] investigated the lubricated sliding wear behavior of in situ, TiB_2 particle reinforced, 2024Al-T4 composites against 52100 steel. They reported that the formation of 10 vol.% of in situ TiB_2 particles (0.3 μm) in 2024Al alloy improved its wear resistance significantly [182]. Fig. 28 shows the cumulative weight loss versus sliding distance for the unreinforced 2024Al alloy and the TiB_2/2024Al composite. This figure also reveals that wear loss of the composite tends to increase at a lower sliding speed, owing to a larger number of formed asperities associated with a reduced lubricant film thickness. Little particle pull-out is observed from TEM micrographs. No voids or other flaws were seen along the Al/TiB_2 interfaces. This implies a strong interfacial bonding between TiB_2 particles and the aluminum alloy matrix [49,182]. In this case, the particles on the wear track, instead of being pulled out, are worn away. The remaining parts are still embedded in the matrix and continue to reinforce the MMC against further wear. The formation of a spall on the wear track is retarded by the presence of the TiB_2 reinforcements. Similarly, Lewis [183] reported that clean interfaces free of brittle reaction zones are formed between TiB_2 particles and the aluminum alloy matrix of XD processed, TiB_2/Al composites. HRTEM study of XD TiB_2/Al composites reveal the presence of atomically abrupt metal–ceramic interfaces [168]. By comparison, in ex situ, SiC particle reinforced, aluminum alloy composites, particle pullout is the major failure mechanism during lubricated sliding wear [184]. This is due to the formation of reaction products at the particle–matrix interface [185].

On the basis of surface chemical analysis of the wear track of in situ TiB_2/2024Al composites by means of X-ray photoelectron spectroscopy (XPS), Caracostas et al. [182] suggest that the

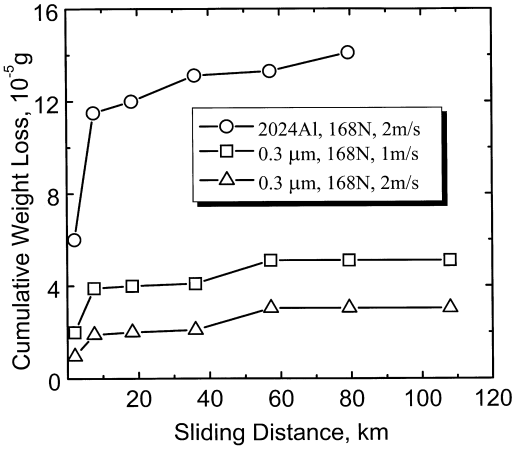

Fig. 28. Cumulative weight loss vs. sliding distance of unreinforced 2024Al alloy and 10 vol.% TiB_2 (0.3 μm)/2024Al composite (reprinted from C.A. Caracostas et al., Tribological properties of aluminum alloy matrix TiB_2 composite prepared by in situ processing, Metallurgical and Materials Transaction A 28A (1997) 494, with permission from TMS and ASM [182]).

Table 11
Nominal content (vol.%) of in situ particles formed in Al-based composites [189]

B/TiO_2 mole ratio	Al_2O_3	TiB_2	Al_3Ti	Al (matrix)
0.5	10.5	2.3	17.8	69.4
1.0	10.5	4.8	11.9	72.8
1.5	10.5	7.1	5.9	76.5
2.0	10.5	9.5	–	80.0

following tribochemical reactions take place during lubricated, sliding wear of the TiB_2/2024Al composites against 52100 steel:

$$2TiB_2 + 5O_2 \rightarrow 2B_2O_3 + 2TiO_2 \quad \text{(R35)}$$

$$B_2O_3 + 3H_2O \rightarrow 2H_3BO_3 \quad \text{(R36)}$$

Both Reactions (R35) and (R36) exhibit negative free energy changes [182]. Boric acid (H_3BO_3) exhibits a triclinic layered crystal structure which is similar to that observed in common solid lubricants, such as MoS_2 and graphite. Moreover, boron, oxygen, and hydrogen atoms form layers parallel to the basal plane of the triclinic structure in boric acid. The layers are held together by weak van der Waals forces [186,187]. During sliding, these layers align themselves along the direction of relative motion. Because of the low shear strength, they slide over one another, thereby providing low friction [188]. Accordingly, TiB_2, apart from reinforcing the aluminum alloy matrix, may also act as a solid lubricant to reduce friction and wear of the composite.

6.4.2. Dry sliding wear

Recently Tjong and coworkers [189] have conducted a preliminary study on dry sliding wear behavior of Al-based composites containing in situ Al_2O_3 and TiB_2 particles and Al_3Ti blocks (Table 11). These in situ composites are fabricated through the exothermic reaction of TiO_2, Al, and B from a TiO_2–Al–B system [20,58–60]. The resultant composites contain a fixed volume content of Al_2O_3 particles (10.5%), but a different volume content of TiB_2 particles. Fig. 29 shows the variation of volumetric wear with sliding distance for composites tested at a sliding velocity of 1.5 m/s and

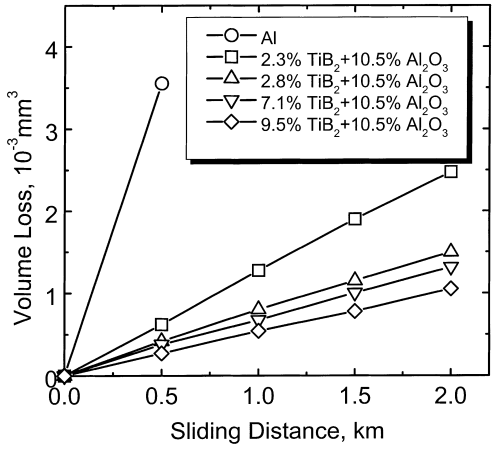

Fig. 29. Wear volume vs. sliding distance for pure Al and in situ ($Al_2O_3 + TiB_2$)/Al composites under a nominal pressure 1.68 MPa and a sliding velocity of 1.5 m/s [189].

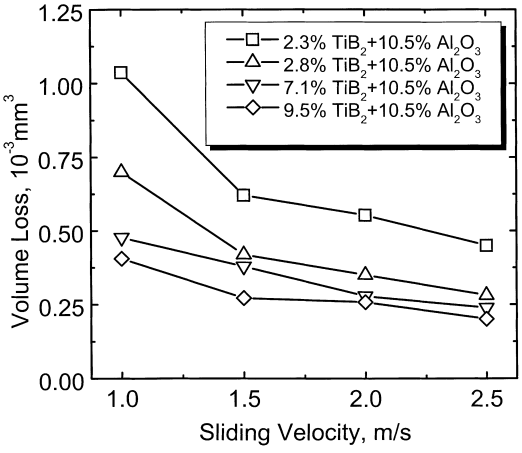

Fig. 30. Wear volume vs. sliding velocity for in situ ($Al_2O_3 + TiB_2$)/Al composites under a nominal pressure 1.68 MPa and a sliding distance of 500 m [189].

under a nominal pressure of 1.68 MPa. This figure clearly indicates that the formation of in situ particles in ductile Al matrix can lead to a sharp decrease in the volumetric wear. Furthermore the higher the TiB_2 content in the composites, the better is their wear resistance. As the in situ Al_2O_3 volume content of the composites investigated is controlled at 10.5 vol.%, mainly only the in situ TiB_2 particles are responsible for improving the wear resistance of Al.

The effect of sliding velocity on the volumetric wear of the composite under a nominal pressure of 1.68 MPa and a sliding distance of 500 m is shown in Fig. 30. The volumetric wear of all the composites decreases with increasing sliding velocity. The composite sample containing 9.5 vol.% TiB_2 particles exhibits a higher wear resistance than other composites at the velocity ranges investigated. Fig. 31 shows the volume loss versus nominal pressure for the composites tested at a sliding velocity of 1.5 m/s and a sliding distance of 500 m. The beneficial effect of the formation of higher TiB_2 volume content in composites is also apparent.

From these results Tjong and coworkers [189] suggest that the excellent wear resistance of (9.5 vol.% TiB_2 + 10.5 vol.% Al_2O_3)/Al composite is not only derived from their higher TiB_2

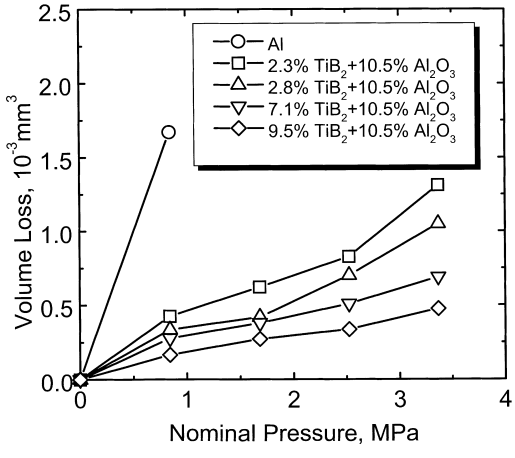

Fig. 31. Wear volume vs. nominal pressure for pure Al and in situ ($Al_2O_3 + TiB_2$)/Al composites under a sliding velocity of 1.5 m/s and a sliding distance 500 m [189].

particle content, but also from the elimination of coarse Al_3Ti blocks. In the latter case large Al_3Ti blocks are detrimental to the wear properties of the composites due to the fact that brittle Al_3Ti blocks often fracture into smaller particles during sliding. Accordingly some cracks are initiated at these fragmented Al_3Ti particles and they tend to propagate toward the top surface region, leading to the delamination of the hardened surface layer. Tjong et al. [189] conclude that there is no pullout or debonding of in situ particles from the matrix due to the existence of strong interfacial bonding and good compatibility between fine in situ particles and the Al matrix. As in situ TiB_2 particles exhibit high hardness they can resist plastic deformation in the subsurface region, thereby improving the wear resistance accordingly.

More recently Tjong et al. [190] further investigated the dry sliding wear behavior of several in situ Al-based composites fabricated from Ti–Al–B, TiO_2–Al–B, TiO_2–Al–B–CuO and TiO_2–Al–B_2O_3. They reported that TiB_2/Al composites prepared from the Ti–Al–B system exhibit the highest wear loss due to the formation of large TiB_2 in situ particles (0.1–5 μm). Such large agglomerated TiB_2 particles are ineffective to resist the shear deformation developed in the wear surface during sliding. By contrast, in situ ($Al_2O_3 + TiB_2$)/Al composite, fabricated from a TiO_2–Al–B system, has the smallest volume wear. This is attributed to the formation of fine TiB_2 and Al_2O_3 particles, which are dispersed uniformly in the aluminum matrix, and to a strong interfacial particle/matrix bonding. The latter enables the in situ particles to be retained in the wear surface during sliding. Among these samples ($Al_2O_3 + TiB_2$)/Al–Cu composite, fabricated from a TiO_2–Al–B–CuO system, exhibits a higher strength compared to ($Al_2O_3 + TiB_2$)/Al composites fabricated from a TiO_2–Al–B system. This is due to the precipitation-strengthening of Al_2Cu [59,60]. However, Al_2Cu precipitates appear to have no effect in reducing the volume wear of the composites [190]. Finally Tjong et al. [190] report that brittle, plate-like, Al_3Ti blocks are prone to cracking in ($Al_2O_3 + TiB_2$)/Al composites fabricated from a TiO_2–Al–B_2O_3 system. The deleterious effect of Al_3Ti blocks on the wear properties of ($Al_2O_3 + TiB_2$)/Al composites has been outlined above [189].

6.5. Creep behavior

6.5.1. Al-based composites

6.5.1.1. Comparison between creep properties of in situ and ex situ composites. The high temperature creep behavior of discontinuously reinforced Al-based MMCs has been studied extensively in the past decade [191–206]. Generally these composites exhibit high values of apparent stress exponent and apparent activation energy. A threshold stress approach is adopted by a number of researchers [194–196,198–206] to explain the creep behavior of these composites. However, most creep studies are focused on the steady-state creep behavior of the conventional ex situ composites. Information on the creep behavior of in situ ceramic particulate reinforced aluminum matrix composites is limited [198,207–211].

Pandey et al. [198] have investigated the high temperature creep behavior of both conventional ex situ 20 vol.% TiB_2/Al and XD-processed in situ 20 vol.% TiB_2/Al composites in compression. They report that both composites exhibit high values of apparent stress exponent and apparent activation energy. The in situ TiB_2/Al composite exhibits an apparent stress exponent of 8–14 at 573 and 623 K, and an apparent activation energy of 339 kJ/mol. These values are much higher than those for creep in pure aluminum. Furthermore they report that the creep resistance of the in situ TiB_2/Al composite is higher than that of the ex situ TiB_2/Al composite. Pandey et al. [198] analyzed the steady-state creep data of both in situ and ex situ TiB_2/Al composites. They show that the steady-state creep data of ex situ TiB_2/Al composite could be rationalized using the substructure invariant

model, by incorporating a threshold stress into the creep equation. However, the creep data of the in situ TiB_2/Al composite could not be explained adequately using existing dislocation creep models, even after considering the threshold stress. This is attributed to the anomalous creep behavior of in situ TiB_2/Al composite observed at higher temperatures [208].

6.5.1.2. Static creep behavior. Krajewski et al. [207] examined the influence of matrix microstructure and reinforcement, with 15 vol.% of in situ TiC particles, on the creep behavior of 2219Al alloy in the temperature range 423–523 K. They reported that at 423 K TiC reinforcements lead to an improvement in creep resistance, while at 523 K both reinforced and unreinforced materials exhibit essentially identical creep behavior. Furthermore essentially identical apparent stress exponents and creep activation energies are observed in both the reinforced and unreinforced materials. Krajewski et al. [207] point out that precipitate spacing in the matrix exerts a predominant influence on minimum creep rate in both the reinforced and unreinforced materials over the temperature range studied. They explain the creep data of both materials using a constant substructure model [212], where precipitate spacing is identified as the pertinent substructure dimension. Further Krajewski et al. suggested that a modest microstructure-independent strengthening from TiC particles observed at 423 K, can be accurately modeled by the existing continuum mechanical models. Also the absence of reinforcement creep strengthening at 523 K can be attributed to the diffusional relaxation processes at higher temperature [207].

Recently Ma and Tjong [209] have investigated the tensile creep behavior of 20 vol.% ($Al_2O_3 + TiB_2$)/Al composites processed by RHP from TiO_2–Al–B and TiO_2–Al–B_2O_3 systems, respectively. Fig. 32 shows the variation of minimum creep rate for two composite specimens under applied stress. This plot shows that these composites exhibit an essentially identical creep resistance. As mentioned in Section 2.1.3, a certain amount of plate-like Al_3Ti blocks, with a size of several tens of micrometers, are generated in the composite fabricated from the TiO_2–Al–B_2O_3 system. An essentially identical creep resistance as observed in Fig. 32 indicates that the coarse Al_3Ti blocks do not exert a significant effect on the creep properties of the composites. The apparent stress exponent and apparent activation energy for creep of both composites, determined from the experimental data, are listed in Table 12. The apparent stress exponents for two in situ composites are 15.8–17.4 and 16.5–17.9, respectively. These values are much higher than those of pure aluminum and solid solution aluminum alloys ($n = 3 - 5$). Moreover the apparent activation energies of the investigated

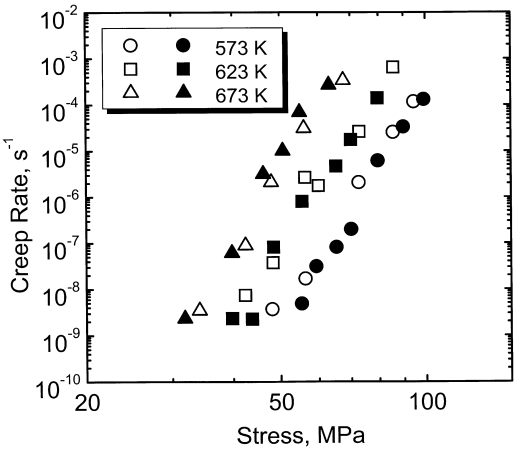

Fig. 32. Variation of minimum creep rate with applied stress for 20 vol.% ($Al_2O_3 + TiB_2$)/Al composites (open symbol for TiO_2–Al–B system and solid symbol for TiO_2–Al–B_2O_3 system) [209].

Table 12
Apparent stress exponent and apparent activation energy for creep of in situ 20 vol.% ($Al_2O_3 + TiB_2$)/Al composites [209]

System	Nominal content of particles (vol.%)		Apparent stress exponent			Apparent activation energy (kJ/mol)
	Al_2O_3	TiB_2	573 K	623 K	673 K	
TiO_2–Al–B	10.5	9.5	15.9	15.8	17.4	242
TiO_2–Al–B_2O_3	14.7	5.3	17.6	16.5	17.9	306

composites are 242 and 306 kJ/mol, respectively, which exceed that for lattice diffusion of aluminum (142 kJ/mol). Such high values of apparent stress exponent and apparent activation energy have been reported by several researchers in creep studies of ex situ SiC/Al or Al_2O_3/Al composites [191–206].

In order to rationalize the strong stress and temperature dependency of creep rate, reported for the discontinuously reinforced, aluminum matrix composites, the concept of an effective stress, previously developed for dispersion-strengthened alloys [213], has been used by several workers [194–206]. In this respect the power-law creep equation

$$\dot{\varepsilon} = A\sigma^{n_a} \exp\left(-\frac{Q_a}{RT}\right) \tag{E14}$$

can be modified as

$$\dot{\varepsilon} = A'\left(\frac{\sigma - \sigma_0}{E}\right)^n \exp\left(-\frac{Q}{RT}\right) \tag{E15}$$

where $\dot{\varepsilon}$ is the minimum creep rate, A and A' are structure dependent parameters, σ is the applied stress, σ_0 is the threshold stress, n_a is the apparent stress exponent, n is the true stress exponent, E is the temperature-dependent Young's modulus, Q_a is the apparent activation energy, Q is the true activation energy, R is the gas constant, and T is the absolute temperature.

Ma and Tjong [209] further examined the creep data of in situ ($Al_2O_3 + TiB_2$)/Al composites using the concept of threshold stress. In order to estimate the value of the threshold stress σ_0, for creep of the ($Al_2O_3 + TiB_2$)/Al composites, a procedure similar to that reported elsewhere [194–196,198–206] is adopted. In this case the data at a single temperature is plotted as $\dot{\varepsilon}^{1/n}$ against σ on double linear scales. Assuming that the creep data of the composites satisfy Eq. (E15) and σ_0 is independent of the applied stress, the data points in the plot of $\dot{\varepsilon}^{1/n}$ versus σ should fit into a straight line. Moreover the extrapolation of this linear regression line to zero strain rate can yield the value of σ_0 for each temperature. The most appropriate value for n is determined by making several plots of the creep data on linear scales as $\dot{\varepsilon}^{1/n}$ versus σ, using different values of n and selecting the value of n that gives the best linear fit to the data points.

Mohamed [214] pointed out that the creep behavior of Al alloys and their composites is related to modified creep behavior of solid solution alloys. Thus, the equations developed for solid solution alloys can be used to describe the creep behavior of composites provided that the applied stress is replaced by an effective stress. The true stress exponent n is usually selected as 3, 5 and 8. These values of n correspond to three well-documented creep cases for metals and alloys: $n = 3$ for creep controlled by viscous glide processes of dislocation [215–217], $n = 5$ for creep controlled by high-temperature dislocation climb (lattice diffusion) [215–217], and $n = 8$ for lattice diffusion-controlled creep with a constant structure [212]. In this case Pandey et al. [195,198] and Gonzalez-Doncel and Sherby [199] have used a true stress exponent of 8 in the plots of $\dot{\varepsilon}^{1/n}$ versus σ for SiC/Al and

TiB_2p/Al composites. However, other research groups [194,196,200–202] have observed that a stress exponent of 5, rather than 8, provides a better description for the creep data of discontinuous SiC/Al composites. Recently Li and Langdon [203] by incorporating a threshold stress into the analysis indicate that the true stress exponent of the Al_2O_3p/6061Al composite fabricated by IM technique is close to 3, and the true activation energy is close to the value for diffusion of Mg in the 6061Al matrix.

Ma and Tjong [209] constructed plots of $\dot{\varepsilon}^{1/n}$ versus σ for $n = 3$, 5 and 8 for $(Al_2O_3 + TiB_2)$/Al composite fabricated from a TiO_2–Al–B system. They report that a stress exponent of 8 yields the best linear fit for this composite (Fig. 33c); for $n = 3$ and 5 the plots exhibit clear curvature with decreasing applied stress (Fig. 33a and b). Similar results are obtained for $(Al_2O_3 + TiB_2)$/Al composite fabricated from a TiO_2–Al–B_2O_3 system. These results definitely indicate that stress exponents of 3 and 5 cannot be used to rationalize the creep data of in situ $(Al_2O_3 + TiB_2)$/Al composites.

Ma and Tjong [209] then estimate the values of the threshold stress from the plots of $\dot{\varepsilon}^{1/8}$ and σ by extrapolation technique (Table 13). The threshold stress obtained for 20 vol.% $(Al_2O_3 + TiB_2)$/Al composites is much higher than that for 20 vol.% SiCp/Al and 20 vol.% TiB_2p/Al composites

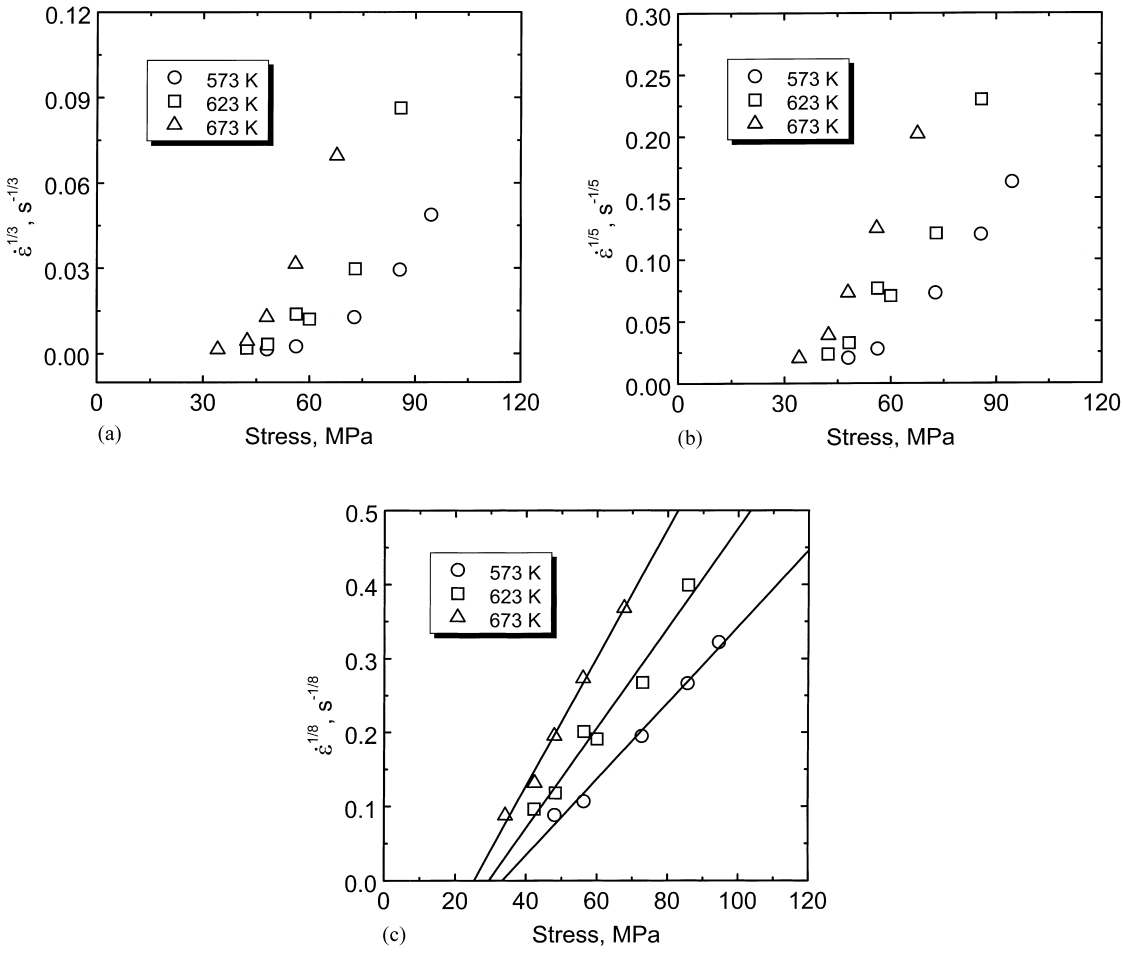

Fig. 33. Variation of (a) $\dot{\varepsilon}^{1/3}$; (b) $\dot{\varepsilon}^{1/5}$ and $\dot{\varepsilon}^{1/8}$ with applied stress on double linear scales for 20 vol.% $(Al_2O_3 + TiB_2)$/Al composite fabricated from TiO_2–Al–B system [209].

Table 13
Threshold stress for creep of 20 vol.% ($Al_2O_3 + TiB_2$)/Al composites determined by extrapolation technique [209]

System	Temperature (K)	Threshold stress (MPa)	σ_0/E
TiO_2–Al–B	573	33.8	6.15×10^{-4}
	623	30.5	5.77×10^{-4}
	673	25.5	5.02×10^{-4}
TiO_2–Al–B_2O_3	573	40.0	7.27×10^{-4}
	623	28.2	5.33×10^{-4}
	673	24.1	4.75×10^{-4}

[195,198] owing to a finer size of the in situ Al_2O_3 and TiB_2 particulates. Furthermore the threshold stress tends to decrease with increasing temperature. This behavior differs from that reported by Pandey et al. [195,198] who reported an essentially temperature-independent threshold stress for SiCp/Al and TiB_2p/Al composites. The temperature dependence of such a threshold stress can best be described by the following empirical relation [196]:

$$\frac{\sigma_0}{E} = B \exp\left(\frac{Q_0}{RT}\right) \tag{E16}$$

where B is a constant and Q_0 is an energy term. To check the validity of Eq. (E16) Ma and Tjong [209] plotted values of σ_0/E, estimated for ($Al_2O_3 + TiB_2$)/Al composite fabricated from a TiO_2–Al–B system, as the logarithm of σ_0/E against $1/T$ (Fig. 34). The Young's modulus E, is estimated from equations for shear modulus, $G\,(\mathrm{MPa}) = 3.0 \times 10^4 - 16T$ and $E = 2(1+\nu)G$, where T is the absolute temperature, and ν is Poisson's ratio [215]. As can be seen from Fig. 34, the data points fit very closely to a straight line for the in situ composite, indicating that the threshold stress determined for this composite can be described by Eq. (E16). Similar results are obtained for ($Al_2O_3 + TiB_2$)/Al composite fabricated from a TiO_2–Al–B_2O_3 system. The value of Q_0 can be estimated from the slope of the linear regression line as shown in Fig. 34. Q_0 is determined to be 6.3 and 13.8 kJ/mol for ($Al_2O_3 + TiB_2$)/Al composites fabricated from TiO_2–Al–B and TiO_2–Al–B_2O_3 systems, respec-

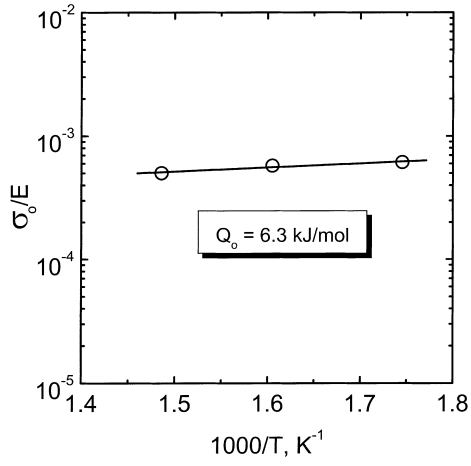

Fig. 34. Plot of the logarithm of the normalized threshold stress, σ_0/E, vs. $1000/T$ for 20 vol.% ($Al_2O_3 + TiB_2$)/Al composite fabricated from TiO_2–Al–B system [209].

tively. This indicates that the value of Q_0 for in situ composites is much lower than that for 30 vol.% SiCp/6061Al (19.3 kJ/mol) and 10 vol.% SiCp/2124Al (24.8 kJ/mol) composites [196,202], i.e. the temperature dependence of threshold stress for the present composites is lower than that for 30 vol.% SiCp/6061Al and 10 vol.% SiCp/2124Al composites.

Recently, Pandey et al. [195,198] explained satisfactorily the creep data of SiCp/Al and TiB_2p/Al composites using the substructure invariant model [212]. Gonzalez-Doncel and Sherby [199] also showed that the creep data of SiC/Al composites can be rationalized by using the substructure invariant model [212]. The substructure invariant model predicts that the creep rate is proportional to the cube of the subgrain size, and the stress exponent is equal to 8, with a stable substructure, during extended creep exposure [212]. The stable substructure can be achieved by introducing second phase particles such as oxide dispersoids in metals. In such a situation, the particles would stabilize the subgrain size. The substructure invariant model [212] can be represented as

$$\dot{\varepsilon} = S\left(\frac{D_L}{b^2}\right)\left(\frac{\lambda}{b}\right)^3\left(\frac{\sigma-\sigma_0}{E}\right)^8 \tag{E17}$$

where D_L is the lattice self-diffusion coefficient, λ is the subgrain size, b is the Burgers vector and S is a constant.

For the substructure invariant model to be applicable in the present study, the substructure should be stabilized by Al_2O_3 and TiB_2 particulates, thereby yielding a stress exponent of 8 and an activation energy equal to the lattice self-diffusion. As mentioned in Section 5.1.1, in situ Al_2O_3 and TiB_2 particulates have an average size of 0.31 μm. This size is much smaller than that of SiC (1.7 μm) and TiB_2 particulate (4 μm) [195,198]. It is very likely that Al_2O_3 and TiB_2 particulates can pin the subgrain boundaries effectively. Thus, the microstructure of the composites remains invariant during creep.

Mohamed et al. [196] have estimated the true activation energy Q, in terms of Q_a, n, σ_0 and Q_0 from the following expression:

$$Q = Q_a + \frac{nRT^2}{G}\frac{\partial G}{\partial T}\left(1+\frac{1}{\sigma/\sigma_0-1}\right) - \frac{nQ_0}{\sigma/\sigma_0-1} \tag{E18}$$

Ma and Tjong [209] applied Eq. (E18) to determine the Q value for in situ $(Al_2O_3 + TiB_2)$/Al composites, using $n = 8$, average temperature $T = 623$ K, average applied stress $\sigma = 55$ MPa, and Q_a values listed in Table 12. The values of the true activation energy Q, for creep are determined as 139 and 147 kJ/mol for $(Al_2O_3 + TiB_2)$/Al composites fabricated from TiO_2–Al–B and TiO_2–Al–B_2O_3 systems, respectively. These values are very close to that for self-diffusion in aluminum (142 kJ/mol) [215]. On the basis of these analyses Ma and Tjong [209] suggest that the creep rate of these two in situ composites is matrix lattice diffusion controlled.

Furthermore, they rationalized the creep data of the two in situ composites by using the diffusivity of aluminum and the threshold stress listed in Table 13. In this respect the minimum creep rate of the composites, normalized to the coefficient of matrix lattice diffusion, $\dot{\varepsilon}/D_L$, is plotted against the effective stress compensated to Young's modulus, $(\sigma-\sigma_0)/E$ (Fig. 35). In the creep data analysis values of the coefficient of lattice self-diffusion in aluminum are obtained using the relation $D_L\,(m^2/s) = 1.71\times10^{-4}\exp(-142.12/RT)$ [218]. Values of the modulus E are obtained as mentioned above. It is noted that data points for all temperatures fit well a single straight line with a slope of 8. Ma and Tjong [209] suggest that the substructure invariant model can provide a satisfactory explanation for in situ $(Al_2O_3 + TiB_2)$/Al composites.

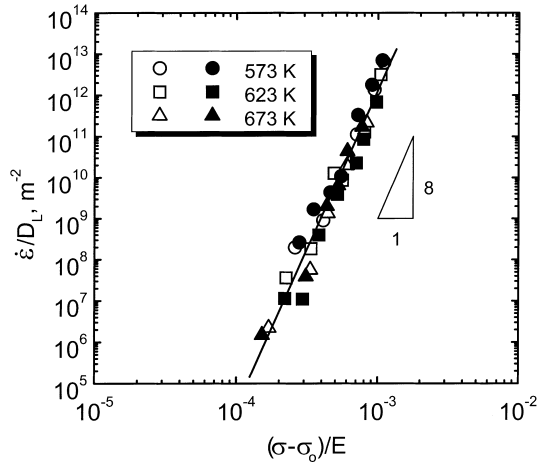

Fig. 35. Variation of diffusivity normalized minimum creep rate, $\dot{\varepsilon}/D_L$, with modulus-compensated effective stress, $(\sigma - \sigma_0)/E$, on double logarithmic coordinates for 20 vol.% $(Al_2O_3 + TiB_2)$/Al composites (open symbol for TiO_2–Al–B system and solid symbol for TiO_2–Al–B_2O_3 system) [209].

Similarly the static creep behavior of in situ 20 vol.% $(Al_2O_3 + TiB_2)$/Al–Cu and 15 vol.% TiB_2/Al composites, fabricated from TiO_2–Al–B–CuO and Ti–Al–B systems, also exhibit high values of apparent stress exponent and creep activation energy [210,211]. Ma et al. [210,211] show that, by incorporating a threshold stress into the analysis, the true stress exponent of these two composites is equal to 8 and the true activation energy is close to the lattice self-diffusion of aluminum. This is the creep behavior of these two composites can also be satisfactorily explained by the substructure invariant model.

6.5.1.3. Cyclic creep behavior. During the past decade the static creep behavior of discontinuously reinforced aluminum matrix composites has been subjected to extensive investigation [191–206]. However, less information is available in the literature concerning the effect of cyclic loading on the creep behavior of Al-based MMCs [219–221]. As many structural components are subjected to repeated loading at elevated temperatures under service conditions, an understanding of the cyclic creep behavior of the composites is of practical importance.

Ma et al. [210] have carried out a pioneering study of the cyclic stress on the effect of the high temperature creep behavior of in situ 20 vol.% $(Al_2O_3 + TiB_2)$/Al–Cu composite. In their study cyclic creep tests were performed under load control conditions, with various percentage amounts of cyclic unloading from the fixed maximum tensile stress. The value of maximum tensile stress amplitude during cyclic loading was adopted as the applied stress for cyclic creep. The largest unloading amount was 90% in order to maintain tension on–off load, and to align the load train. The cyclic creep rate is defined as the net increment of peak strain (envelope strain) per second, i.e. the envelope creep rate is used as the cyclic creep rate.

Fig. 36 shows the variation of static and cyclic steady-state creep rates versus applied stress for this composite. A loading frequency of 0.5 Hz and unloading amount of 90% are used for cyclic creep. Apparently the steady-state creep rate for cyclic creep at 573 and 623 K is significantly lower than that for static creep. This implies that cyclic creep retardation (CCR) occurs in 20 vol.% $(Al_2O_3 + TiB_2)$/Al–Cu composite for the stress and temperature ranges investigated. Furthermore, it is noted that the magnitude of cyclic creep retardation increases with decreasing applied stress. The apparent stress exponent and apparent activation energy for static and cyclic creep of

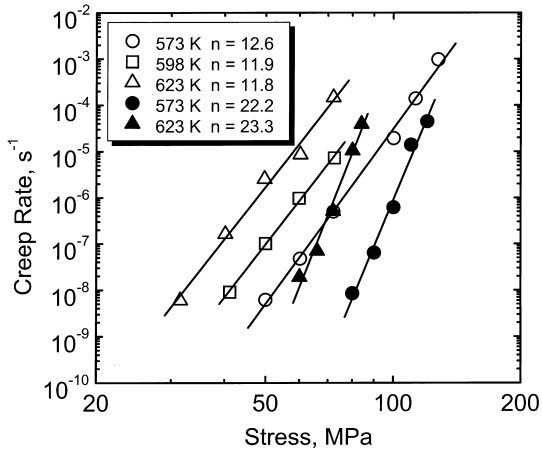

Fig. 36. Variations of static and cyclic steady-state creep rates with applied stress for 20 vol.% ($Al_2O_3 + TiB_2$)/Al–Cu composite. For cyclic creep, applied stress is defined as the maximum tensile stress amplitude. (Open symbol for static creep and solid symbol for cyclic creep with loading frequency of 0.5 Hz and unloading amount of 90% [210].)

($Al_2O_3 + TiB_2$)/Al–Cu composites are summarized in Table 14. This table shows that the apparent stress exponent and apparent activation energy for cyclic creep of ($Al_2O_3 + TiB_2$)/Al–Cu composite are much higher than those for static creep.

Ma et al. [210] suggested that the CCR behavior of in situ composites, like that of oxide dispersion strengthened (ODS) alloy [222,223], can be explained in terms of the storage of anelastic strain. Such strain results in a delay of the non-recoverable creep during the on-load cycles, i.e. the storage of anelastic strain must first take place, before non-recoverable creep can occur. The anelastic strain does not contribute to the net cyclic creep rate, as it is recovered during the subsequent off-load period. The greater the frequency, the greater the decrease in the net cyclic strain rate [222,223]. In terms of the threshold stress, the apparent stress exponent and apparent activation energy for creep are expressed by the following two equations, which can be derived from Eqs. (E14) and (E15):

$$n_a = \frac{n(1 - d\sigma_0/d\sigma)}{1 - (\sigma/\sigma_0)} \tag{E19}$$

$$Q_a = Q - \frac{nRT^2}{\sigma - \sigma_0}\frac{d\sigma_0}{dT} - \frac{nRT^2}{E}\frac{dE}{dT} \tag{E20}$$

where $d\sigma_0/dT$ and dE/dT have negative values.

Table 14
Apparent stress exponents and apparent activation energies for static and cyclic creep of 20 vol.% ($Al_2O_3 + TiB_2$)/Al–Cu composite [210]

Test mode	Temperature (K)	Apparent stress exponent	Apparent activation energy (kJ/mol)
Static creep	573	12.6	337
	598	11.9	
	623	11.8	
Cyclic creep	573	22.2	421
	623	23.3	

The threshold stress is generally considered as applied stress independent, so the apparent stress exponent for creep is determined by the value of σ_0/σ (Eq. (E19)). The effective stress, $\sigma - \sigma_0$, driving non-recoverable creep will essentially be zero during the earliest stages of the on-load cycle, and gradually increase to the value appropriate for a static test as the storage of anelastic strain saturates, assuming the on-load period is sufficiently long. Thus, a small average effective stress, i.e. a large average value of σ_0/σ, is available during the on-load period to drive non-recoverable creep, leading to a lower strain rate for cyclic creep. Therefore, a higher value of apparent stress exponent for cyclic creep is observed.

It is noted from Eq. (E20) that increasing values of σ_0/σ, $d\sigma_0/dT$ and dE/dT all result in increasing Q_a. Since the temperature dependence of the elastic modulus (dE/dT) is the same for both static and cyclic creep, the higher value of Q_a for cyclic creep lies in the temperature dependence ($d\sigma_0/dT$) and the magnitude (σ_0) of the threshold stress. According to Nardone et al. [222] the anelastic recovery is controlled by a thermally activated process, and the recovery of the anelastic strain exhibits an exponential dependence with respect to temperature. Therefore, the value of σ_0, for cyclic creep, is more sensitive to temperature than that for static creep, i.e. a higher value for the $d\sigma_0/dT$ term under cyclic creep conditions. As discussed above the average value of σ_0/σ for cyclic creep is larger than that for static creep. Thus, the larger value of $d\sigma_0/dT$ and smaller value of effective stress, $\sigma - \sigma_0$, in turn result in a higher value of apparent activation energy Q_a, for cyclic creep.

Furthermore, the steady-state creep rates of $(Al_2O_3 + TiB_2)$/Al–Cu composite tend to decrease with increasing loading frequency (Fig. 37), i.e. the magnitude of CCR increases with increasing loading frequency. A similar behavior was previously reported by Nardone et al. [222,223] in ODS alloys. Ma et al. [210] suggested that the frequency dependence of cyclic creep deceleration is related to the time constant of anelastic relaxation. Following the load application, the non-recoverable creep rate reaches the static value only after an on-load time approaches the anelastic relaxation time constant. For shorter cyclic periods (higher frequencies) the anelastic strain is less completely stored, due to a small on-load time. Thus, the envelope creep rate (time-averaged rate of non-recoverable creep) is considerably reduced, resulting in the occurrence of non-recoverable creep at a lower rate. Therefore, the magnitude of cyclic creep retardation increases with increasing loading frequency.

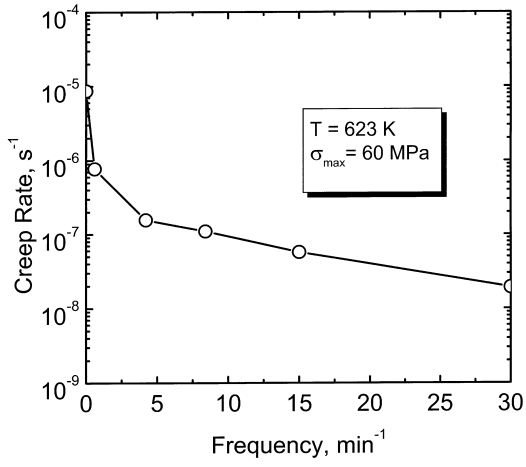

Fig. 37. Variation of steady-state creep rate with loading frequency for 20 vol.% $(Al_2O_3 + TiB_2)$/Al–Cu composite with a constant maximum stress of 60 MPa and an unloading amount of 90% [210].

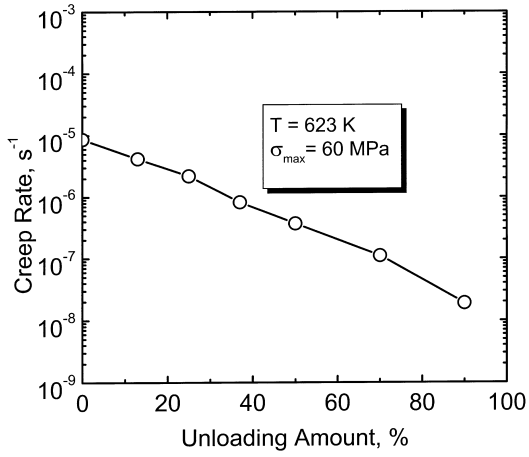

Fig. 38. Variation of steady-state creep rate with percentage of unloading amount for 20 vol.% ($Al_2O_3 + TiB_2$)/Al–Cu composite with a loading frequency of 0.5 Hz and a constant maximum stress of 60 MPa [210].

Finally, steady-state creep rates of in situ composite tend to decrease continuously with increasing percentage of unloading (Fig. 38), i.e. CCR behavior is enhanced with increasing percentages of unloading. Ma et al. [210] proposed that increase of unloading results in decrease of the mean stress and a corresponding decrease of cyclic creep rate for constant peak stress and loading frequency.

6.5.2. Ti-based composites

Zhu et al. [224] have conducted a preliminary study on high temperature creep behavior of in situ TiBw/Ti–6Al–4V composite prepared by RHP. They report that the creep resistance of the composite is higher than that of Ti–6Al–4V alloy by two orders of magnitude. However, the stress and temperature dependence of creep rates in this Ti-based composite agree with that for unreinforced Ti alloy. They suggest that a decrease in creep rate of the composite could be explained by transfer of load form matrix to reinforcements. Creep failure of the composite is caused by debonding of reinforcements from the matrix and by cleavage of the reinforcements. Fracture of the matrix is mainly intragranular [224].

Soboyejo et al. [96] have investigated high temperature creep properties of RSP-processed in situ TiBw/Ti–Al–V composites at 813 and 923 K. Compared with the IM produced matrix alloy, they report that TiB reinforcements decrease the creep rate by approximately two to three orders of magnitude. However, creep rates of the in situ composites are approximately one-order of magnitude lower than those for monolithic PM alloy. Furthermore, they show that in situ composites with different microstructural features exhibit a similar creep resistance. They suggest that deformation restraint and pinning/locking of grain boundaries by TiB reinforcements, are the two most likely creep resistance mechanisms.

Ranganath and Mishra [225] investigated the steady-state compressive creep behavior of Ti_2C/Ti and (TiB + Ti_2C)/Ti composites at 823–923 K. They report that the measured steady-state creep rate of composites is two to three orders of magnitude lower than unreinforced Ti in the temperature ranges investigated. Fig. 39 shows typical creep rate versus stress plots for Ti and 25 vol.% Ti_2C/Ti composite. The apparent stress exponent and apparent activation energy for creep of these investigated materials are summarized in Table 15. This reveals that values of stress exponent are higher for all composites than for unreinforced Ti at 823 K, whereas the difference in value is not

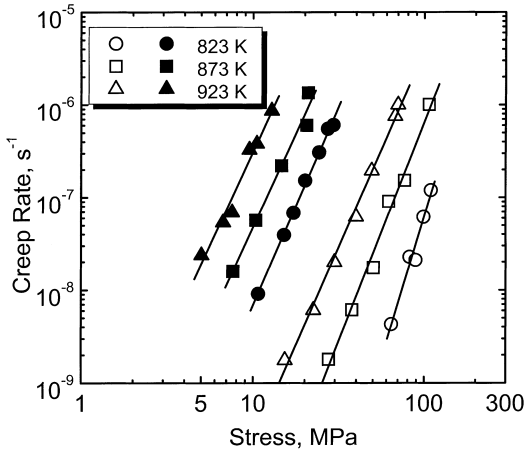

Fig. 39. Variation of steady-state creep rate with applied stress for unreinforced Ti (solid symbol) and 25 vol.% Ti_2C/Ti composite (open symbol) (reprinted from S. Ranganath, R.S. Mishra, Steady-state creep behavior of particulate-reinforced titanium matrix composites, Acta Materialia 44 (1996) 931, with permission from Elsevier [225]).

significant at 873 and 923 K. Furthermore, the value of apparent activation energies for creep is significantly higher than that for Ti, and increases with increasing volume fraction of reinforcements. Ranganath and Mishra [225] suggested that creep deformation of unreinforced Ti is governed by the climb-controlled creep mechanism. They proposed two possibilities to explain the origin of the high stress exponent at 823 K and the higher activation energy for the composites, i.e. (a) the presence of a threshold stress; (b) a change in the creep mechanism at 823 K. In this respect they estimated the values of threshold stress for the composites from the plots of σ versus $\dot{\varepsilon}^{1/4.1}$ by extrapolating the linear regression line to zero creep rate. However, even after compensating for threshold stress, Ranganath and Mishra [225] observed that the presence of reinforcement lead to lower values of creep constant. Thus, they suggest that there is a change in the steady-state creep mechanism from lattice-diffusion control ($n = 5$) to pipe pipe-diffusion control for which $n = 7$ is expected. Further, the constitutive equation for the composites should include a volume fraction term in order to explain creep strengthening. They also introduced a dimensionless constant, $A = 3.2 \times 10^5 \exp(-24.2\, V_r)$ for the lattice diffusion regime and $A = 9.4 \times 10^7 \exp(-28.1\, V_r)$ for the pipe-diffusion regime, to account for the influence of reinforcements on creep kinetics, where V_r is the volume fraction of reinforcements. By incorporating this volume fraction dependence and threshold stress into the power-law creep equation, the constitutive equation for creep of Ti-based composites in lattice

Table 15
Apparent stress exponent and apparent activation energy for creep of composites and unreinforced Ti[a]

Materials	Apparent stress exponent			Apparent activation energy (kJ/mol)
	823 K	873 K	923 K	
Ti	4.3	4.1	4.1	236
10 vol.% (TiB + Ti_2C)/Ti	4.9	4.9	4.8	284
15 vol.% (TiB + Ti_2C)/Ti	7.2	4.7	4.1	336
25 vol.% Ti_2C/Ti	6.1	4.7	4.3	353

[a] Reprinted from S. Ranganath, R.S. Mishra, Steady-state creep behavior of particulate-reinforced titanium matrix composites, Acta Materalia 44 (1996) 932 with permission from Elsevier [225].

diffusion and pipe-diffusion regimes can be expressed, respectively, as

$$\dot{\varepsilon} = 3.2 \times 10^5 \exp(-24.2V_r)\frac{EbD_L}{kT}\left(\frac{\sigma - \sigma_0}{E}\right)^{4.1} \quad \text{(E21)}$$

$$\dot{\varepsilon} = 9.4 \times 10^7 \exp(-28.1V_r)\frac{EbD_p}{kT}\left(\frac{\sigma - \sigma_0}{E}\right)^{6.1} \quad \text{(E22)}$$

where $\dot{\varepsilon}$ is the steady-state creep rate, σ the applied stress, σ_0 the threshold stress, E is the temperature-dependent Young's modulus, b is the Burgers vector, k is the Boltzmann constant, T is the absolute temperature, D_L is the lattice self-diffusion coefficient, and D_p is the pipe-diffusion coefficient.

Recently Tsang et al. [64] have examined the effect of volume fraction of reinforcement on the tensile creep properties of in situ TiB/Ti composites fabricated by CAC. Their experimental data are plotted in Fig. 40 as steady-state creep rate versus applied stress. Apparently the steady-state creep rate of the composites is one to two orders of magnitude lower than that for unreinforced Ti, and decreases further with increasing volume fraction of TiB reinforcement. Higher modulus, induced by load transfer from the matrix to stiffer reinforcement, and threshold stress, induced by the interaction between dislocation and reinforcement, are responsible for an increase in creep strength of the Ti-based composites. It is noted from Fig. 40 that the stress exponent of the composites is evidently greater than that for unreinforced Ti and shows a tendency to increase with increasing volume fraction of reinforcement. Tsang et al. [64] estimate the threshold stress for the composites from plots of σ versus $\dot{\varepsilon}^{1/4.2}$ by extrapolating the linear regression to zero creep rate. The threshold stress is determined to be 25, 31 and 35 MPa for 5, 10 and 15 vol.% TiB/Ti, respectively. Further they present creep data in terms of creep rate versus modulus-compensated effective stress, in double logarithm plots (Fig. 41). Clearly all creep data for unreinforced Ti and composites merge into a straight linear line with a slope of 4.2. Based on these results, Tsang et al. [64] suggest that both creep mechanisms for pure Ti and in situ Ti-based composites are associated with the lattice-diffusion controlled dislocation climb. No transition of creep mechanism occurs in Ti-based composites at 823 K, over the investigated stress range. They point out that a transition from lattice to pipe diffusion at 823 K, as proposed by Ranganath and Mishra [225], arises from the fact that the factor of modulus, which

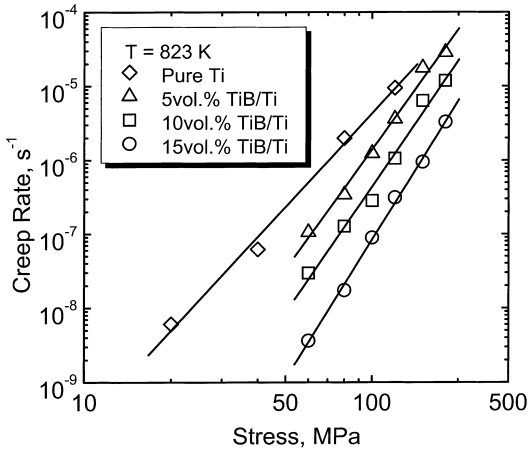

Fig. 40. Variation of steady-state creep rate with applied stress for unreinforced Ti and TiB/Ti composite at 823 K (reprinted from H.T. Tsang et al., Effects of volume fraction of reinforcement on tensile and creep properties of in situ TiB/Ti MMC, Scripta Materialia 37 (1997) 1362, with permission from Elsevier [64]).

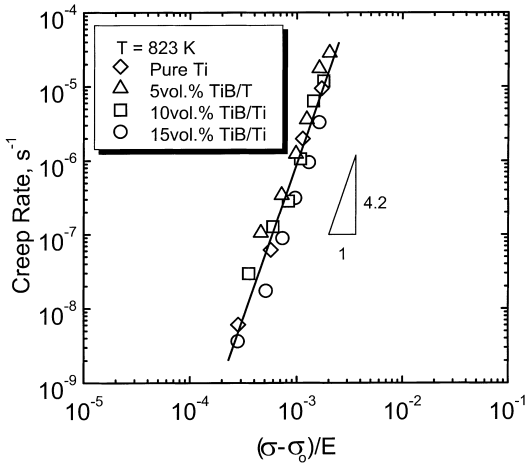

Fig. 41. The plot of the creep rate vs. the modulus-compensated effective stress for unreinforced Ti and TiB/Ti composite at 823 K (reprinted from H.T. Tsang et al., Effects of volume fraction of reinforcement on tensile and creep properties of in situ TiB/Ti MMC, Scripta Materialia 37 (1997) 1364, with permission from Elsevier [64]).

increases with increasing reinforcement fraction, is not introduced in the plots of creep rate against effective stress. After compensating the modulus term, the creep data tested from various volume fraction of reinforcement may merge. Thus, the volume fraction terms are no longer need to be introduced into the constitutive creep equation for Ti-based composites.

More recently Ma et al. [226] further examined compressive creep behavior of in situ 15 vol.% TiB/Ti and 15 vol.% (TiB + TiC)/Ti composites at 873–923 K. They report that the creep rate of the composites is about one-order of magnitude lower than that of unreinforced Ti. However, creep resistance of the (TiB + TiC)/Ti composite is higher than that of the TiB/Ti composite. The higher creep resistance of the (TiB + TiC)/Ti composite is attributed to smaller size of reinforcements [226]. It is interesting to note that both composites exhibit identical stress exponents of 4.5–4.7 at 873–923 K. These values are close to those of 15 vol.% (TiB + Ti_2C)/Ti composite (4.8–4.9) as reported by Ranganath and Mishra [225].

6.5.3. Cu-based composites

In recent years creep behavior of oxide dispersion-strengthened (DS), copper alloys have been reported [227,228]. Similar to Al-based MMCs, the creep behavior of oxide dispersion-strengthened copper composites is characterized by high apparent stress exponents and high apparent activation energies. Giberling and coworkers point out that an attractive particle-dislocation interaction is the dominant factor in controlling creep behavior of Al_2O_3 dispersion-strengthened copper [228]. By contrast, creep characteristics of copper alloys reinforced with borides is not well understood. Recently Ma and Tjong [172] performed a pioneering study on the effect of in situ TiB_2 reinforcement on high temperature creep behavior of copper at 773–873 K. They reported that the creep rate of monolithic Cu exhibits an exponential dependence on applied stress, whereas the power-law relationship prevailed for the experimental data from the 15 vol.% TiB_2/Cu composite. Fig. 42 shows the comparison between creep resistances of monolithic Cu and TiB_2/Cu composite. Apparently the creep rate of the 15 vol.% TiB_2/Cu composite is several orders of magnitude lower than that of the monolithic Cu. This indicates that the incorporation of in situ TiB_2 particulates into the Cu matrix can increase the creep resistance of Cu significantly. The composite exhibited a stress exponent of 25.5, 20.6 and 22.1 at 773, 823 and 873 K, respectively. These values are close to those

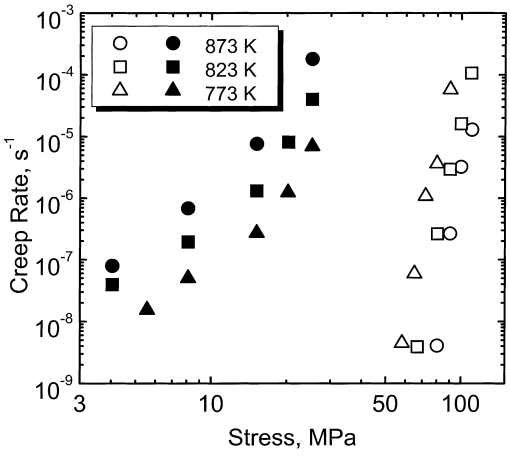

Fig. 42. Comparison in creep resistance between unreinforced Cu (solid symbol) and 15 vol.% TiB_2/Cu composite (open symbol) [172].

reported for Al_2O_3 dispersion-strengthened copper alloy at 748–773 K [228]. Furthermore, the creep activation energy of in situ TiB_2/Cu composite (444 kJ/mol) is much higher than that of unreinforced Cu (187 kJ/mol). To rationalize the high values of apparent stress exponent and apparent activation energy, the concept of threshold stress is again introduced for the TiB_2/Cu composite. In this case the creep can be described by a modified power-law creep equation (Eq. (E15)). Values of threshold stress are determined from the plot of $\dot{\varepsilon}^{1/4.8}$ versus σ by means of extrapolation. Here a stress exponent of 4.8 is selected because Frost and Ashby [229] report that the stress exponent for creep of pure copper is ~4.8 under the power-law creep condition. The value of threshold stress is determined to be 73.6, 65.1 and 35.1 MPa, respectively. The threshold stress also exhibits a strong temperature dependence and is similar to that of some aluminum-based MMCs [194,196,199–206,209–211]. Temperature dependence of threshold stress for TiB_2/Cu composite can be described by Eq. (E16) [196]. The value of Q_0 in Eq. (E16) is determined as 13.4 kJ/mol. This value is very close to that reported for some aluminum matrix composites [209,211]. On the basis of these results, Ma and Tjong [172] estimate the value of the true activation energy for creep of the TiB_2/Cu composite by means of Eq. (E18) using $n = 4.8$, average temperature $T = 823$ K, $Q_a = 444$ kJ/mol, and average applied stress $\sigma = 88$ MPa. The value of the true activation energy, Q, for creep is determined as 208 kJ/mol. This value is very close to that for self-diffusion in copper (197 kJ/mol) [229]. It implies that the creep rate of this in situ Cu-based composite is matrix lattice diffusion controlled. In Fig. 43 the minimum creep rate of the composite, normalized to the coefficient of matrix lattice diffusion, $\dot{\varepsilon}/D_L$, is plotted against the effective stress, compensated to the shear modulus G, $(\sigma - \sigma_0)/G$. It can be seen that the data points for all temperatures fit well a single straight line with a slope of 4.8. This indicates again that creep of in situ TiB_2/Cu composite is controlled by lattice-diffusion.

7. Summary and outlook

In this review article current developments in fabrication, mechanism, microstructure and mechanical properties of MMCs reinforced with in situ ceramic phases have been addressed. With regard to processing of in situ MMCs, a variety of techniques have evolved over the last decade. A

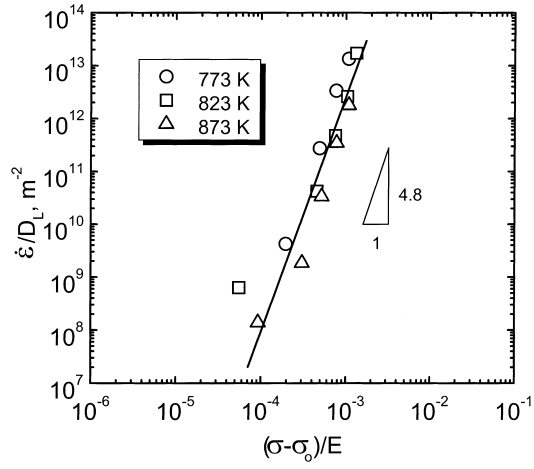

Fig. 43. Variation of diffusivity normalized minimum creep rate, $\dot{\varepsilon}/D_L$, with modulus-compensated effective stress, $(\sigma - \sigma_0)/G$, on double logarithmic coordinates for 15 vol.% TiB_2/Cu composite [172].

review of the available literature shows that these processing techniques can be classified as solid–liquid reaction, vapor–liquid–solid reaction, solid–solid reaction, and liquid–liquid reaction. Among these processes the solid–liquid reaction process is extensively adopted to produce in situ MMCs. The features, advantages and disadvantages, of various processing routes are examined and discussed.

The thermodynamics and kinetics of in situ reactions involved in preparing in situ MMCs are examined. The mechanism responsible for in situ formation of ceramic reinforcements for some reactive systems is still not well-understood. Among the many ceramic reinforcements, titanium boride and diboride are of particular importance because they can be formed in situ in Al-, Cu- and Ti-based composites. Accordingly the in situ MMCs, particularly Al-based composites reinforced with TiB_2 particles, exhibit higher strength, modulus, creep and wear resistance than conventional ex situ composites. These unique properties make them attractive for use as structural component materials in the aerospace and automotive industries.

The microstructure of in situ MMCs is generally characterized by fine reinforcing particles, which are uniformly distributed in the metal matrix, and by a clean particle–matrix interface. The interface is atomically abrupt and free from any interfacial phase. Direct contact on an atomic scale is established between in situ reinforcement and the metal matrix. In aluminum matrix composites both incoherent and semicoherent interfaces are observed, whereas coherent interfaces are reported in titanium matrix composites.

Finally in situ production of reinforcing particles in the metal matrix appears to be a promising route to fabricate composites in terms of both technical and economic considerations. The in situ formation of a ceramic second phase provides greater control of the size and level of reinforcement, as well as the matrix–reinforcement interface, yielding better tailorability of the composite properties. In the latter case it is more cost effective to form the in situ ceramic reinforcing phase in the metals/alloys rather than produce ex situ MMCs via incorporation of expensive ceramic reinforcements in metal matrices. Moreover one can take advantage of conventional, established, processing technologies for large-scale casting and subsequent metal-working to produce in situ MMCs. Although a number of challenges still exist, the novel composite technologies of in situ production of reinforcing particles offer very attractive possibilities for commercial success.

References

[1] S.G. Fishman, J. Met. 38 (1986) 26.
[2] Y. Flom, R.J. Arsenault, J. Met. 38 (1986) 31.
[3] Y. Flom, R.J. Arsenault, Mater. Sci. Eng. 77 (1986) 191.
[4] A.H.M. Howes, J. Met. 38 (1986) 28.
[5] A. Mortensen, M.N. Gugor, J.A. Cornie, M.C. Flemings, J. Met. 38 (1986) 30.
[6] A. Mortensen, J.A. Cornie, M.C. Flemings, J. Met. 40 (1988) 12.
[7] V.C. Nardone, K.W. Prewo, Scripta Metall. 20 (1986) 43.
[8] T.W. Chow, A. Kelly, A. Okura, Composites 16 (1986) 187.
[9] H.J. Rack, in: P. Kumar, K. Vedula, A. Ritter (Eds.), Processing and Properties of Powder Metallurgy Composites, The Metallurgical Society, Warrendale, PA, 1988, p. 155.
[10] I.A. Ibrahim, F.A. Mohamed, E.J. Lavernia, J. Mater. Sci. 26 (1991) 1137.
[11] J.J. Lewandowski, C. Liu, in: P. Kumar (Ed.), Proceedings of the Processing and Properties for Powder Metallurgy Composites, TMS, Warrendale, PA, 1987, p. 107.
[12] A. Mortensen, J.A. Cornie, M.J.C. Flemings, Metall. Trans. 19A (1988) 709.
[13] Y. Wu, E.J. Lavernia, Metall. Trans. 23A (1992) 2923.
[14] Z.Y. Ma, J. Liu, C.K. Yao, J. Mater. Sci. 26 (1991) 1971.
[15] Z.Y. Ma, J. Bi, Y.X. Lu, M. Luo, Y.X. Gao, Scripta Metall. Mater. 29 (1993) 225.
[16] S.V. Nair, J.K. Tien, R.C. Bates, Int. Met. Rev. 30 (1985) 275.
[17] Z.Y. Ma, X.G. Ning, Y.X. Lu, J.H. Li, J. Bi, Y.Z. Zhang, Mater. Lett. 21 (1994) 69.
[18] S.C. Tjong, K.C. Lau, S.Q. Wu, Metall. Mater. Trans. 30A (1999) 2551.
[19] A.R.C. Westwood, Metall. Trans. 19A (1988) 749.
[20] Z.Y. Ma, J.H. Li, M. Luo, X.G. Ning, Y.X. Lu, J. Bi, Y.Z. Zhang, Scripta Metall. Mater. 31 (1994) 635.
[21] S. Ranganath, M. Vijayakumar, J. Subrahmanyam, Mater. Sci. Eng. A149 (1992) 253.
[22] C. Biselli, D.G. Morris, N. Randall, Scripta Metall. Mater. 30 (1994) 1327.
[23] Y. Choi, J.K. Lee, M.E. Mullins, J. Mater. Sci. 32 (1997) 1717.
[24] C. Raghunath, M.S. Brat, P.K. Rohatgi, Scripta Metall. Mater. 32 (1995) 577.
[25] M.J. Koczak, M.K. Premkumar, JOM 1 (1993) 44.
[26] A.G. Merzhanov, I.P. Borovinskaya, Dokl. Akad. Nauk. SSSR 204 (1972) 366.
[27] I.P. Borovinskaya, A.G. Merzhanov, N.P. Novikov, A.K. Filonenko, Combust. Explos. Shock Waves 10 (1974) 2.
[28] A.G. Merzhanov, A.K. Filonenko, I.P. Borovinskaya, Dokl. Akad. Nauk. SSSR 208 (1973) 892.
[29] A.G. Merzhanov, G.G. Karyuk, I.P. Borovinskaya, V.A. Prokudina, E.G. Dyad'ko, Sov. Powder Metall. Met. Ceram. 20 (1981) 709.
[30] N.D. Corbin, J.W. McCauley, MTL MS 86-1, USAMTL, Watertown, MA, 1986.
[31] J.B. Holt, Z.A. Munir, J. Mater. Sci. 21 (1986) 251.
[32] A.A. Zenin, A.G. Merzhanov, G.A. Nersisyan, Fiz. Goren. Vzryva 17 (9181) 63.
[33] Z.A. Munir, J.B. Holt, J. Mater. Sci. 22 (1987) 710.
[34] I.P. Borovinskaya, V.E. Loryan, Sov. Powder Metall. Met. Ceram. 191 (1979) 851.
[35] T.M. Maksimov, M.K. Ziatdinov, A.G. Raskolenlo, O.K. Lepakova, Combust. Explos. Shock Waves 15 (1979) 415.
[36] A.R. Sarkisyan, S.K. Dolukhanyan, I.P. Borovinskaya, Sov. Powder Metall. Met. Ceram. 17 (1978) 424.
[37] K.A. Philpot, Z.A. Munir, J.B. Holt, J. Mater. Sci. 22 (1987) 159.
[38] S. Sampath, S. Khatri, E. Shtessel, M.J. Koczak, in: V.A. Ravi, T.S. Srinvatsan (Eds.), Processing and Fabrication of Advanced Materials for High Temperature Applications II, TMS, Warrendale, PA, 1993, p. 223.
[39] S.D. Dunmead, D.W. Readey, C.E. Semler, J.B. Holt, Rep. UCRL-98773, Lawrence Livemore National Laboratory, 1988.
[40] J.B. Holt, Rep. UCRL-53258, Lawrence Livemore National Laboratory, 1982.
[41] Y. Miyamoto, K. Hirao, M. Koizumi, in: Proceedings of the International Symposium on Fundamental Research Strategy in Development of New Materials for Efficient Energy Conversion, Osaka, 1987.
[42] A.N. Tabachenko, T.A. Panteleeva, V.I. Itin, Combust. Explos. Shock Waves USSR 20 (1984) 387.
[43] Y. Choi, M.E. Mullins, K. Wijayatilleke, J.K. Lee, Metall. Trans. 23A (1992) 2387.
[44] I. Gotman, M.J. Koczak, E. Shtessel, Mater. Sci. Eng. A187 (1994) 189.
[45] L. Chrstodoulou, D.C. Nagle, J.M. Brupbacher, International Patent No. WO86/06366 (1986).
[46] L. Chrstodoulou, et al., US Patent 4,751,084 (1988).
[47] J.M. Brupbacher, et al., US Patent 4,836,982 (1989).
[48] A.K. Kuruvilla, K.S. Prasad, V.V. Bhanuprasad, Y.R. Mahajan, Scripta Metall. Mater. 24 (1990) 873.
[49] C.A. Caracostas, W.A. Chiou, M.E. Fine, H.S. Cheng, Scripta Metall. Mater. 27 (1992) 167.
[50] R. Mitra, W.A. Chiou, J.R. Weertman, M.E. Fine, R.M. Aikin Jr., Scripta Metall. Mater. 25 (1991) 2689.
[51] G.M. Vyletel, D.C.V. Aken, J.E. Allison, Scripta Metall. Mater. 25 (1991) 2405.
[52] G.M. Vyletel, J.E. Allison, D.C.V. Aken, Metall. Trans. 24A (1993) 2545.

[53] P.E. Krajewski, J.E. Allison, J.W. Jones, Metall. Trans. 24A (1993) 2731.
[54] D.C.V. Aken, P.E. Krajewski, G.M. Vyletel, J.E. Allison, J.W. Jones, Metall. Mater. Trans. 26A (1995) 1395.
[55] G.M. Vyletel, J.E. Allison, D.C.V. Aken, Metall. Mater. Trans. 26A (1995) 3143.
[56] Z.Y. Ma, J. Bi, Y.X. Lu, H.W. Shen, Y.X. Gao, in: L. Arnberg, et al. (Eds.), Proceedings of the Third International Conference on Aluminum Alloys, Trondheim, Norway, Norwegian Institute of Technology, 1992, p. 435.
[57] Z.Y. Ma, J. Bi, Y.X. Lu, H.W. Shen, Y.X. Gao, Composites Interface 1 (1993) 287.
[58] Z.Y. Ma, J.H. Li, S.X. Li, X.G. Ning, Y.X. Lu, J. Bi, J. Mater. Sci. 31 (1996) 741.
[59] Z.Y. Ma, S.C. Tjong, Metall. Mater. Trans. 28A (1997) 1931.
[60] Z.Y. Ma, J.H. Li, M. Luo, X.G. Ning, Y.X. Lu, J. Bi, Y.Z. Zhang, J. Mater. Sci. Technol. 12 (1996) 25.
[61] D.Z. Wang, Z.R. Liu, C.K. Yao, M. Yao, Mater. Sci. Prog. 7 (1993) 467 (in Chinese).
[62] Y. Lin, R.H. Zee, B.A. Chin, Metall. Trans. 22A (1991) 859.
[63] H.T. Tsang, C.G. Chao, C.Y. Ma, Scripta Mater. 35 (1996) 1007.
[64] H.T. Tsang, C.G. Chao, C.Y. Ma, Scripta Mater. 37 (1997) 1359.
[65] W.J. Lu, X.N. Zhang, D. Zhang, R.J. Wu, Y.J. Pian, W.P. Fang, Acta Metall. Sinica 35 (1999) 536.
[66] X. Zhang, W. Lu, D. Zhang, R. Wu, Scripta Mater. 41 (1999) 39.
[67] P.C. Maity, S.C. Panigrahi, P.N. Chakraborty, Scripta Metall. Metall. 28 (1993) 549.
[68] H. Nakata, T. Choh, N. Kanetake, J. Mater. Sci. 30 (1995) 1719.
[69] A. Chrysanthou, G. Erbaccio, J. Mater. Sci. 30 (1995) 6339.
[70] Z. Wang, S. Zeng, Q. Li, C. Li, S. Wang, B. Liu, Acta Metall. Sinica 30 (1994) 314.
[71] E. Zhang, S. Zeng, X. Zeng, Q. Li, Trans. Nonferrous Met. Soc. China 6 (1996) 114.
[72] E. Zhang, B. Yang, S. Zeng, Q. Li, M. Ma, Trans. Nonferrous Met. Soc. China 8 (1998) 92.
[73] S. Luo, J. Sun, Trans. Nonferrous Met. Soc. China 7 (1997) 113.
[74] E. Zhang, S. Zeng, B. Yang, Q. Li, M. Ma, Metall. Mater. Trans. 30A (1999) 1147.
[75] E. Zhang, S. Zeng, B. Yang, Q. Li, M. Ma, Metall. Mater. Trans. 30A (1999) 1153.
[76] P.J. Davies, J.L.F. Kellie, J.V. Wood, UK Patent No. 2,257985A, ASM, Paris, September 1992.
[77] J. Kellie, J.V. Wood, Mater. World 3 (1995) 10.
[78] P.J. Davies, J.L.F. Kellie, J.V. Wood, Key Eng. Mater. 77/78 (1993) 357.
[79] J.V. Wood, P. Davies, J.L.F. Kellie, Mater. Sci. Technol. 9 (1993) 833.
[80] L. Lu, M.O. Lai, F.L. Chen, Acta Mater. 45 (1997) 4297.
[81] Y. Chen, D.D.L. Chung, J. Mater. Sci. 31 (1996) 311.
[82] Y. Chen, D.D.L. Chung, J. Mater. Sci. 30 (1995) 4609.
[83] Z.Y. Chen, Y.Y. Chen, Q. Shu, G.Y. An, Acta Metall. Sinica 35 (1999) 874.
[84] D.C. Dunand, J.L. Sommer, A. Mortensen, Metall. Trans. 24A (1993) 2161.
[85] E. Taheri-Nassaj, M. Kobashi, T. Choh, Scripta Mater. 34 (1996) 1257.
[86] E. Taheri-Nassaj, M. Kobashi, T. Choh, Scripta Mater. 37 (1997) 605.
[87] D. Muscat, R.A.L. Drew, Metall. Trans. 25A (1994) 2357.
[88] M. Nanabe, P.B. Aswath, J. Mater. Res. 11 (1996) 1562.
[89] M. Nanabe, P.B. Aswath, Acta Mater. 45 (1997) 4067.
[90] M.K. Aghajanian, N.N. Macmilan, C.R. Kennedy, S.J. Luszcz, R. Roy, J. Mater. Sci. 24 (1989) 658.
[91] A.W. Urquhart, Mater. Sci. Eng. A144 (1991) 75.
[92] O. Salas, H. Ni, V. Jayaram, K.C. Vlach, C.G. Levi, R. Mehrabian, J. Mater. Res. 6 (1991) 1964.
[93] V.S.R. Murthy, B.S. Rao, J. Mater. Sci. 30 (1995) 3091.
[94] W.O. Soboyejo, R.J. Lederich, S.M.L. Sastry, in: S.K. Das, C.P. Ballard, F. Marikar (Eds.), High Performance Composites for the 1990s, TMS, Warrendale, PA, 1991, p. 127.
[95] T.C. Peng, D.M. Bowden, S.M.L. Sastry, in: T.G. Gassbarre, W.F. Jandeska (Eds.), Advances in Powder Metallurgy IV, 387 MPIF, Princeton, NJ, 1989, p. 387
[96] W.O. Soboyejo, R.J. Lederich, S.M.L. Sastry, Acta Metall. Mater. 42 (1994) 2579.
[97] S. Ragarajan, P.B. Aswath, W.O. Soboyejo, Scripta Mater. 35 (1996) 239.
[98] S. Dubey, W.O. Soboyejo, T.S. Srivatsan, Appl. Compos. Mater. 4 (1997) 361.
[99] X.C. Tong, N.F. Shen, B.C. Liu, J. Mater. Sci. 30 (1995) 3680.
[100] X.C. Tong, J. Mater. Sci. 33 (1998) 5365.
[101] X.C. Tong, H.S. Fang, Metall. Mater. Trans. 29A (1998) 875.
[102] X.C. Tong, H.S. Fang, Metall. Mater. Trans. 29A (1998) 893.
[103] H. Fugunaka, X. Wang, Y. Aramaki, J. Mater. Sci. Lett. 9 (1990) 23.
[104] J. Pan, Ph.D. Dissertation, Harbin Institute of Technology, 1994.
[105] J. Pan, J.H. Li, H. Fukunaka, X.G. Ning, H.Q. Ye, Z.K. Yao, M. Yang, Composites Sci. Technol. 57 (1997) 319.
[106] D.Z. Wang, Z.R. Liu, C.K. Yao, M. Yao, J. Mater. Sci. Lett. 9 (1990) 23.
[107] H.X. Peng, D.Z. Wang, L. Geng, C.K. Yao, J.F. Mao, Scripta Mater. 37 (1997) 199.
[108] M.J. Koczak, K.S. Kumar, US Patent 4,808,372 (1989).
[109] P. Sahoo, M.J. Koczak, Mater. Sci. Eng. A144 (1991) 37.
[110] P. Sahoo, M.J. Koczak, Mater. Sci. Eng. A131 (1991) 69.

[111] M.K. Prekumar, M.G. Chu, Metall. Trans. 24A (1993) 2358.
[112] M.K. Prekumar, M.G. Chu, Mater. Sci. Eng. A202 (1995) 172.
[113] P. Sahoo, M.J. Koczak, in: Proceedings of the TMS Conference on Advanced Metal and Ceramic Matrix Composites, February 1990.
[114] C.X. Chu, R.J. Wu, G.D. Zhang, J. Mater. Sci. Technol. 12 (1996) 365.
[115] L. Chen, S. Han, Physical Chemistry, Shanghai Science and Technology Press, 1980 (in Chinese).
[116] J.S. Bejamin, Metall. Trans. 1 (1970) 2943.
[117] J.S. Bejamin, Sci. Am. 234 (1976) 40.
[118] P.G. Gilman, J.S. Bejamin, Annu. Rev. Mater. Sci. 13 (1983) 279.
[119] J.S. Bejamin, T.E. Volin, Metall. Trans. 5 (1974) 1929.
[120] G. Frommeyer, S. Beer, K.V. Oldenburg, Z. Metallkd. 85 (1994) 5.
[121] G. Jangg, F. Kutner, G. Korb, Powder Metall. Int. 9 (1977) 24.
[122] G. Jangg, in: E. Arzt, L. Schultz (Eds.), New Materials by Mechanical Alloying Techniques, Proceedings of the DGM Conference Calw-Hirsau, October 1988, DGM Informationsgesellschaft, Oberursel, 1988, p. 39.
[123] C.C. Koch, O.B. Calvin, C.G. Mckamey, J.O. Scarbrough, J. Appl. Phys. Lett. 43 (1983) 1017.
[124] J. Bi, Z.Y. Ma, S.J. Wu, Y.X. Lu, H.W. Shen, J. Mater. Sci. Technol. 9 (1993) 61.
[125] Z.Y. Ma, X.G. Ning, Y.X. Lu, J. Bi, L.S. Wen, S.J. Wu, G. Jangg, H. Daninger, Scripta Metall. Mater. 31 (1994) 131.
[126] L. Lu, M.O. Lai, X.P. Niu, H.N. Ho, Z. Metallkd. 89 (1998) 567.
[127] Y.X. Lu, J. Bi, D.X. Li, D.H. Ping, Z.Y. Ma, H.W. Shen, in: C.T. Sun, T.T. Loo (Eds.), Proceedings of the Second International Symposium on Composite Materials and Structures, Peking University Press, Beijing, 1992, p. 882.
[128] D.X. Li, D.H. Ping, Y.X. Lu, H.Q. Ye, Mater. Lett. 16 (1993) 322.
[129] L. Wang, M. Niinomi, S. Takahashi, M. Hagiwara, S. Emura, Y. Kawabei, S.J. Kim, Mater. Sci. Eng. A263 (1999) 319.
[130] S.S. Sahay, K.S. Ravichandran, R. Atri, B. Chen, J. Rubin, J. Mater. Res. 14 (1999) 4214.
[131] Z.Y. Ma, S.C. Tjong, L. Geng, Scripta Mater. 42 (2000) 367.
[132] K. Satyaprasad, Y.R. Mahajan, V.V. Bhanuprasad, Scripta Metall. Mater. 26 (1992) 711.
[133] R. Mitra, M.E. Fine, J.R. Weerman, J. Mater. Res. 8 (1993) 2370.
[134] B.C. Giessen, US Patent 4,540,546 (1985).
[135] A.K. Lee, L.E. Sanchez-Caldera, S.T. Oktay, N.P. Suh, Adv. Mater. Proc. 8 (1992) 31.
[136] R.A. Rapp, X. Zheng, Metall. Trans. 22A (1991) 3071.
[137] T. Nukami, M.C. Flemings, Metall. Mater. Trans. 26A (1995) 1877.
[138] B. Yang, Y.Q. Wang, B.L. Zhou, Acta Metall. Sinica 34 (1998) 100.
[139] I. Barin, O. Knacke, Thermodynamical Properties of Inorganic Substances, Springer, Berlin, 1973.
[140] O. Knacke, O. Kubaschewski, R. Hesselman, Thermodynamical Properties of Inorganic Substances, 2nd Edition, Springer, Berlin, 1991.
[141] M.G. Chu, M.K. Premkumar, Metall. Trans. 24A (1993) 2803.
[142] L.F. Mondolfo, Aluminum Alloys: Structure and Properties, Butterworths, Woburn, MA, 1976, p. 236.
[143] K.L. Tee, L. Lu, M.O. Lai, Z. Metallkd. 91 (2000) 251.
[144] Y. Tanaeoka, O. Odawara, Y. Kaeida, J. Am. Ceram. Soc. 72 (1989) 72.
[145] R.Z. Yuan, Z.Y. Fu, Z.A. Munir, X.X. Zhou, Z.L. Yang, J. Mater. Synth. Process. 1 (1993) 153.
[146] Z.Y. Fu, R.Z. Yuan, Z.A. Munir, Int. J. SHS 2 (1993) 261.
[147] Z.Y. Fu, R.Z. Yuan, Z.A. Munir, Z.L. Yang, Int. J. SHS 1 (1993) 119.
[148] H.J. Brinkman, J. Duazczyk, L. Katgerman, Scripta Mater. 37 (1997) 293.
[149] H.J. Brinkman, J. Duazczyk, L. Katgerman, Mater. Sci. Technol. 14 (1998) 873.
[150] A.M. Kanury, Metall. Trans. 23A (1992) 2349.
[151] S. Khatri, M. Koczak, Mater. Sci. Eng. A162 (1993) 153.
[152] C.F. Feng, L. Froyen, Scripta Mater. 39 (1998) 109.
[153] C.F. Feng, L. Froyen, Scripta Mater. 36 (1997) 467.
[154] P.S. Gilman, W.D. Nix, Metall. Trans. 12A (1981) 813.
[155] R. Schultz, M. Trudeau, J.Y. Huot, A.V. Neste, Phys. Rev. Lett. 62 (1989) 2849.
[156] M. Atzmon, Phys. Rev. Lett. 64 (1990) 487.
[157] E. Ma, J. Pagan, G. Cranford, M. Atzmon, J. Mater. Res. 8 (1993) 1836.
[158] Y.H. Park, H. Hashimoto, T. Abe, Mater. Sci. Eng. A181/A182 (1994) 1291.
[159] J.Y. Huang, L.L. Ye, K. Wu, H.Q. Ye, Metall. Mater. Trans. 26A (1995) 2755.
[160] J.Y. Huang, L.L. Ye, K. Wu, H.Q. Ye, Acta Mater. 44 (1996) 1781.
[161] Z.G. Liu, J.T. Guo, L.L. Ye, G.S. Li, Z.Q. Hu, Appl. Phys. Lett. 65 (1994) 2666.
[162] L.L. Ye, Z.G. Liu, M.X. Quan, Z.Q. Hu, J. Appl. Phys. 80 (1996) 1910.
[163] J.J. Valencia, C. McCullough, J. Rosler, C.G. Levi, R. Mehrabian, in: P. Rohatgi, et al. (Eds.), Solidification of Metal Matrix Composites, Warrendale, PA, TMS, 1990, p. 133.
[164] M.E. Hyman, C. McCullough, J.J. Valencia, C.G. Levi, R. Mehrabian, Metall. Trans. 20A (1989) 1847.

[165] M.V. Swain, in: R.W. Cahn, P. Haasen, E.K. Kramer (Eds.), Materials Science and Technology, Vol. 11, Weinhelm VCH, Verlagsgesellschaft mbH, 1994, p. 183.
[166] S. Raganath, T. Roy, R.S. Mishra, Mater. Sci. Technol. 12 (1996) 219.
[167] T. Nukami, J. Mater. Sci. Lett. 17 (1998) 276.
[168] R. Mitra, W.A. Chiou, J.R. Weertman, M.E. Fine, J. Mater. Res. 8 (1993) 2380.
[169] A.R.C. Westwood, S.R. Winzer, in: P.A. Psaras, H.D. Langford (Eds.), Advanced Materials Research, National Academy Press, Washington, DC, 1987, p. 225.
[170] V.V. Bhanuprasad, Int. J. Powder 27 (1991) 227.
[171] J. Lee, N.J. Kim, J.Y. Jung, E.. Lee, S. Ahn, Scripta Mater. 39 (1998) 1063.
[172] Z.Y. Ma, S.C. Tjong, Mater. Sci. Eng. A284 (2000) 70.
[173] S.M. Pickard, B. Berdy, J. Harding, M. Taya, Scripta Metall. 22 (1988) 601.
[174] C.C. Perng, J.R. Hwang, J.L. Doong, Scripta Metall. Mater. 29 (1993) 311.
[175] C.C. Perng, J.R. Hwang, J.L. Doong, Mater. Sci. Eng. A171 (1993) 213.
[176] R.U. Vaidya, A.K. Zurek, J. Mater. Sci. 30 (1995) 2541.
[177] A. Kalambur, I.W. Hall, Scripta Mater. 37 (1997) 193.
[178] S.C. Tjong, Z.Y. Ma, R.K.Y. Li, Mater. Lett. 38 (1999) 39.
[179] M. Guden, I.M. Hall, Mater. Sci. Eng. A232 (1997) 1.
[180] S.I. Hong, G.T. Gray III, J.J. Lewandowski, Acta Metall. Mater. 41 (1995) 2337.
[181] J.H. Shackelford, A. Alexandu, J.S. Park (Eds.), CRC Materials Science, Engineering Handbook, 2nd Edition, CRC Press, Ann Arbor, 1994, pp. 470–471.
[182] C.A. Caracostas, W.A. Chiou, M.E. Fine, H.S. Cheng, Metall. Mater. Trans. 28A (1997) 491.
[183] D. Lewis III, in: R.K. Everet, R.J. Arsenault (Eds.), Metal Matrix Composites: Processing and Interfaces, Academic Press, New York, 1991, p. 121.
[184] Y.M. Pan, Ph.D. Dissertation, Northwestern University, Evanston, IL, 1990.
[185] T. Iseki, T. Kameda, T. Maruyama, J. Mater. Sci. 19 (1984) 1692.
[186] A. Erdemir, Lubric Eng. 47 (1991) 168.
[187] A. Erdemir, G.R. Fenske, R.A. Erck, F.A. Nichols, D.E. Busch, Lubric Eng. 47 (1991) 179.
[188] M.B. Peterson, M. Kanakia, in: F.A. Smidt, P.J. Blau (Eds.), Engineering Materials for Advanced Friction and Wear Applications, ASM, Metals Park, OH, 1988, p. 153.
[189] S.Q. Wu, H.G. Zhu, S.C. Tjong, Metall. Mater. Trans. 30A (1999) 243.
[190] S.C. Tjong, S.Q. Wu, H.G. Zhu, Composites Sci. Technol. 59 (1999) 1341.
[191] T.G. Nieh, Metall. Trans. 15 (1984) 139.
[192] T.G. Nieh, K. Xia, T.G. Langdon, J. Eng. Mater. Technol. 110 (1988) 77.
[193] T. Morimoto, T. Yamaoka, H. Lilholt, M. Taya, J. Eng. Mater. Technol. 110 (1988) 70.
[194] K.T. Park, E.J. Lavernia, F.A. Mohamed, Acta Metall. Mater. 38 (1990) 2149.
[195] A.B. Pandey, R.S. Mishra, Y.R. Mahajan, Acta Metall. Mater. 40 (1992) 2045.
[196] F.A. Mohamed, K.T. Park, E.J. Lavernia, Mater. Sci. Eng. A150 (1992) 21.
[197] M. Furukawa, J. Wang, Z. Horita, M. Nemoto, Y. Ma, T.G. Landon, Mater. Metall. Trans. 26A (1995) 633.
[198] A.B. Pandey, R.S. Mishra, Y.R. Mahajan, Mater. Sci. Eng. A189 (1994) 95.
[199] G. Gonzalez-Doncel, O.D. Sherby, Acta Metall. Mater. 41 (1993) 2797.
[200] K.T. Park, F.A. Mohamed, Metall. Trans. 26A (1995) 3119.
[201] J. Cadek, H. Oikawa, V. Sustek, Mater. Sci. Eng. A190 (1995) 9.
[202] Y. Li, F.A. Mohamed, Acta Mater. 45 (1997) 4775.
[203] Y. Li, T.G. Langdon, Acta Mater. 45 (1997) 4797.
[204] Z.Y. Ma, S.C. Tjong, Composites Sci. Technol. 59 (1999) 737.
[205] S.C. Tjong, Z.Y. Ma, Composites Sci. Technol. 59 (1999) 1117.
[206] Z.Y. Ma, S.C. Tjong, Mater. Sci. Eng. A278 (2000) 5.
[207] P.E. Krajewski, J.E. Allison, J.W. Jones, Metall. Trans. 24A (1993) 2731.
[208] A.B. Pandey, R.S. Mishra, Y.R. Mahajan, Scripta Metall. Mater. 29 (1993) 1199.
[209] Z.Y. Ma, S.C. Tjong, Mater. Sci. Eng. A256 (1998) 120.
[210] Z.Y. Ma, S.C. Tjong, Z.G. Wang, Mater. Sci. Eng. A264 (1999) 177.
[211] Z.Y. Ma, S.C. Tjong, S.X. Li, J. Mater. Res. 14 (1999) 4541.
[212] O.D. Sherby, R.H. Klundt, A.K. Miller, Metall. Trans. 8A (1977) 843.
[213] S. Purushothman, J.K. Tien, Acta Metall. 26 (1978) 519.
[214] F.A. Mohamed, Mater. Sci. Eng. A245 (1998) 242.
[215] J.E. Bird, A.K. Mukherjee, J.E. Dorn, in: D.G. Brandon, A. Rosen (Eds.), Quantitative Relation between Properties and Microstructure, Israel University Press, Jerusalem, 1969, p. 225.
[216] O.D. Sherby, P.M. Burke, Prog. Mater. Sci. 13 (1968) 325.
[217] F.A. Mohamed, T.G. Langdon, Acta Metall. 22 (1974) 779.
[218] T.S. Lundy, J.F. Murdock, J. Appl. Phys. 33 (1962) 1671.
[219] P.L. Liu, Z.G. Wang, W.L. Wang, Mater. Sci. Technol. 13 (1997) 667.

[220] P.L. Liu, Z.G. Wang, H. Toda, T. Kobayashi, Scripta Mater. 36 (1997) 807.
[221] S.C. Tjong, Z.Y. Ma, Z.G. Wang, Mater. Sci. Technol. 15 (1999) 666.
[222] V.C. Nardone, D.E. Matejczyk, J.K. Tien, Metall. Trans. 14A (1983) 1435.
[223] V.C. Nardone, W.L. Kimmerle, J.K. Tien, Metall. Trans. 17A (1986) 1577.
[224] S.J. Zhu, Y.X. Lu, Z.G. Wang, J. Bi, in: Antonio Miravete (Ed.), Proceedings of the Ninth International Conference on Composite Materials (ICCM/9), Vol. 1, University of Zaragona and Woodhead Publishing Limited, 1993, p. 549.
[225] S. Ranganath, R.S. Mishra, Acta Mater. 44 (1996) 927.
[226] Z.Y. Ma, S.C. Tjong, S.X. Li, unpublished work.
[227] M.S. Nagorka, G.E. Lucas, C.G. Levi, Metall. Mater. Trans. 26A (1995) 873.
[228] S.E. Broyles, K.R. Anderson, J.R. Groza, J.C. Gibeling, Metall. Mater. Trans. 27A (1996) 1217.
[229] H.J. Frost, A.F. Ashby, Deformation-Mechanism Maps: The Plasticity and Creep of Metals and Ceramics, Pergamon Press, Oxford, UK, 1982, pp. 113–131.